Abstract

BLOCK, NATHAN ROBERT. Comparison of mixing length, standard k-ε, and renormalized group k-ε turbulence models in GOTHIC 7.2. (Under the direction of Dr. James W. Leach.)

Scores of CFD codes are available for computing flow properties in complex geometries. Many of these codes require significant effort for producing the models and large amounts of computational power for even simple simulations. Within the nuclear industry, large-scale transient simulations are required that would take considerable time to compute with a standard CFD code. Instead of utilizing a CFD code, the GOTHIC thermal-hydraulic code can be used to compute various thermal and flow properties for these large-scale simulations. For calculating flow properties, GOTHIC has several turbulence models that can be used for computing the Reynolds stresses. The purpose of this work is to evaluate the effectiveness of the mixing length, k-ε, and RNG k-ε turbulence models in predicting flow properties using coarse meshes in GOTHIC. Experiments given in literature for an axi-symmetric jet, mixing layer flow, and channel flow are modeled with GOTHIC and compared to the experimental results.

Various flow properties such as the turbulent kinetic energy, spreading rates, velocity profiles, mixing region growth rates, and centerline velocities generated by GOTHIC are compared with experimental data. The results show that the mixing length model does poorly at predicting any of the flow properties, especially the turbulent kinetic energy. The RNG k-ε model does significantly better at predicting the flows, but takes much longer to run. Overall, however, the standard k-ε model provides the best replication of the

experimental results for the coarse meshes utilized. In conclusion, the standard k-ε model should continue to be used for the default turbulence model in future validation of GOTHIC.

Comparison of mixing length, standard k-ε, and renormalized group k-ε turbulence models in GOTHIC 7.2

by

Nathan Robert Block

(Under the direction of Dr. James W. Leach)

A thesis submitted to the Graduate Faculty of

North Carolina State University

In partial fulfillment of the requirements for the degree of

Masters of Science

in

Mechanical Engineering

Raleigh

October 21, 2005

Approved by

Dr. Herbert Eckerlin	Dr. Richard Gould

Dr. James Leach

Chair of Advisory Committee

Biography

Nathan Robert Block was born to Gene and Edith Block in Indianapolis, Indiana on July 29, 1981. Nathan is the oldest of four children including two brothers, Stephen and Douglas, and a sister, Rachel. He was raised in Durham, North Carolina where he enjoyed working on cars and computers during his childhood. In addition, he was heavily involved with the Royal Ranger program, finishing 3rd in its 1996 National Ranger of the Year competition.

Nathan was home instructed for both primary school and high school. During the final two years of high school, he attended Durham Technical Community College concurrently, obtaining transfer credits in mathematics, science, and English. After graduating high school in the spring of 1999, he enrolled at North Carolina State University where his prior interest in the automotive field led him to purse a degree in mechanical engineering. Nathan received a Bachelor of Science degree in Mechanical Engineering in December 2002 and immediately enrolled in N.C. State's graduate program the following spring. Under the direction of Dr. Jim Leach, he began research on turbulence modeling in GOTHIC transient analysis code. Simultaneously, Nathan worked for the Industrial Assessment Center where he performed energy assessments of manufacturing facilities and helped write reports on improving energy conservation, productivity, and reducing waste. In May 2003, Nathan married his high school sweetheart, Kerri Williams.

Nathan is employed by the developer of the GOTHIC code, Numerical Applications, Inc. He and his wife currently reside in Cary, North Carolina.

Contents

List of Tables v

List of Figures vi

List of Symbols xii

1. Introduction 1

2. Background 4

2.1. GOTHIC 4
2.1.1. Control volumes 6
2.1.2. Boundary conditions 10
2.1.3. Flow paths 12
2.1.4. 3-D flow connectors 15
2.1.5. Initial conditions 16
2.2. Turbulence modeling 18
2.2.1. Derivation of Reynolds stress 18
2.2.2. Prandtl mixing length model 22
2.2.3. Standard k-ε model 24
2.2.4. RNG k-ε model 28

3. Axi-Symmetric Jet Model 30

3.1. Experimental setup from literature 30
3.2. GOTHIC model 31
3.3. Results 33
3.3.1. Mixing length models 34
3.3.2. Standard k-ε model 42
3.3.3. RNG k- ε model 47
3.3.4. Comparison between turbulence models 50

4. Channel Flow Model 59

4.1. Experimental setup from literature 59
4.2. GOTHIC model 60
4.3. Results 63
4.3.1. Mixing length models 64
4.3.2. Standard k-ε model 74
4.3.3. RNG k- ε model 79
4.3.4. Comparison between turbulence models 84

5. Mixing Layer Flow Model 97

5.1. Experimental setup from literature 97

5.2. GOTHIC model 98
5.3. Results 101
5.3.1. Mixing length models 102
5.3.2. Standard k-ε model 109
5.3.3. RNG k- ε model 112
5.3.4. Comparison between turbulence models 115

6. Conclusions 122

7. References 126

Appendix A. Axi-Symmetric Jet GOTHIC Input Deck 129

Appendix B. Channel Flow GOTHIC Input Deck 141

Appendix C. Mixing Layer Flow GOTHIC Input Deck 152

List of Tables

Table 2.1: Model constants for the standard k-ε model 27

Table 2.2: Model constants for RNG k-ε model 29

List of Figures

Figure 2.1: Flow path momentum direction options 15

Figure 2.2: Randomness of fluid properties in a turbulent flow [adapted from Cebeci & Smith (1974) [7]] 19

Figure 3.1: Diagram of apparatus for axi-symmetric jet experiment 31

Figure 3.2: Axi-symmetric jet GOTHIC noding diagram 32

Figure 3.3: 3-D mesh of jet facility 33

Figure 3.4: Axi-symmetric jet velocity profile at various downstream distances (0.001 mix) 36

Figure 3.5: Axi-symmetric jet lateral velocity profile at various downstream distances (0.001 mix) 37

Figure 3.6: Axi-symmetric jet centerline velocities (0.001 mix) 38

Figure 3.7: Axi-symmetric jet velocity profile at various downstream distances (0.01 mix) 39

Figure 3.8: Axi-symmetric jet lateral velocity profile at various downstream distances (0.01 mix) 39

Figure 3.9: Axi-symmetric jet centerline velocities (0.01 mix) 40

Figure 3.10: Axi-symmetric jet velocity profile at various downstream distances (0.1 mix) 41

Figure 3.11: Axi-symmetric jet lateral velocity profile at various downstream distances (0.1 mix) 41

Figure 3.12: Axi-symmetric jet centerline velocities (0.1 mix) 42

Figure 3.13: Axi-symmetric jet velocity profile at various downstream distances (k-ε) .. 43

Figure 3.14: Axi-symmetric jet lateral velocity profile at various downstream distances (k-ε) 45
Figure 3.15: Axi-symmetric jet centerline velocities (k-ε) 46
Figure 3.16: Axi-symmetric jet turbulent kinetic energy profile at various downstream distances (k-ε) 46
Figure 3.17: Axi-symmetric jet velocity profile at various downstream distances (RNG) 48
Figure 3.18: Axi-symmetric jet lateral velocity profile at various downstream distances (RNG) 48
Figure 3.19: Axi-symmetric jet centerline velocities (RNG) 49
Figure 3.20: Axi-symmetric jet turbulent kinetic energy profile at various downstream distances (RNG) 50
Figure 3.21: Axi-symmetric jet velocity profile comparison (y=2) 51
Figure 3.22: Axi-symmetric jet velocity profile comparison (y=3) 52
Figure 3.23: Axi-symmetric jet velocity profile comparison (y=4) 52
Figure 3.24: Axi-symmetric jet lateral velocity profile comparison (y=2) 54
Figure 3.25: Axi-symmetric jet lateral velocity profile comparison (y=3) 54
Figure 3.26: Axi-symmetric jet lateral velocity profile comparison (y=4) 55
Figure 3.27: Axi-symmetric jet turbulent kinetic energy profile comparison (y=2) 56
Figure 3.28: Axi-symmetric jet turbulent kinetic energy profile comparison (y=3) 56
Figure 3.29: Axi-symmetric jet turbulent kinetic energy profile comparison (y=4) 57
Figure 3.30: Axi-symmetric jet centerline velocity profile comparison 58
Figure 4.1: Channel GOTHIC noding diagram 61

Figure 4.2: 3-D mesh of channel..... 62

Figure 4.3: Velocity normalized by friction velocity over entire channel (mix 0.1)..... 65

Figure 4.4: Mean velocity profile of channel close to wall (mix 0.1) 65

Figure 4.5: Velocity profile normalized by channel mean velocity (mix 0.1)..... 67

Figure 4.6: Mean velocity defect across channel (mix 0.1)..... 67

Figure 4.7: Turbulent kinetic energy normalized by the friction velocity (mix 0.1)..... 68

Figure 4.8: Velocity normalized by friction velocity over entire channel (mix 0.01)..... 69

Figure 4.9: Mean velocity profile of channel close to wall (mix 0.01) 70

Figure 4.10: Velocity profile normalized by channel mean velocity (mix 0.01)..... 70

Figure 4.11: Mean velocity defect across channel (mix 0.01)..... 71

Figure 4.12: Turbulent kinetic energy normalized by the friction velocity (mix 0.01).... 71

Figure 4.13: Velocity normalized by friction velocity over entire channel (mix 0.001).. 72

Figure 4.14: Mean velocity profile of channel close to wall (mix 0.001) 72

Figure 4.15: Velocity profile normalized by channel mean velocity (mix 0.001)..... 73

Figure 4.16: Mean velocity defect across channel (mix 0.001)..... 73

Figure 4.17: Turbulent kinetic energy normalized by the friction velocity (mix 0.001).. 74

Figure 4.18: Velocity normalized by friction velocity over entire channel (k-ε) 76

Figure 4.19: Mean velocity profile of channel close to wall (k-ε)..... 76

Figure 4.20: Velocity profile normalized by channel mean velocity (k-ε)..... 77

Figure 4.21: Mean velocity defect across channel (k-ε)..... 78

Figure 4.22: Turbulent kinetic energy normalized by the friction velocity (k-ε) 79

Figure 4.23: Velocity normalized by friction velocity over entire channel (RNG)..... 80

Figure 4.24: Mean velocity profile of channel close to wall (RNG) 81

Figure 4.25: Velocity profile normalized by channel mean velocity (RNG) 82
Figure 4.26: Mean velocity defect across channel (RNG)..... 83
Figure 4.27: Turbulent kinetic energy normalized by the friction velocity (RNG)..... 84
Figure 4.28: Comparison of normalized velocity for different models (y=2) 86
Figure 4.29: Comparison of normalized velocity for different models (y=3) 86
Figure 4.30: Comparison of normalized velocity for different models (y=4) 87
Figure 4.31: Comparison of normalized velocity (near wall) for different models (y=2) 88
Figure 4.32: Comparison of normalized velocity (near wall) for different models (y=3) 88
Figure 4.33: Comparison of normalized velocity (near wall) for different models (y=4) 89
Figure 4.34: Comparison of velocity profiles normalized by channel mean velocity for different models (y=2) 90
Figure 4.35: Comparison of velocity profiles normalized by channel mean velocity for different models (y=3) 91
Figure 4.36: Comparison of velocity profiles normalized by channel mean velocity for different models (y=4) 91
Figure 4.37: Comparison of mean velocity defect across channel for different models (y=2)..... 93
Figure 4.38: Comparison of mean velocity defect across channel for different models (y=3)..... 93
Figure 4.39: Comparison of mean velocity defect across channel for different models (y=4)..... 94
Figure 4.40: Comparison of turbulent kinetic energy normalized by the friction velocity for different models (y=3)..... 95

Figure 4.41: Comparison of turbulent kinetic energy normalized by the friction velocity for different models (y=4) 96
Figure 5.1: Diagram of apparatus for mixing layer experiment 98
Figure 5.2: Mixing layer GOTHIC noding diagram 99
Figure 5.3: 3-D mesh of mixing layer facility 100
Figure 5.4: Mixing layer velocity profile (0.001 mix) 103
Figure 5.5: Mixing region growth rates (0.001 mix) 104
Figure 5.6: Kinetic energy profile of mixing region (0.001 mix) 105
Figure 5.7: Mixing layer velocity profile (0.01 mix) 106
Figure 5.8: Mixing region growth rates (0.01 mix) 106
Figure 5.9: Kinetic energy profile of mixing region (0.01 mix) 107
Figure 5.10: Mixing layer velocity profile (0.1 mix) 107
Figure 5.11: Mixing region growth rates (0.1 mix) 108
Figure 5.12: Kinetic energy profile of mixing region (0.1 mix) 108
Figure 5.13: Mixing layer velocity profile (k-ε) 109
Figure 5.14: Mixing region growth rates (k-ε) 111
Figure 5.15: Kinetic energy profile of mixing region (k-ε) 112
Figure 5.16: Mixing layer velocity profile (RNG) 113
Figure 5.17: Mixing region growth rates (RNG) 114
Figure 5.18: Kinetic energy profile of mixing region (RNG) 115
Figure 5.19: Comparison of mixing layer velocity profiles for different models (y=2). 116
Figure 5.20: Comparison of mixing layer velocity profiles for different models (y=3). 117
Figure 5.21: Comparison of mixing layer velocity profiles for different models (y=4). 117

Figure 5.22: Comparison of mixing region growth rates ($z_{0.1}$) 119

Figure 5.23: Mixing region growth rate for k-ε model offset by 0.115 ft. 119

Figure 5.24: Comparison of mixing region growth rates ($z_{0.5}$) 120

Figure 5.25: Comparison of mixing region growth rates ($z_{0.95}$) 120

Figure 5.26: Comparison of kinetic energy profiles of mixing region 121

List of Symbols

d	Jet nozzle diameter
e	Specific internal energy
$f(\xi)$	Scaled cross-stream velocity
h	Specific enthalpy
k	Turbulent kinetic energy
p	Instantaneous static pressure
P	Mean static pressure
q_j	Heat flux vector
r	Distance from centerline of jet
$r_{1/2}$	Jet half-width
t	Time
t_{ij}	Instantaneous viscous stress tensor
T	Time domain
u	Instantaneous velocity
u'	Velocity fluctuation
u^+	Scaled mean velocity
u_τ	Friction velocity
U	Mean velocity in longitudinal direction
U_0	Jet centerline longitudinal velocity
U_c	Mixing layer convection velocity
U_h	Mixing layer longitudinal velocity of injected fluid
U_J	Jet nozzle velocity
U_l	Mixing layer longitudinal velocity of stagnant fluid
U_m	Average entrance velocity
V	Jet lateral velocity
y	Distance downstream of the jet nozzle, channel entrance, and mixing layer entrance
z	Arbitrary fluid property, Mixing layer distance from interface between stagnant and injected fluid
z^+	Scaled distance from wall
z_α	Mixing layer cross-stream distance

δ	Channel half thickness, characteristic flow width
μ	Molecular viscosity
ρ	Density
τ_w	Wall shear stress
υ	Kinematic viscosity
ξ	Cross-stream non-dimensional coordinate
ζ	Scaled cross-stream coordinate

1. Introduction

Many Computational Fluid Dynamics (CFD) codes such as FLUENT, FLOWTRAN, and CFX are available for engineers to use to compute flow properties involving complex geometries. To analyze flow properties, such codes typically require the user to create, or import, a CAD model. Once a model is created and a grid mesh is applied to the model, boundary conditions can be specified and the flow simulation initiated. While these codes can provide accurate approximations of the flow, a substantial effort is required to determine flow properties for a single time point. The use of such codes for long transient problems, such as is often required in the nuclear industry, would require substantial computational resources and significant amounts of time. For time sensitive analyses, CFD codes are not practical for the nuclear industry. In addition, many transient analyses in the nuclear industry require the modeling of multiple compartments, rooms, and elevations. Very large CAD models would be required to compute such flow properties in CFD codes. Thus, there is little practical use for CFD codes for performing analyses in the nuclear industry.

GOTHIC is a computer program for performing thermal-hydraulic transient analyses on multi-phase flows in complex geometries [15]. It was originally developed for performing safety analyses on primary and secondary containments in commercial nuclear power plants. It performs its analysis by solving the continuity, momentum, and energy equations in each volume being analyzed. GOTHIC is better suited for creating and solving transient thermal-hydraulic problems that are typically found at nuclear plants than the CFD codes previously identified. It has many special components such as heat exchangers, pumps, etc. that are not available in CFD codes. Large-scale models can be quickly modeled using GOTHIC's graphics-driven preprocessor. Depending on the importance of the properties in a given

location, each control volume of the model can be modeled with as little or as much detail as required. The amount of detail modeled includes the grid resolution for each control volume. This allows the computational time for performing transient analyses, which would take considerable resources with a traditional CFD code, to be minimized.

Currently, GOTHIC has the ability to model both laminar and turbulent flows in the vapor phase. The turbulence modeling options available in its current version (7.1) are the Prandtl mixing length and the standard k-ε model proposed by Jones and Launder [12]. The development version of the code (7.2 dev) contains three additional turbulence models. These include a renormalized group theory (RNG) k-ε model, as well as quadratic and cubic k-ε models that have been tested and implemented by Analytis, Andreani, and others [2, 3, 4, 5]. In this work we will compare experimental and computational results with numerical results provided by GOTHIC. Specifically, we will analyze the accuracy of the mixing length, standard k-ε, and RNG k-ε turbulence models in relatively coarse grids. The grids used for modeling the flows will be maintained as coarse as possible to minimize the computational time for the analyses. This is a requirement of this work since one of the major advantages of GOTHIC is its ability to quickly compute the flow properties. We will be using GOTHIC to model simple experiments provided in literature to determine the ability of the code to predict the properties of these flows. In particular, we will be looking at a channel flow, an axi-symmetric jet, and a mixing layer flow. GOTHIC's ability to compute the flow properties for these simple geometries will act to validate the use of the turbulence models in coarse grids within GOTHIC. Although GOTHIC is primarily used for transient analysis, in this work we will ignore the transient solution and analyze only the steady-state

solution. If the code properly predicts the steady-state solution, further research can be done to determine the accuracy of its transient solution.

2. Background

In order to provide the reader with a better understanding of the important features of this study, the following sections provide additional background on the GOTHIC code as well as the turbulence models being studied. The development of the GOTHIC code and its important parameters as they pertain to this study are developed in Section 2.1. In addition, the Reynolds stress equation and the turbulence models are derived in Section 2.2. These sections assist the reader in understanding the GOTHIC parameters, limiting the need for significant development of inputs in the GOTHIC model sections, and familiarize the reader with the turbulence models being studied.

2.1. GOTHIC

GOTHIC (Generation of Thermal-Hydraulic Information for Containments) is a computer code for solving a variety of transient fluid flow and heat transfer problems. It is currently one of the leading software packages used within the commercial nuclear industry and is maintained by Numerical Applications, Inc. for the Electric Power Research Institute (EPRI). EPRI's members, and thus its funding, include over 90% of the U.S.'s electricity generating capacity [1]. The purpose of GOTHIC was to provide a thermal-hydraulic code to the utilities that could be used by its personnel without having to continually bring in outside contractors such as General Electric (GE), Westinghouse, and Babcox and Wilcox, whenever a safety issue was discovered or operability study was required. Using GOTHIC, utilities can create their own thermal hydraulic models that can be maintained in-house, providing substantial cost savings and faster response to time-critical issues. The companies identified above have each developed suites of

thermal-hydraulic packages for doing various types of transient analyses such as calculating vessel blowdown, containment temperature and pressure, suppression pool temperatures, environmental qualification (EQ) profiles, room heat-up analyses, etc. GOTHIC provides the ability to perform all of the analyses identified above, as well as a host of other analyses, in a single, easy-to-use package.

The GOTHIC software package consists of a pre/postprocessor, solver, and graphics generation module. The pre/postprocessor is a graphical, menu-driven program that is used to create the input deck for the solver. Model components and their connections are added to a schematic diagram that the preprocessor interprets for the input deck. This facilitates beginner development of a model, alleviates modeling errors, and significantly reduces troubleshooting of an incorrect model. The postprocessor portion of the program allows the user to quickly produce publish-quality graphs of over 150 predefined parameters such as temperature, pressure, velocity, etc. Imported data can also be added to the graphs and control variables can also be graphed. Complete manipulation of the dependent and independent graph parameters is also available including multiplication and adder factors as well as integration and division of curves. Vector and contour plots of certain parameters such as velocity and temperature are also available.

The software is primarily used to model large systems such as power plant containments, buildings, etc. However, it can also be used to model complex configurations using a variety of blockage geometries. Complex models that have been developed and successfully defended to the Nuclear Regulatory Commission (NRC) include water hammer analyses and the propagation of a bubble in a slightly inclined pipe [6, 19]. The software contains numerous components useful for HVAC modeling such as

thermal conductors, valves, doors, fans, coolers, heaters, heat exchangers, and flow paths. In addition, it also contains components particularly useful for the nuclear industry including hydrogen igniters, pumps, spray nozzles, vacuum breakers, and radioactive isotope tracking. Fluid and vapor initial conditions can be defined for each cell in the model through the preprocessor. Functions, component trips, and user-defined control variables provide the user with the ability to create extremely complex control systems. The software also has a grid generation scheme for three-dimensional models that allows the user to create logarithmic, linear, or user-defined rectangular grids in all three dimensions. The following sections provide detailed information on the GOTHIC components that are relevant to this research. Specifically, the input parameters required for each component are identified and their use in the solver is explained. Parameters not explicitly mentioned have no bearing on the analyses and are left at their default values.

2.1.1. Control volumes

A model in GOTHIC is created using lumped and/or subdivided volumes. As the title implies, a lumped volume calculates a single value for the each of the properties irrespective of the size of the volume. Thus, a velocity, temperature, or any other property in a lumped volume is the same at the top, bottom, front, or back. This is useful for modeling a volume whose property gradients are unimportant to the problem, i.e., an atmosphere where a pipe flow is exiting. A lumped volume can be divided into a subdivided volume using a built-in grid generation system. Using a subdivided volume allows velocity profiles and other gradients to develop in a control volume. In addition, inlets and outlet locations can be specified within a subdivided volume.

In order for GOTHIC to run properly, several parameters must be specified for each lumped volume. These include the following:

1. *Volume*

   The volume is the total free volume of the cell. The volume is used with the density to determine the mass contained within the volume. (**Note:** GOTHIC can be set to utilize either SI or English units. Since all of the analyses were performed using SI units, all of the parameters will be identified in such units.)

2. *Hydraulic diameter*

   The hydraulic diameter is calculated using a formula familiar from fluid mechanics.

$$D_h = \frac{4V}{A_w} \tag{2.1}$$

   where, $V =$ volume and $A_w =$ wettable surface area

   The hydraulic diameter is used for calculating heat transfer coefficients, which are not used in this analysis.

3. *Height*

   The height of the volume must be specified in order for the code to run. The volume is divided by the height to determine an effective Liquid to Vapor Interface area for pool regions. This is not applicable for these analyses.

Subdivided volumes require specification of significantly more parameters than lumped volumes. In addition to the three required for the lumped volume, subdivided volumes also require the following:

1. *Volume dimensions*

   The dimensions of the overall control volume must be specified in the x, y, and z directions. These values are used to calculate a new volume that over-rides the volume specified in the Volume parameter.

2. *Grid line locations*

   Grid lines in the x, y, and z directions can be located two ways. First, the user can select the desired location of the grid line on the control volume in the preprocessor window. The other option is to use the built-in grid generator to produce linear or logarithmic gridlines. These can be used with a range option to produce fine meshes in one part of the control volume and coarser meshes in another.

3. *Blockages*

   Since many applications involve geometries that are not rectangular, the blockage option was added to allow complex geometries to be produced. Similar to the solid modeling capabilities of 3-D modeling packages such as SolidWorks and Pro-Engineer, rectangular, circular, and wedge geometries can be added and subtracted to produced the desired model geometry.

4. *Slip conditions*

   A slip or no slip condition can be applied to the inside surfaces of the control volume. This can be used to produce models with symmetry constraints. For example, in a channel flow the velocity profile is symmetric about the centerline and the velocity perpendicular to the mean flow is negligibly small. Thus, this flow can be modeled using only half of the channel and a slip

condition can be applied to the centerline. This would reduce the grid size and the computational time required for the analysis.

5. *Turbulence parameters*

   Under these parameters the user can decide whether the code should consider molecular diffusion or not. In addition, a turbulence model can be provided.

   a. *Molecular diffusion*

      This option can be toggled ON or OFF depending on the user's preference.

   b. *Turbulence model*

      If no model is chosen, the flow is modeled using laminar theory [11]. The code has the ability to apply the following turbulence models [11]:

      i. Mixing length model
      ii. Standard k-ε model
      iii. RNG k-ε model
      iv. k-ε model with 2nd order source for the Reynolds stress term
      v. k-ε model with 3rd order source for the Reynolds stress term

GOTHIC also contains special parameters that can be set to provide additional capabilities such as hydrogen burn models, laminar and turbulent leakages, and additional sources for turbulent kinetic energy and dissipation. However, since these parameters are not relevant to this study, their details are not provided. If the reader so desires, this information can be obtained from the GOTHIC user manual [11].

2.1.2. Boundary conditions

As with most CFD packages, boundary conditions must be specified by the user. GOTHIC allows the user to specify a pressure, flow, or coupled boundary condition (BC). Pressure BCs act as a sink or source for fluid, depending on the conditions of the attached volume. Flow BCs can also act as a sink or source, but the flow rate is independent of any other BC or volume, unless specified by the user with a control variable (more information on this is provided below). Coupled BCs can be used to split flow between two volumes, but are not used in this study. The following discusses the parameters that must be specified for each type of BC for the code to run.

For both the pressure and flow boundary conditions, the following parameters must be specified:

1. *Temperature*

   The temperature of the fluids must be specified in the appropriate units (˚F or ˚C). If steam were located in the boundary condition, the temperature would be used in conjunction with the pressure to determine a liquid/steam split for the fluid.

2. *Pressure*

   The absolute pressure of the boundary condition must be given.

3. *Flow*

   For pressure BCs, the Flow option is toggled OFF and no value can be specified. For flow BCs, the flow rate is specified in units of mass/second (kg./s. or lbm./s.) by default, with a negative value indicating the flow is

entering the boundary condition and a positive value indicating flow leaving the BC. Volumetric flow rates ($m.^3/s.$ or $ft.^3/s.$) can also be specified by placing a 'V' in front of the value specified for the flow.

4. *Temperature/Pressure/Flow FF*

   Forcing functions can also be applied to the nominal value specified for the temperature, pressure, or flow. This function can be a user specified function utilizing data points, or it can be a user-defined control variable.

5. *Liquid volume fraction*

   Since GOTHIC is utilized for multiphase, multicomponent flows, the incoming fluid can be a mixture of fluids in vapor, mist, liquid, or droplet form and multiple gases such as air, hydrogen, etc. All of the experiments analyzed in the following sections utilize only air. Thus, this parameter is set to zero for this study.

6. *Steam volume fraction*

   For the same reasons mentioned above, this parameter is also set to zero. These two parameters are only mentioned because they must be set to a value in order for the code to execute. By placing an 'H' in front of the value specified, the relative humidity of the air in the BC can be specified. For the experiments modeled in Sections 3 through 5, the authors do not specify humidity conditions. Thus, they are assumed to be low and negligible for the experiments.

7. *Gas volume fraction*

   The volume fraction for gas 1, air, is set to 1.0 since all the analyses utilize air

as their medium. By default, GOTHIC chooses to only consider air. However, additional gases can be added to a boundary condition. If this is done, a volume fraction for each gas must be specified.

2.1.3. Flow paths

Flow paths are used to connect control volumes to each other and to boundary conditions. The following parameters must be set in order for the model to run:

1. *End elevations & heights*

   Elevation and heights for each side of the flow path must be specified. In addition, these parameters must fall within the location where it is attached to a control volume. For example, if a control volume is located at an elevation of 5 ft. with a height of 2 ft., the flow path entering the control volume can be placed at an elevation of 5 ft. and a height of 2 ft. Additionally, it could be placed at an elevation of 5.5 ft. and have a height up to 1.5 ft. However, it could not be placed at 5.5 ft. and have a height of 2 ft. because the flow path would fall outside of the surface of the control volume. This is also the case for subdivided volumes. The elevation and height must place the flow path within a single cell of the subdivided volume. As it relates to these analyses, these parameters are unimportant as long as they are specified such that the code can run.

2. *Flow areas*

   The cross-sectional area of the flow path must be designated in the appropriate units ($m.^2$ or $ft.^2$).

3. *Hydraulic diameter*

   A hydraulic diameter must be provided for the flow path. If none is given, GOTHIC provides a warning and assumes the hydraulic diameter to be the same as the flow path height. This parameter is used in conjunction with the friction length and friction factor to calculate an equivalent loss factor for the flow path (see item 5 below).

4. *Inertia length*

   The inertia length is used to calculate momentum transfer between the two control volumes or the boundary condition and control volume. According to the GOTHIC user manual [11], this value should be equivalent to the distance from the centers of the two volumes if the volumes are of the same order of magnitude or the width of the smaller cell if they are not. If the flow path attaches a control volume to a boundary condition, the length of the volume should be utilized. The inertia length and flow area are used to calculate an effective junction mass. This value is the mass that is accelerated in the momentum equation of the Navier-Stokes equations. Thus, it should be provided a reasonable value in order to calculate a correct solution.

5. *Friction length*

   The friction length is used to determine the friction force being applied to the fluid by the wall. The friction length is used with the hydraulic diameter to calculate an effective loss coefficient according to the following:

$$K = \frac{fL_f}{D_h} \tag{2.2}$$

where, f = friction factor, L_f = friction length, and D_h = hydraulic diameter.

6. *Forward/Reverse Loss Coefficient*

   Forward and reverse loss coefficients are provided to allow for calculating minor losses through the flow path. In addition, entrance and exit loss coefficients should be added to these values. The forward loss coefficient is applied to fluid flow from side A to side B of the junction while the reverse loss coefficient is applied if the flow is in the opposite direction.

The flow paths are connected to subdivided volumes by placing a marker in the grid where you desire the flow be applied. Depending on where in the grid the marker is placed, the momentum of the flow can be directed toward any of the six cell faces (up, down, left, right, front, back). These are identified by markers 1b, 6b, 3b, 2b, 4b, and 5b, in Figure 2.1, respectively. It is important that this marker inject the flow in the direction the user intends. Otherwise, it will provide erroneous results in both the transient and steady state analysis.

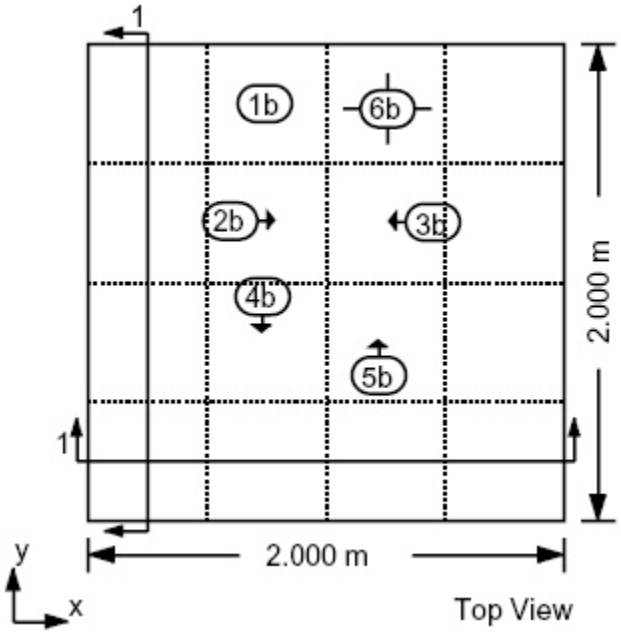

Figure 2.1: Flow path momentum direction options

2.1.4. 3-D flow connectors

Three dimensional flow connectors are used to provide multiple hydraulic connections between two subdivided volumes or subdivided and lumped volumes. The 3-D connectors can only be used between two control volumes. For these analyses, 3-D connectors are used to essentially connect the apparatus' being modeled to inlet and outlet (atmospheric) conditions. The only critical parameters for this component are outlined below.

1. *Loss Coefficient*

   This is the same loss coefficient that would be specified for a flow path to produce a pressure drop across the junction. For these analyses, the volumes are assumed to be directly connected to the apparatus' and no loss coefficient is required. However, in some of the models backflow into the 3-D volume can create unrealistic oscillations, preventing a

steady-state value from being reached. For these cases, the reverse loss coefficient is set to an arbitrarily large value to eliminate any backflow. This eliminates oscillations and allows steady-state solutions to develop in the 3-D volumes.

2. *LP Volume Momentum*

   This parameter controls the transport of momentum from one volume to the other. The available options for this parameter are CONSERVE and DISCARD. In order to ensure a proper inlet velocity to the apparatuses, the CONSERVE option is specified for all the connections. Setting this value to DISCARD would effectively add a loss coefficient of 1.0 (an exit loss) to the junction [11].

2.1.5. Initial conditions

Initial conditions must be provided to every volume/cell in the model prior to execution of the code. Default values can be assigned that are provided to any volume/cell that does not have its initial conditions explicitly specified. The following parameters for the initial conditions must be specified.

1. *Total Pressure*

   This provides the absolute pressure for the fluid in the volume/cell at the midpoint of the cell. If the cell is contains liquid, care should be taken to account for the head of the fluid if it accounts for more than 50% of the cell volume. For these analyses, these values are typically set to the same value as the atmospheric flow source.

2. *Vapor Temperature*

   This is the temperature of the steam and/or gas in the volume. This value is also set to the same value as that used for the atmosphere unless specified otherwise.

3. *Liquid Temperature*

   This is the temperature of the liquid in the volume. Since no liquid is used in the analyses, the value of this parameter is unimportant. However, it is set to the same value as the vapor temperature for consistency.

4. *Relative Humidity*

   This parameter sets the relative humidity of the vapor in the volume. No humidity is assumed in any of the analyses. Thus, this value is specified as zero.

5. *Liquid Volume Fraction*

   If liquid exists initially in the volume, the fraction of the volume that it occupies is specified here. Since air is the medium of choice in the experiments modeled, this value is set to zero also.

6. *Gas Volume Fractions*

   The volume fraction of each gas is specified through this parameter. GOTHIC assumes that all gases act as an ideal gas. Thus, the volume fraction specified is the same as the mole fraction. While steam may also be present in the cell, its effective volume fraction is subtracted first (also assuming that it acts as an ideal gas, i.e., if the cell pressure is 250 kPa and the steam pressure is 25 kPa, then the volume fraction of the cell that is

occupied by steam is 0.10 (25/250).) [11]. The value specified for the gas volume fraction is the percentage of the remaining volume that is not occupied by the steam. For these analyses, the only non-condensable present is air. Thus, its gas volume fraction is set to 1.0.

2.2. Turbulence modeling

In order to provide background for the reader to understand the use of a turbulence model, the following derivation is provided.

2.2.1. Derivation of Reynolds stress

Turbulent flows are, in general, very difficult to describe mathematically. In fact, no closed form solution for a turbulent flow exists because turbulent flows are inherently random and three-dimensional phenomena. However, observation of property measurements in turbulent flows shows that the properties fluctuate about a mean value. Figure 2.2 shows this comparison for a turbulent velocity profile. Thus, these properties can be represented as the sum of a mean value, represented with an over-bar, and a fluctuating value, designated with a prime symbol. In making this assumption, we must assume that the time over which the values are documented must be sufficiently long that they are no longer a function of time.

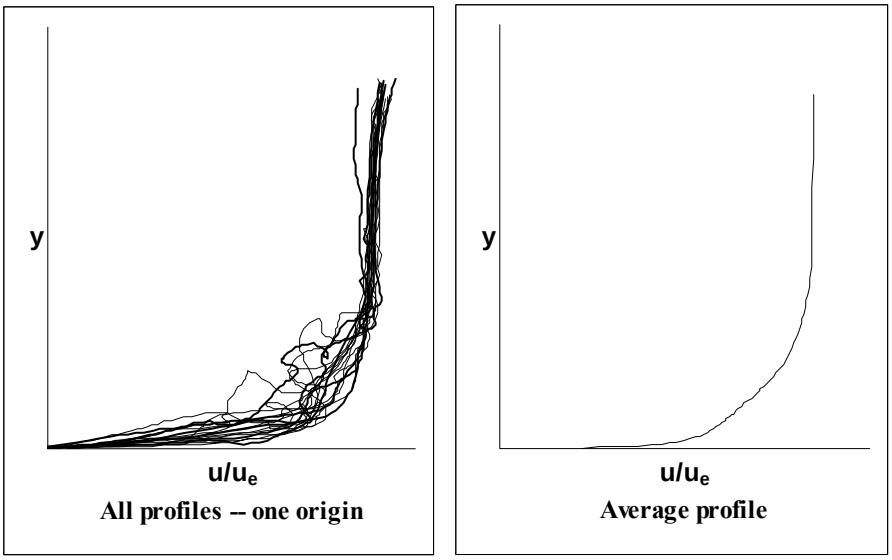

Figure 2.2: Randomness of fluid properties in a turbulent flow [adapted from Cebeci & Smith (1974) [7]]

Noting that the fluctuations in the velocity are small compared to the mean, we can describe them using a mean component and a fluctuating component as shown by Wilcox [20]. Thus, the velocity u_i can be described as

$$u_i = U_i + u_i' \tag{2.3}$$

where U_i refers to the mean velocity and u_i' refers to the velocity fluctuation.

Using a technique known as Reynolds time averaging allows us to define a mean fluid property, $\bar{z}$, as

$$\bar{z} = \frac{1}{T}\int_t^{t+T} z\,dt \tag{2.4}$$

In order to calculate the mean velocity, we can substitute each component of the velocity definition into the Reynolds time averaging equation.

$$\overline{U_i} = \frac{1}{T}\int_t^{t+T} U_i \, dt \qquad \overline{u_i'} = \frac{1}{T}\int_t^{t+T} u_i' \, dt \tag{2.5}$$

Since the mean velocity is constant with respect to time, this implies that

$$\overline{U_i} = U_i \qquad \overline{u_i'} = 0 \tag{2.6}$$

An analysis of fluids requires the consideration of the Navier-Stokes equations. The Navier-Stokes continuity, momentum, and energy equations in index notation are given by the following.

$$\frac{\partial \rho}{\partial t} + \frac{\partial}{\partial x_i}\left(\rho u_i\right) = 0 \tag{2.7}$$

$$\frac{\partial}{\partial t}\left(\rho u_i\right) + \frac{\partial}{\partial x_j}\left(\rho u_i u_j\right) = -\frac{\partial p}{\partial x_i} + \frac{\partial t_{ij}}{\partial x_j}, \qquad t_{ij} = \mu\left(\frac{\partial u_i}{\partial x_j} + \frac{\partial u_j}{\partial x_i}\right) \tag{2.8}$$

$$\frac{\partial}{\partial t}\left[\rho\left(e + \frac{1}{2}u_i u_i\right)\right] + \frac{\partial}{\partial x_j}\left[\rho u_j\left(h + \frac{1}{2}u_i u_i\right)\right] = \frac{\partial}{\partial x_j}\left(u_i t_{ij}\right) - \frac{\partial q_j}{\partial x_j}, \qquad h = e + p/\rho \tag{2.9}$$

The analysis outlined in this paper considers only low speed (incompressible) flows without any energy analysis. This results in a decoupling of the continuity, momentum, and energy equations and eliminates the need to consider the energy equation at all. Based on these assumptions, the simplified Navier-Stokes equations are:

$$\frac{\partial u_i}{\partial x_i} = 0 \tag{2.10}$$

$$\frac{\partial u_i}{\partial t} + \frac{\partial}{\partial x_j}\left(u_i u_j\right) = -\frac{1}{\rho}\frac{\partial p}{\partial x_i} + \nu\frac{\partial^2 u_i}{\partial x_j \partial x_j} \tag{2.11}$$

Now that we have developed a description for the velocity and a way to average a value, we can substitute the velocity, u_i, into the Navier-Stokes equations. Substitution and averaging of the continuity equation gives

$$\frac{\partial U_i}{\partial x_i} = 0 \Rightarrow \frac{\partial \overline{u_i'}}{\partial x_i} = 0 \tag{2.12}$$

Substituting into the momentum equation gives

$$\frac{\partial \left(U_i + u_i'\right)}{\partial t} + \frac{\partial}{\partial x_j}\left(\left(U_i + u_i'\right)\left(U_j + u_j'\right)\right) = -\frac{1}{\rho}\frac{\partial \left(P + p'\right)}{\partial x_i} + \nu \frac{\partial^2 \left(U_i + u_i'\right)}{\partial x_j \partial x_j} \tag{2.13}$$

As is apparent, all of the fluctuations will disappear except for the double fluctuation term associated with the inertial term. The double fluctuation term remains because the variables u_i' and u_j' are correlated.

$$\overline{\left(U_i + u_i'\right)\left(U_j + u_j'\right)} = \overline{U_i U_j} + \overline{U_i u_j'} + \overline{U_j u_i'} + \overline{u_i' u_j'} \tag{2.14}$$

$$\overline{\left(U_i + u_i'\right)\left(U_j + u_j'\right)} = U_i U_j + \overline{u_i' u_j'} \tag{2.15}$$

Thus, the mean momentum equation now simplifies to

$$\frac{\partial U_i}{\partial t} + \frac{\partial \left(U_i U_j\right)}{\partial x_j} = -\frac{1}{\rho}\frac{\partial P}{\partial x_i} + \frac{1}{\rho}\frac{\partial}{\partial x_j}\underbrace{\left(\mu \frac{\partial U_i}{\partial x_j}\right)}_{(1)} \underbrace{- \rho \overline{u_i' u_j'}}_{(2)} \tag{2.16}$$

Term (1) in the above equation is known as the laminar stress, while (2) is the turbulent, or Reynolds, stress. This quantity describes the effect of the velocity fluctuations on the mean flow. Most modern turbulence models attempt to close this

equation by modeling the Reynolds stress term. In order to simplify, we will rewrite (2) in terms of stress.

$$\tau_{ij} = \overline{u_i' u_j'} = \mu_T \frac{\partial U_i}{\partial x_j} \tag{2.17}$$

2.2.2. Prandtl mixing length model

From derivations in classical physics, the shear stress in a perfect gas is given by

$$t_{xy} = \mu \frac{dU}{dy} \tag{2.18}$$

This same derivation gives molecular viscosity as a function of the thermal velocity, v_{th}, and the mean free path of the molecule, l_{mfp}.

$$\mu = \frac{1}{2} \rho v_{th} l_{mfp} \tag{2.19}$$

In the early twentieth century, Prandtl proposed a turbulence model that was analogous to this definition. Instead of using the mean free path and the thermal velocity, Prandtl proposed using a mixing length, l_{mix}, and a mixing velocity, v_{mix} [20].

$$\mu_T = \rho v_{mix} l_{mix} \tag{2.20}$$

In addition, Prandtl assumed that the mixing velocity could be described as

$$v_{mix} = l_{mix} \left| \frac{dU}{dy} \right| \tag{2.21}$$

Thus, the turbulent viscosity, μ_T, could be described as

$$\mu_T = \rho l_{mix}^2 \left| \frac{dU}{dy} \right| \tag{2.22}$$

For wall bounded shear flows, the mixing length is proportional to the distance from the wall according to

$$l_{mix} = \kappa y \tag{2.23}$$

where κ is an empirical constant and y is the distance to the wall. Since all of the unknowns in the equations above have now been defined, the equations are closed and a Reynolds stress can be calculated for the flow.

In GOTHIC, the mixing length is user specified rather than calculated using equation (2.23) above. Prandtl's mixing length model was developed for flow over a flat plate [20]. It does not appear practical to calculate the mixing length using equation (2.23) because volumes in GOTHIC are wall bounded on all sides. Thus, it would be difficult to determine what distance, y, should be used to calculate the mixing length. To get around this, the code's authors decided to allow the user to provide the mixing length, which is highly dependent on the application. Thus, experimental data needs to be provided in order to calibrate the mixing length for the flow. The downfall of this methodology is that the code cannot be used to calculate flow properties a priori. Rather, a model needs to be calibrated to known conditions and then changes can be made to see their effect on the system. As will be shown in the results for the experiments modeled, this may allow the code to model an overall flow property, such as the total velocity through a channel, but does not provide good

results for predicting the cross-stream properties. Thus, this model is not ideal for calculation of flow properties.

2.2.3. Standard k-ε model

Unlike the mixing length model presented above, the k-ε models specify both the length and velocity scale of turbulence with transport equations. Most two-equation turbulence models use the turbulence kinetic energy equation for providing the velocity scale. (**Note: Turbulence kinetic energy, turbulent kinetic energy, and kinetic energy are used interchangeably in the remainder of this paper.**) This equation is derived from the Reynolds-stress equation, which is given below.

$$\frac{\partial \tau_{ij}}{\partial t} + U_k \frac{\partial \tau_{ij}}{\partial x_k} = -\tau_{ik} \frac{\partial U_j}{\partial x_k} - \tau_{jk} \frac{\partial U_i}{\partial x_k} + \varepsilon_{ij} - \Pi_{ij} + \frac{\partial}{\partial x_k}\left[\nu \frac{\partial \tau_{ij}}{\partial x_k} + C_{ijk} \right] \tag{2.24}$$

where

$$\Pi_{ij} = \overline{\frac{p'}{\rho}\left(\frac{\partial u_i'}{\partial x_j} + \frac{\partial u_j'}{\partial x_i} \right)} \qquad \varepsilon_{ij} = 2\nu \overline{\frac{\partial u_i'}{\partial x_k} \frac{\partial u_j'}{\partial x_k}}$$

$$\rho C_{ijk} = \rho \overline{u_i' u_j' u_k'} + \overline{p' u_i'} \delta_{jk} + \overline{p' u_j'} \delta_{ik} \tag{2.25}$$

Prandtl postulated an additional velocity scale using this equation [20]. In classical physics, we define the kinetic energy, K, of a moving object by

$$K = \frac{1}{2} m v^2 \tag{2.26}$$

Prandtl defined the turbulence kinetic energy of a flow by

$$k = \frac{1}{2}\overline{u_i' u_i'} \tag{2.27}$$

Since the Reynolds stress is defined as

$$\tau_{ij} = -\overline{u_i' u_j'} \tag{2.28}$$

We can take the trace of this equation by setting $j = i$. By doing so, we determine a relationship between equations (2.27) and (2.28) above.

$$\tau_{ii} = -2k \tag{2.29}$$

Thus, we can take the trace of the Reynolds stress equation to provide a transport equation for the turbulent kinetic energy. Doing so provides the following equation.

$$\begin{aligned}\frac{\partial \tau_{ii}}{\partial t} + U_k \frac{\partial \tau_{ii}}{\partial x_k} = &-\tau_{ik}\frac{\partial U_i}{\partial x_k} - \tau_{ik}\frac{\partial U_i}{\partial x_k} + 2\nu\overline{\frac{\partial u_i' \partial u_i'}{\partial x_k \partial x_k}} - \Pi_{ii} \\ &+ \frac{\partial}{\partial x_k}\left[\nu\frac{\partial \tau_{ii}}{\partial x_k} - \overline{u_k' u_i' u_i'} + \frac{2\overline{p' u_i'}}{\rho}\delta_{ik}\right]\end{aligned} \tag{2.30}$$

Simplifying equation (2.30) above gives the final form of the turbulence kinetic energy equation.

$$\frac{\partial k}{\partial t} + U_k \frac{\partial k}{\partial x_k} = \tau_{ik}\frac{\partial U_i}{\partial x_k} - \varepsilon + \frac{\partial}{\partial x_k}\left[\nu\frac{\partial k}{\partial x_k} - \frac{1}{2}\overline{u_k' u_i' u_i'} + \frac{\overline{p' u_i'}}{\rho}\delta_{ik}\right] \tag{2.31}$$

In order to solve this equation, the double and triple correlation terms must be modeled. For this model, the diffusive transport terms are modeled as

$$\frac{1}{2}\overline{u_k' u_i' u_i'} + \frac{\overline{p' u_i'}}{\rho}\delta_{ik} = \frac{\nu_T}{\sigma_k}\frac{\partial k}{\partial x_k} \tag{2.32}$$

Since $k = \frac{1}{2}\left(u_1' u_1' + u_2' u_2' + u_3' u_3'\right)$, the velocity scale for turbulence is defined as $\sqrt{k}$.

Now that the velocity scale has been defined, we only need to define the length scale in order to calculate the turbulent viscosity and close the system of equations. A procedure similar to the derivation of the turbulent kinetic energy, k, exists for deriving dissipation, ε. However, this procedure yields a much more complex equation which has many additional double and triple correlations that must be modeled in order to solve the equation. Instead of proceeding in this direction, we will assume that the dissipation equation takes the same form as the turbulent kinetic energy equation, having a production, dissipation, and diffusion term. Taking this course yields an equation for dissipation as follows.

$$\frac{\partial \varepsilon}{\partial t} + U_k \frac{\partial \varepsilon}{\partial x_k} = C_{\varepsilon 1} \frac{\varepsilon}{k} \tau_{ik} \frac{\partial U_i}{\partial x_k} - C_{\varepsilon 2} \frac{\varepsilon^2}{k} + \frac{\partial}{\partial x_k}\left[\left(\nu + \frac{\nu_T}{\sigma_\varepsilon}\right)\frac{\partial \varepsilon}{\partial x_k}\right] \tag{2.33}$$

where $c_{\varepsilon 1}$, $c_{\varepsilon 2}$, and σ_ε are closure coefficients which must be determined from homogenous turbulence, the log law of the wall, and/or other experimental data. In addition, we must define the turbulent viscosity, ν_T, to close the system of equations. For the k-ε model, the turbulent viscosity is modeled as

$$\nu_T = C_\mu \frac{k^2}{\varepsilon} \tag{2.34}$$

Using the equations above and closure constants provided by Rodi [18] (Table 2.1), the effect of turbulence on the mean flow is calculated in GOTHIC:

Table 2.1: Model constants for the standard k-ε model

Constant	Value
C_{μ}	0.09
$C_{\varepsilon 1}$	1.44
$C_{\varepsilon 2}$	1.92
σ_{ε}	1.0
σ_{k}	1.3

Note to the reader: In general, GOTHIC can be used for compressible flows. In this case, there is an additional production term that is a result of the fluid's buoyancy. In this study, the fluid is assumed to be incompressible. Thus, this buoyancy term is neglected and the closure coefficient related to it is not provided.

Using the logarithmic law of the wall, GOTHIC uses a relationship developed by Rodi [18] for determining the turbulent flow properties at cells adjacent to a wall [10]. Rodi's method calculates the friction velocity from the following:

$$U_f = \frac{\tau_w}{\mu} \tag{2.35}$$

With this, the kinetic energy is given by

$$k = \frac{U_f}{\sqrt{C_{\mu}}} \tag{2.36}$$

and the dissipation is

$$\varepsilon = \frac{U_f^3}{Ky} \tag{2.37}$$

where K is von Karman's constant (0.4) and y is defined as

$$y = \frac{D_h}{8} \tag{2.38}$$

with D_h being the cell hydraulic diameter.

This correlation allows GOTHIC to predict turbulence properties without having to create fine meshes near wall boundaries. Using the turbulent kinetic energy, dissipation, turbulent viscosity, and momentum equations, mean flow properties can be determined.

2.2.4. RNG k-ε model

The renormalized group theory k-ε model (RNG) developed by Yakhot and Orszag (1986) [23] uses the same equations as the standard k-ε model for the turbulence kinetic energy, dissipation, and turbulent viscosity. However, it also introduces an equation for calculating one of the constants. Instead of $C_{\varepsilon 2}$ being equal to 1.92, it is now defined by

$$C_{\varepsilon 2} = \widetilde{C}_{\varepsilon 2} + \frac{C_\mu \lambda^3 \left(1 - \lambda / \lambda_0\right)}{1 + \beta \lambda^3} \tag{2.39}$$

where

$$\lambda \equiv \frac{k}{\varepsilon} \sqrt{2 S_{ij} S_{ji}} \tag{2.40}$$

and $S_{ij} = S_{ji}$ is the mean strain rate tensor defined by the following

$$S_{ij} = \frac{\partial u_i}{\partial x_j} + \frac{\partial u_j}{\partial x_i} \tag{2.41}$$

Changing the value of $C_{\varepsilon 2}$ from a constant to an equation causes the remaining closure constants to change.

Table 2.2, below shows the values of the closure constants proposed by Yakhot and Orszag, which are utilized in GOTHIC [10].

Table 2.2: Model constants for RNG k-ε model

Constant	Value
C_μ	0.085
$C_{\varepsilon 1}$	1.42
$\widetilde{C}_{\varepsilon 2}$	1.68
σ_ε	0.719
σ_k	0.719
β	0.012
λ_0	4.38

3. Axi-Symmetric Jet Model

The experiment modeled for the axi-symmetric jet flow was performed at Boeing Research Labs by Wygnanski and Fiedler in 1968 [21]. The following sections explain the physical setup of the experiment, explain how it is modeled in GOTHIC, and provides a comparison of GOTHIC's results with the experimental data.

3.1. Experimental setup from literature

In order to take measurements of a self-preserving, axi-symmetric jet, Wygnanski and Fiedler [21] placed their experimental apparatus in a space-conditioned room. Particulates in the air larger than 0.04 microns were removed using an electrostatic precipitator and the room temperature was maintained within ±1°F during the entire experiment. The apparatus consisted of two concentric cages made of 1/16-in. mesh screens placed 2½ in. apart. This setup helped to eliminate any drafts in the room due to the HVAC system and allowed for accurate measurement of the flows a significant distance downstream of the nozzle. The dimensions of the internal cage were 7½ ft. high by 8 ft. wide by 17 ft. long with the far end of the cage open. A 1.04-in. diameter nozzle was placed in the middle of the 7½ ft. high wall, directing the flow towards the open end of the cage, parallel to the floor (see Figure 3.1). Most of the flow measurements were taken using a nozzle velocity of 51 m./s. giving a Reynolds number on the order of 1E+5 (based on the nozzle diameter). Some measurements were also taken with a nozzle velocity of 72 m./s., but this case was not replicated with the GOTHIC model. The flow measurements were taken using linearized, constant-temperature hotwire anemometers and the signals were processed using a variety of circuits to integrate and differentiate the

readings of the hotwires. Using the apparatus described above, experimental data was taken over a long period of time to obtain good statistical averages of the flow parameters, as required and discussed in Section 2.2.1.

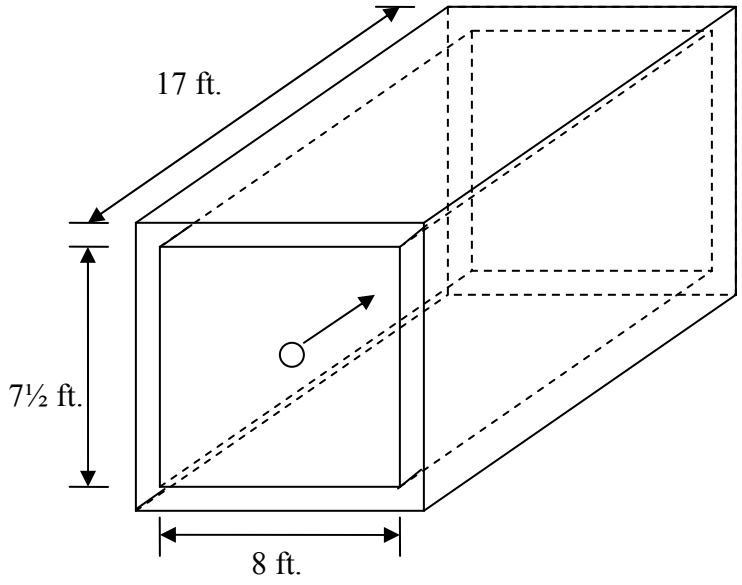

Figure 3.1: Diagram of apparatus for axi-symmetric jet experiment

3.2. GOTHIC model

The GOTHIC model representing the axi-symmetric jet apparatus is modeled with control volumes, 3-D connectors, flow paths, and boundary conditions. Volume 2s (see Figure 3.2) represents the caged apparatus diagrammed in Figure 3.1. Volume 1 is the sink (atmosphere) for the open end of the cage at the end of the room opposite the jet nozzle. A 3-D connector is used to hydraulically connect the cage to the atmosphere. A flow boundary condition with a volumetric flow sufficient to produce a nozzle velocity of 51 m./s. is forced through flow path 1. Flow path 1 connects the flow boundary condition and the cell where the jet nozzle is located. Flow path 2 provides an exit from the

atmosphere control volume to the pressure boundary condition. This boundary conditions acts as a mass sink for the flow leaving the apparatus.

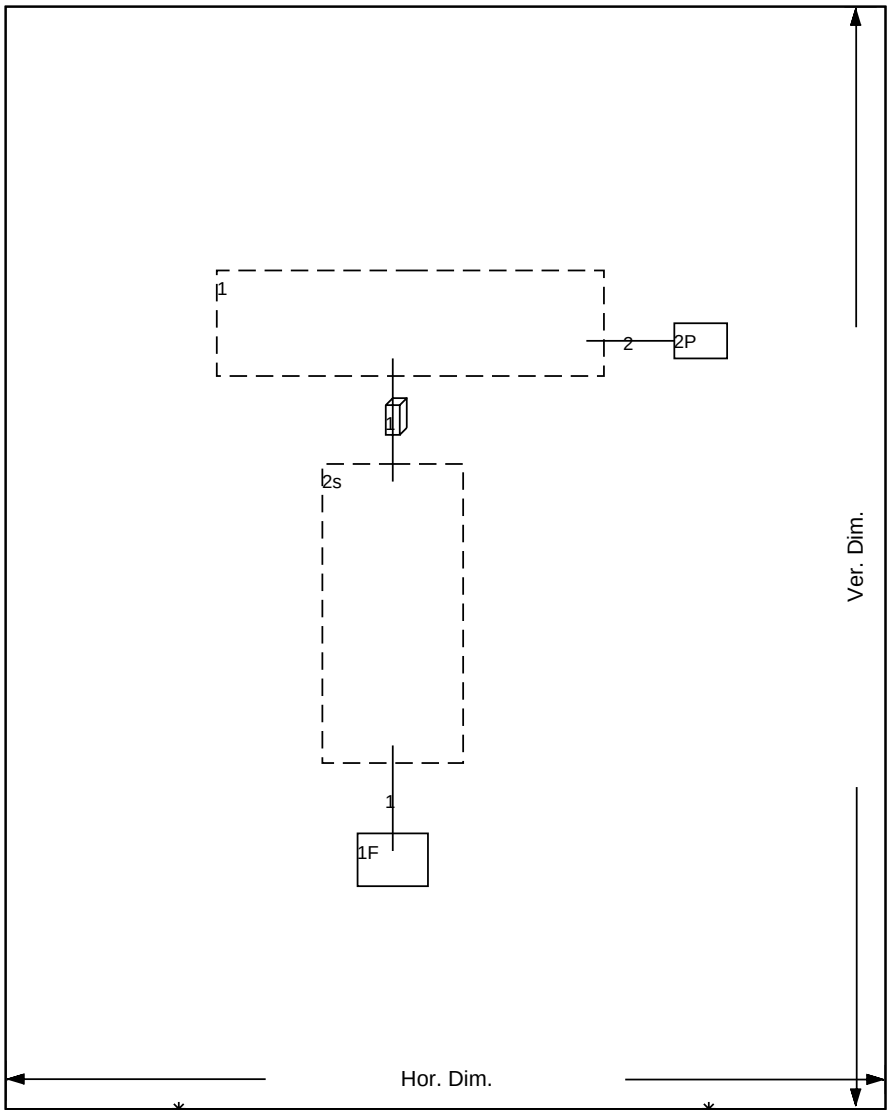

Figure 3.2: Axi-symmetric jet GOTHIC noding diagram

The three-dimensional mesh of the jet facility is given in Figure 3.3. In the x-direction, perpendicular to the mean flow and parallel to the ground, the volume is subdivided into 56 cells. The grid is coarser on the outside (near the min and max x values) than in the middle, where the jet is injected. In the y direction, the mean flow

direction, the volume is subdivided into five cells of equal length. In the z direction, perpendicular to the mean flow and the ground, the volume is divided into 21 equal cells. The jet flow is injected into the flow path at a reference coordinate (x, y, z) of (23, 1, 11). The 3-D connector is attached to the end of the volume from coordinates (1, 5, 1) to (56, 5, 21). Using this setup, the axi-symmetric jet experiment was replicated.

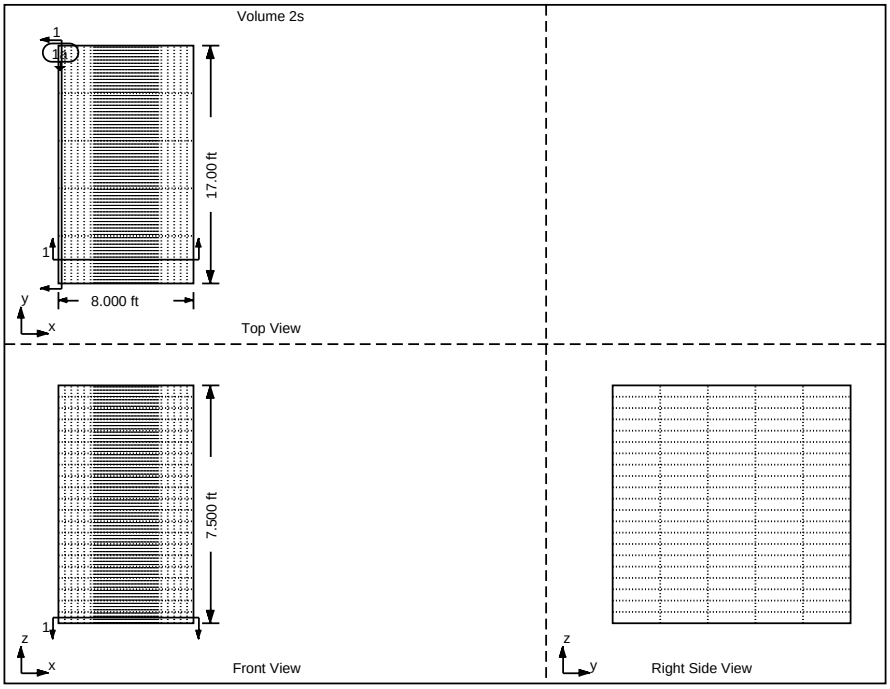

Figure 3.3: 3-D mesh of jet facility

3.3. Results

The following sections provide the results for each of the turbulence models analyzed. The ability of each model to predict experimental data is evaluated in the first three sections. The final section compares the computational results for each of the models against both the experimental data and the other models. The following

definitions are used for producing non-dimensional values which allow comparison of the GOTHIC and experimental data.

U	Jet longitudinal velocity
U_J	Jet nozzle velocity, 51 m./s.
U_0	Jet centerline longitudinal velocity
V	Jet lateral velocity
d	Jet nozzle diameter, 1.04 in.
y	Distance downstream of the jet nozzle
r	Distance from centerline of jet
$r_{1/2} \equiv r\big\|_{U=\frac{1}{2}U_0}$	Jet half-width
k	Turbulent kinetic energy

3.3.1. Mixing length models

As stated in Section 2, the mixing length model in GOTHIC is specified prior to the execution of the code. The length specified must be a constant value and is not calculated by the code. Results for each of the three mixing lengths specified are given below.

The time required to run the models to a transient time of 50 seconds (at which point steady-state profiles are reached) for the 0.001 ft., 0.01 ft., and 0.1 ft. mixing lengths are 1.21, 1.24, and 1.22 hours, respectively. These computer runs were completed on a Pentium 4 computer running WindowsXP with a 1.7 GHz processor and 768 MB of RAM. Figure 3.4 gives the velocity profile in the direction of the jet flow at several locations downstream of the jet nozzle for the mixing length of 0.001

ft. (0.012 in.). The velocity profile at y =2, 3, and 4 are equivalent to distances of 6.8, 10.2, and 13.6 ft. downstream, respectively. Of the profiles given, the velocity 6.8 ft. from the jet matches the experimental data most closely. However, further review of the data shows that there are actually an insufficient number of data points available within the range of the experimental data provided to evaluate the accuracy of the GOTHIC results. This is due to the skewed velocity profile that occurs since the mixing length model does not do a good job of estimating the dissipation of the jet. The centerline velocity, U_0, for the 0.001 ft. mixing length model is significantly higher than calculated for the two-equation models, and the velocity decelerates quite quickly when moving outside of the centerline of the jet. This results in a jet half-width, $r_{1/2}$, that is too small. Since the profile is given in terms of the jet half-width, the number of data points available in the data set is reduced since the differencing scheme of GOTHIC is fixed for the analysis. Thus, Figure 3.4 provides little useful information other than to show that the dissipation for the 0.001 ft. mixing length model is under predicted. Based on this conclusion it is not surprising to see the lateral velocity profile given in Figure 3.5. Here again, there are very few data points available within the experimental data range to compare with. However, the lateral profile is extremely flat, which is inconsistent with experiment. Thus, this figure also provides little useful information regarding GOTHIC's ability to model the axi-symmetric jet with the mixing length model.

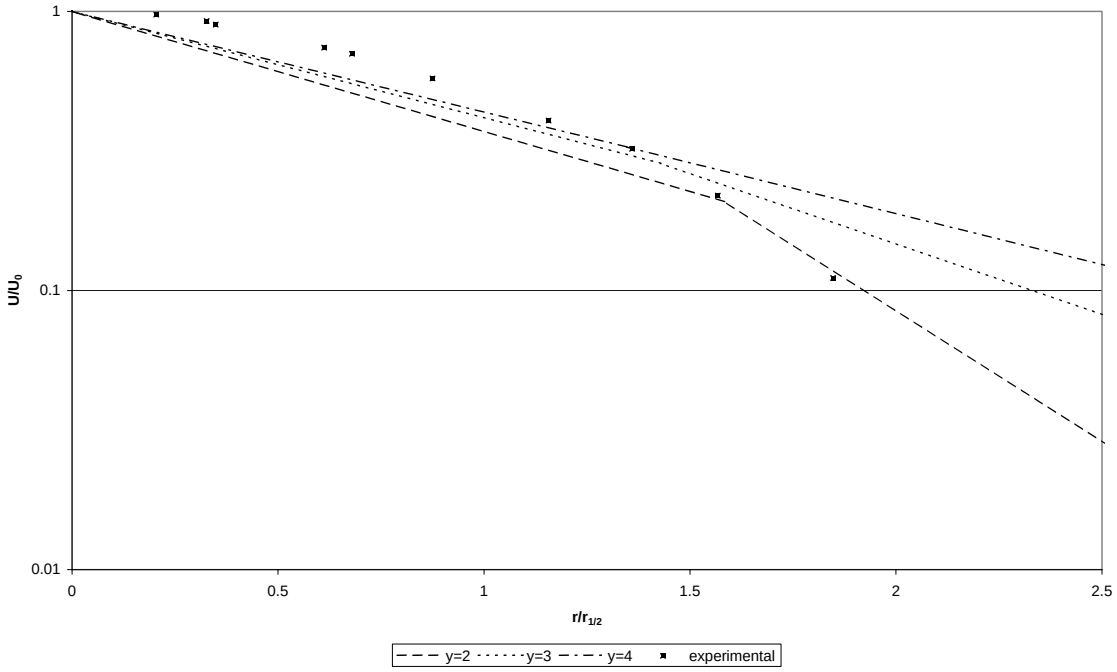

Figure 3.4: Axi-symmetric jet velocity profile at various downstream distances (0.001 mix)

The ability of the model to correctly predict flow properties of the jet is further put in question by the results of Figure 3.6. The data-fitted equation line corresponds to the line provided by the constant of $x_0/d = 4$ and velocity-decay constant B = 5.8 in the following equation from Reference [17]:

$$\frac{U_0(x)}{U_J} = \frac{B}{(x - x_0)/d} \tag{3.1}$$

As Figure 3.6 shows, the velocity-decay constant of the regression line for the GOTHIC data is negative. This would indicate that the centerline velocity of the jet is increasing as the plume moves downstream. Such data is inconsistent with physics and does not properly represent the behavior of the jet.

For the reasons documented above, the turbulence model with a mixing length of 0.001 ft. does not do a good job of predicting the flow properties of the axi-symmetric

jet. This should not come as a surprise as the mixing length model was developed for flow over a flat plate [20]. Typically, the mixing length utilized is related to the distance from a bounding surface, which, by definition, does not exist for a free shear flow such as a jet. The lack of such a surface greatly impedes the ability of the model to properly predict the properties of the jet. Thus, the mixing length model using a length of 0.001 ft. does not accurately predict the flow properties of the jet.

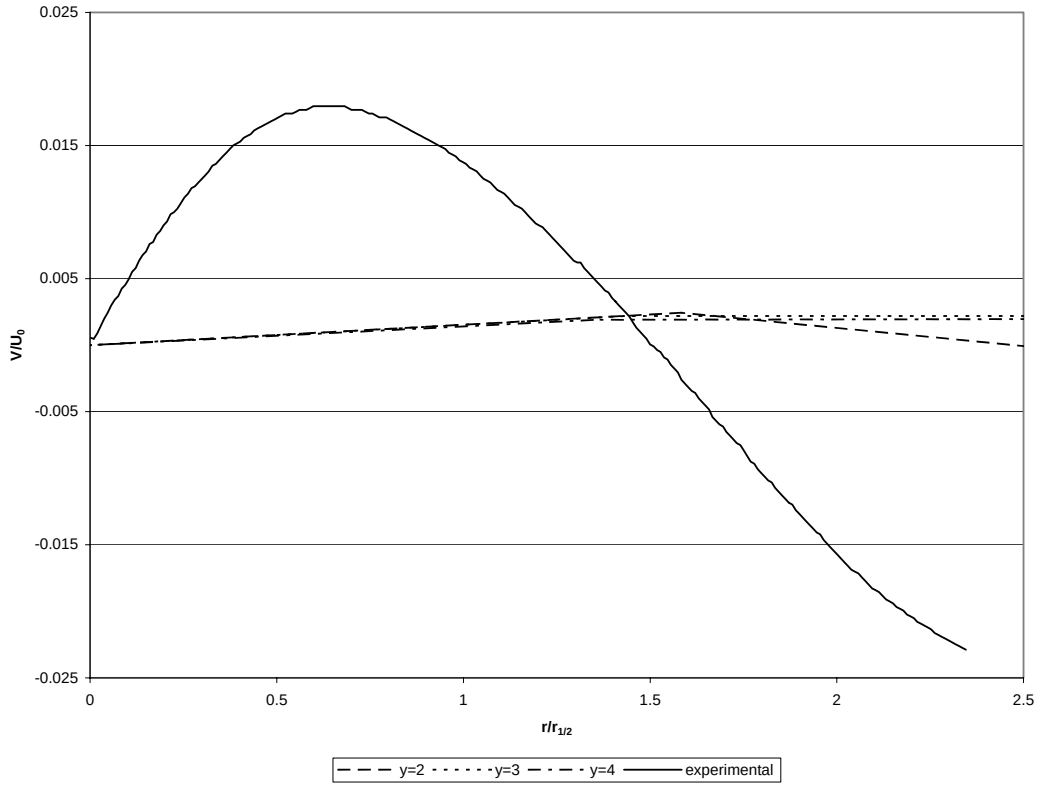

Figure 3.5: Axi-symmetric jet lateral velocity profile at various downstream distances (0.001 mix)

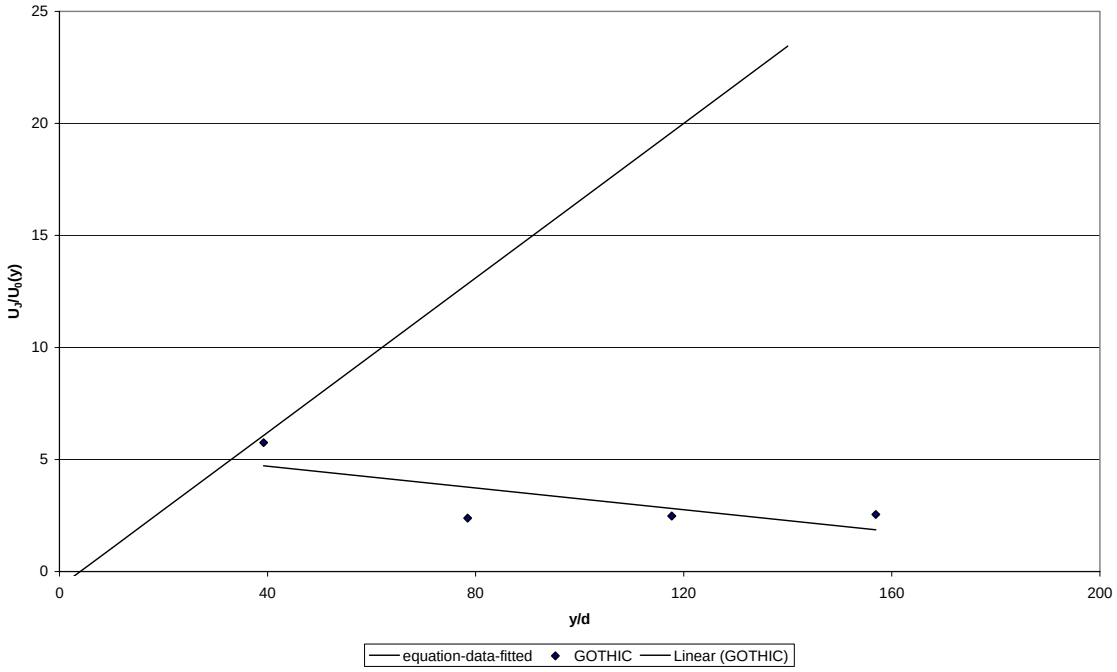

Figure 3.6: Axi-symmetric jet centerline velocities (0.001 mix)

The results for the mixing length model with a mixing length of 0.01 ft. are similar to that of the 0.001 ft. length. Here again there are not a sufficient number of data points within the GOTHIC noding scheme to accurately model the jet. This is again shown in Figure 3.7 where only a few data points in the experimental data range are available. Figure 3.8 and Figure 3.9 also show similar results to their respective graphs for the 0.001 ft. mixing length model. The lateral velocity given in Figure 3.8 is also inaccurate due to a lack of data points within the experimental data set. Figure 3.9 also gives a jet centerline velocity similar to that of Figure 3.6, which is also invalid. Thus, the results of the 0.01 ft. mixing length model are invalid and do not provide useful data to compare with experimental data.

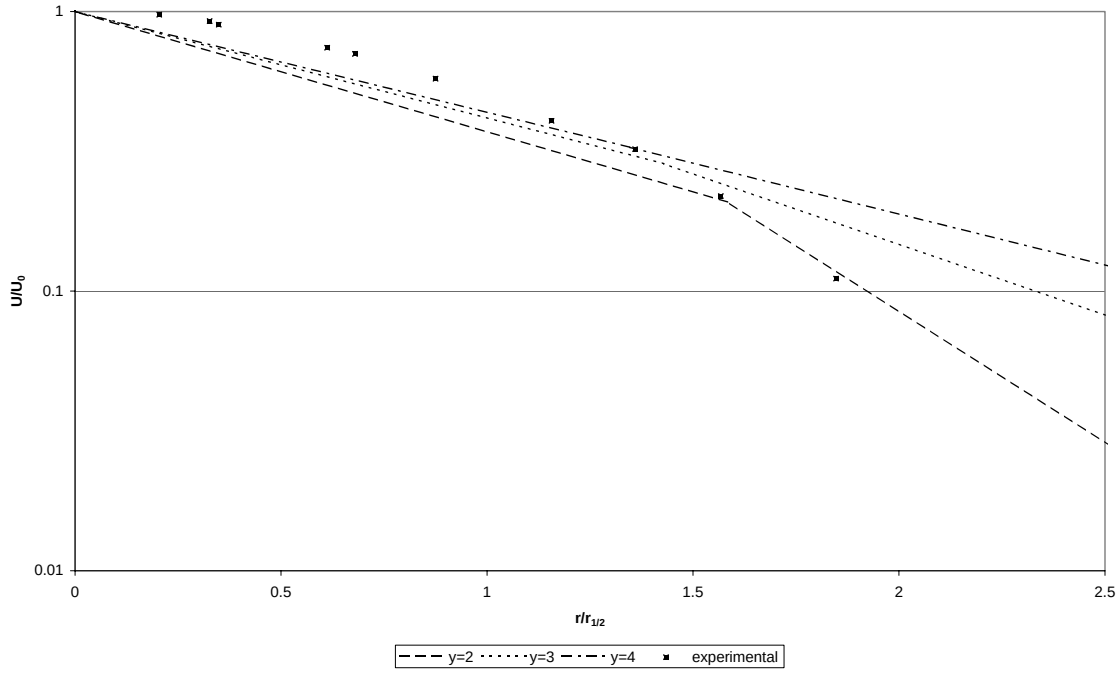

Figure 3.7: Axi-symmetric jet velocity profile at various downstream distances (0.01 mix)

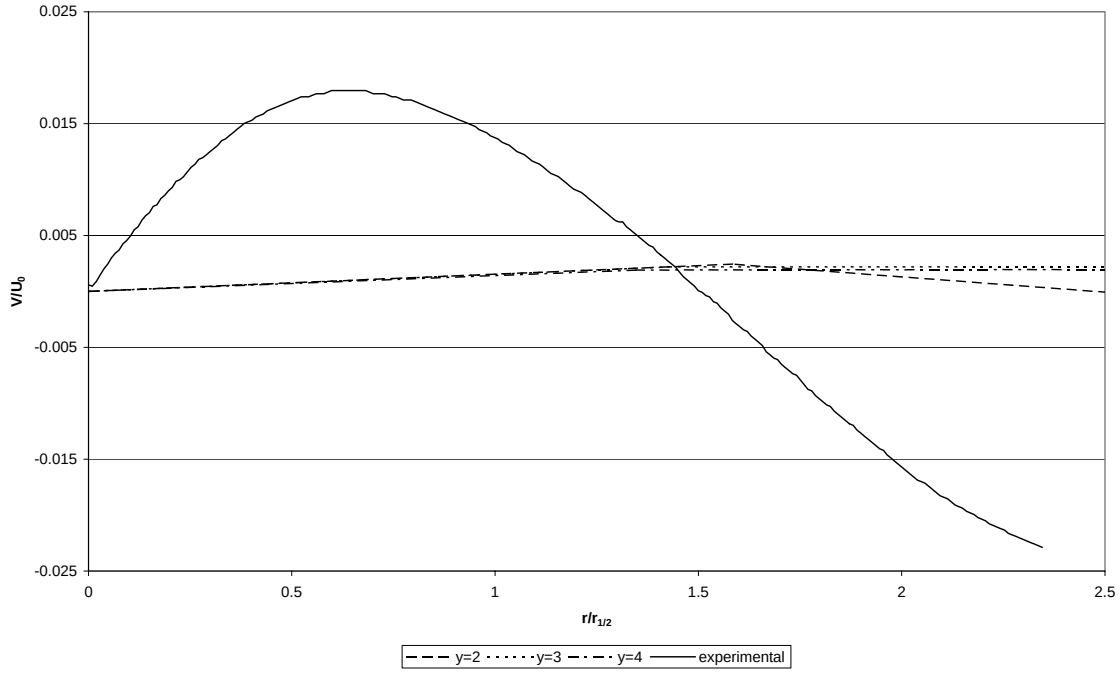

Figure 3.8: Axi-symmetric jet lateral velocity profile at various downstream distances (0.01 mix)

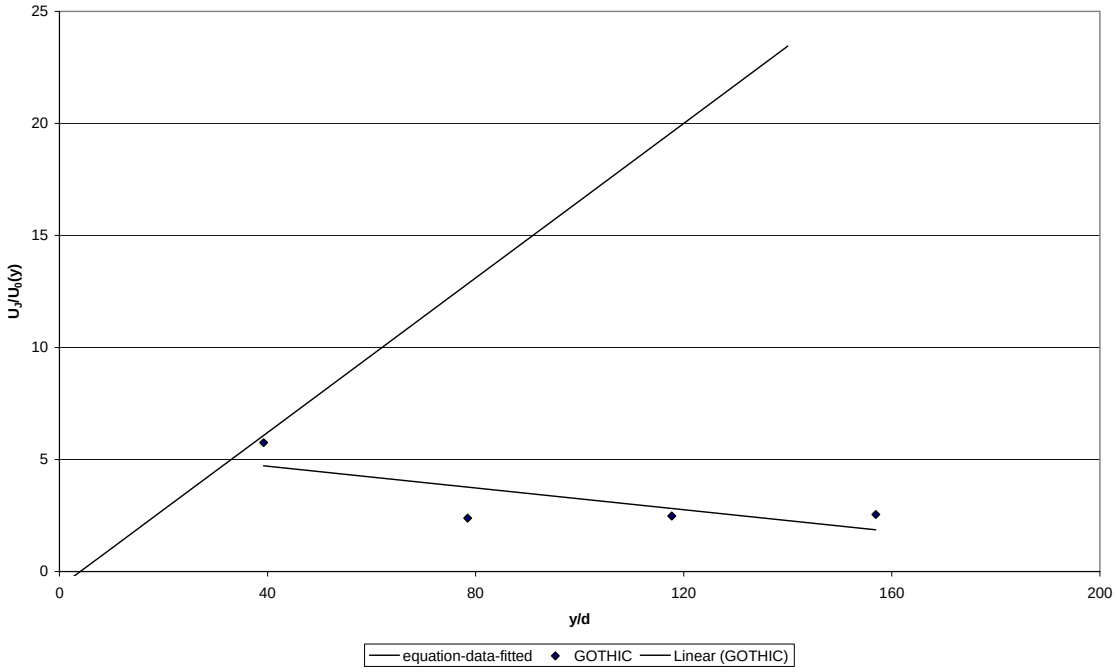

Figure 3.9: Axi-symmetric jet centerline velocities (0.01 mix)

Figure 3.10, Figure 3.11, and Figure 3.12 show the results for the mixing model with a length of 0.1 ft. A comparison of these results to those presented earlier for the 0.01 ft. and 0.001 ft. models show no significant difference between the results. Thus, the results for the 0.1 ft. mixing length model are also invalid based on the accuracy of the other mixing lengths documented previously.

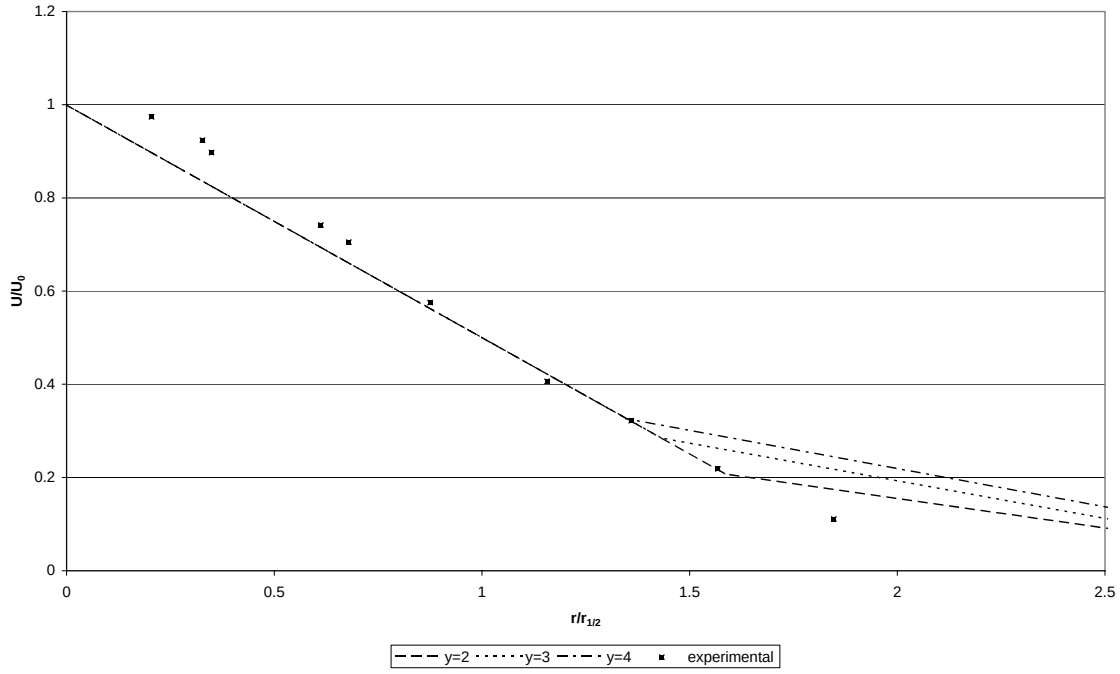

Figure 3.10: Axi-symmetric jet velocity profile at various downstream distances (0.1 mix)

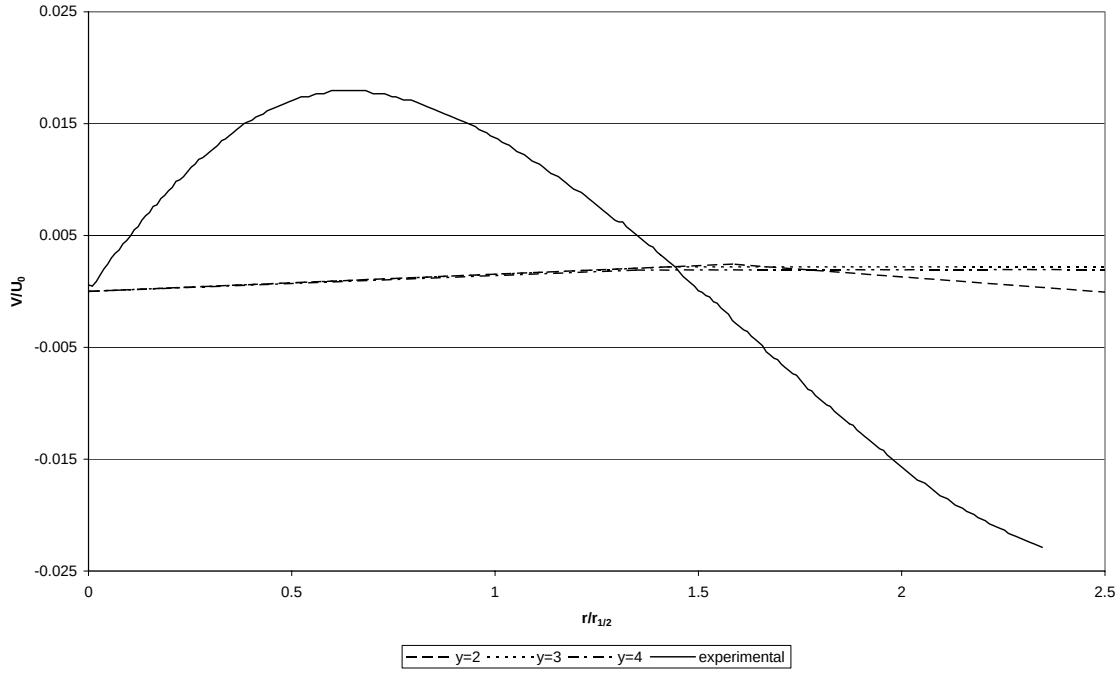

Figure 3.11: Axi-symmetric jet lateral velocity profile at various downstream distances (0.1 mix)

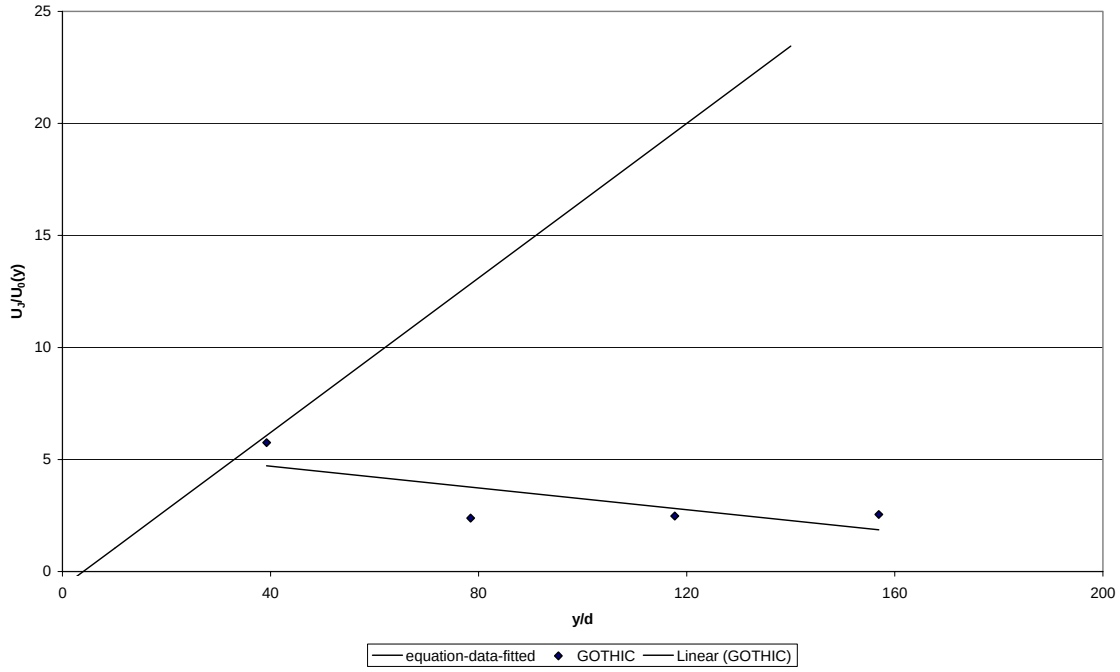

Figure 3.12: Axi-symmetric jet centerline velocities (0.1 mix)

3.3.2. Standard k-ε model

As will be shown in this section, the standard k-ε model does a better job of determining flow properties for the axi-symmetric jet than the mixing length models. A 50 second transient of the axi-symmetric jet required 19.46 hours of computational time on the computer system previously identified. Figure 3.13 gives the velocity profile across the jet at several downstream distances. As stated in Section 3.3.1, the distances downstream of the jet nozzle corresponding to y = 2, 3, and 4 are equivalent to 6.8, 10.2, and 13.6 ft., respectively. In terms of the jet diameter, these are located at distances of 39, 78, and 117 nozzle diameters downstream of the nozzle. The velocity profile at distances of 6.8 ft. and 10.2 ft. show that GOTHIC is still developing the velocity profile in this region. For these profiles, the predicted velocities are very close to that of experiment for distances up to one jet half-width

from the centerline. As the profile moves beyond the half-width, the velocity profiles begin to diverge significantly from experiment. The velocity profile at y = 4 most closely corresponds to the experimental data of Wygnanski, et al. [21], across the full width of the jet. Near the jet centerline, the velocity computed by GOTHIC is slightly smaller than the experimental data while the opposite holds true on the outer edge of the jet. The GOTHIC half-width velocity predicted appears to be very close to where that of the experimental data would fall. Thus, GOTHIC does a reasonable job of predicting the velocity profile of the axi-symmetric jet with the standard k-ε turbulence model.

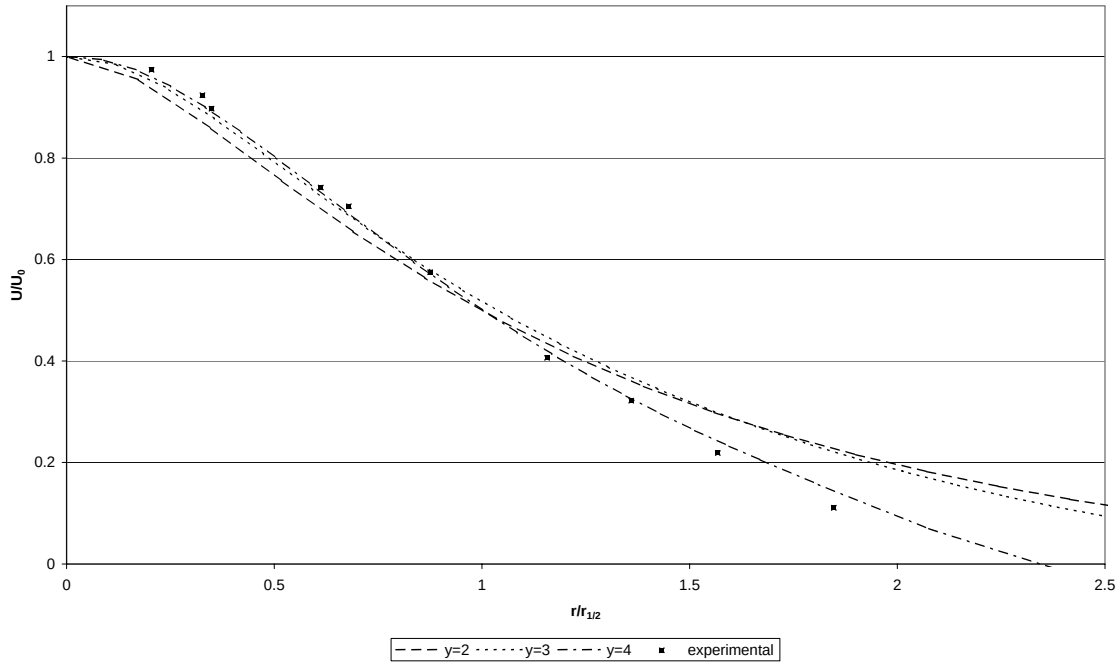

Figure 3.13: Axi-symmetric jet velocity profile at various downstream distances (k-ε)

Since the longitudinal velocity profile of Figure 3.13 is reasonable, one would assume that the lateral velocity profile would also be accurate. Figure 3.14 gives the lateral velocity profile for the standard k-e model. The peak lateral velocity predicted

by GOTHIC coincides well with that given by the experimental data for all of the profiles. While the peak lateral velocity is relatively accurate, the profile and the entrainment of the stagnant air into the jet (the negative velocity region) are not. GOTHIC predicts a much faster increase in the lateral velocity than provided by experiment. Once the peak is reached, the slope of the velocity follows the experiment well to a distance of 1.5 half-widths. Beyond this point, the lateral velocity profiles again diverge from the experimental data. The jet centerline velocity profile, Figure 3.15, again compares the GOTHIC results to experimentally fitted data. At the first data point, near a y/d of 40, the GOTHIC predicted velocity is near that of the experimental results. However, further downstream GOTHIC predicts a slower dissipation of the centerline velocity resulting in a smaller slope of the centerline velocity profile. Despite this, GOTHIC's standard k-ε model does a reasonable job of predicting the velocity profiles of the axi-symmetric jet.

For the standard k-ε and RNG k-ε models, a normalized turbulent kinetic energy profile is also given for the jet. The turbulent kinetic energy profile for the standard k-ε model is shown in Figure 3.16. Here the turbulent kinetic energy profile at y = 2 most accurately reflects the experimental data of Wygnanski and Fiedler [21]. For this profile, the kinetic energy at the jet centerline is very close to that of the experimental data. Moving out from the centerline, the GOTHIC turbulent kinetic energy increases significantly faster than experiment. From approximately half of the jet half-width to more than twice the half-width, the profile at y = 2 closely resembles that of the experimental data, although GOTHIC's values are slightly smaller. In this region the profiles at y = 3 and y = 4 more closely resemble that of experiment.

Overall, however, the profile at y = 2 provides the best representation of the experimental data. Thus, the turbulent kinetic energy predicted by the standard k-ε model is fairly accurate.

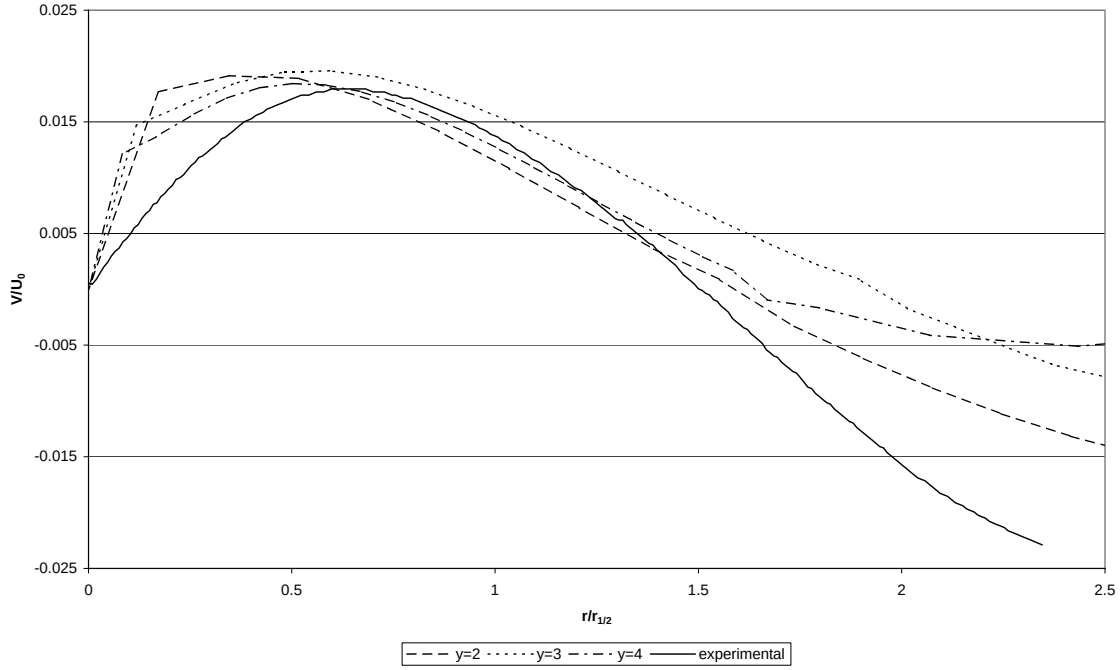

Figure 3.14: Axi-symmetric jet lateral velocity profile at various downstream distances (k-ε)

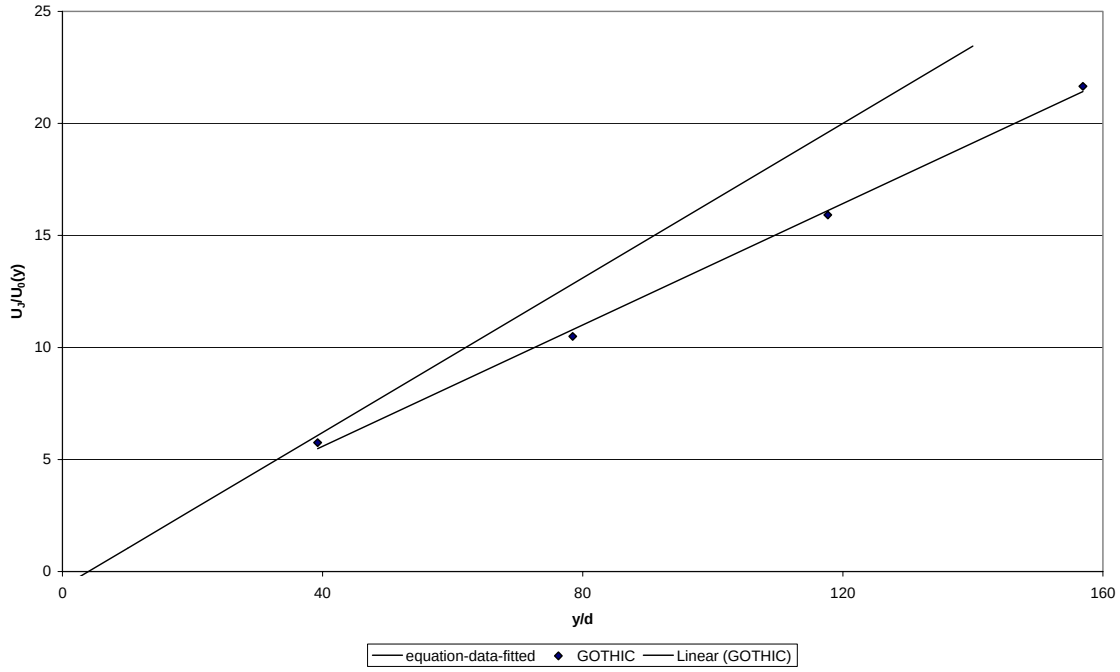

Figure 3.15: Axi-symmetric jet centerline velocities (k-ε)

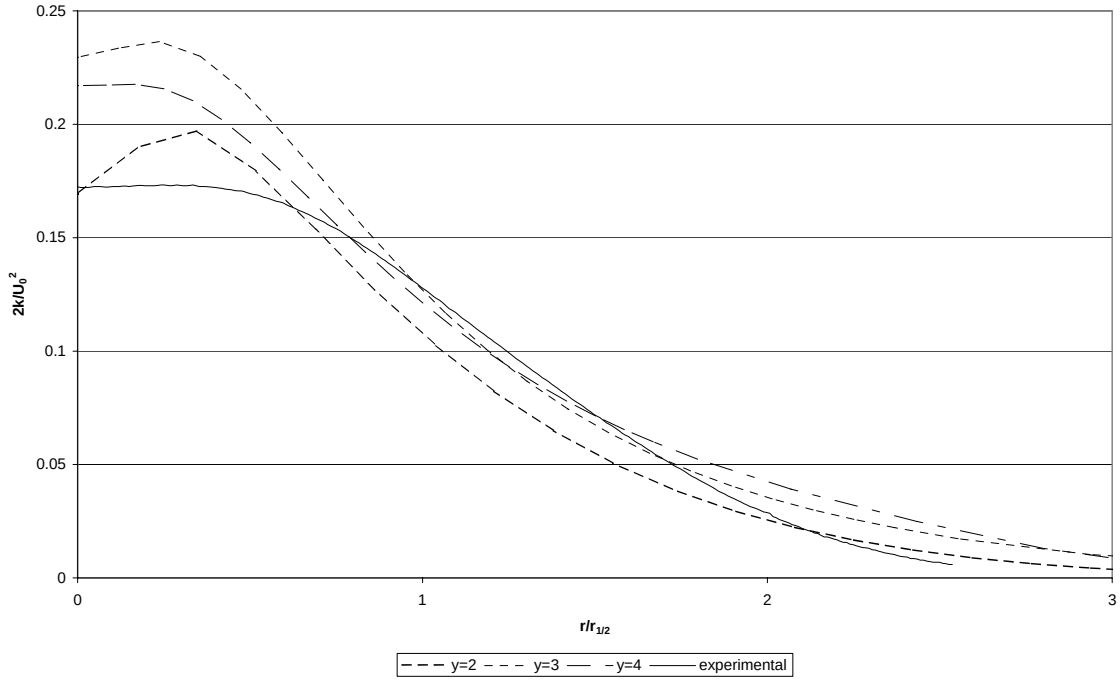

Figure 3.16: Axi-symmetric jet turbulent kinetic energy profile at various downstream distances (k-ε)

3.3.3. RNG k- ε model

As will be shown in this section, the RNG k-ε model produces the results that are most consistent with the experimental data. The RNG model required 20.46 hours to compute a 50 second transient. Figure 3.17 gives the longitudinal velocity profile produced by GOTHIC's RNG k-ε model for the axi-symmetric jet at various downstream distances, along with experimental results. Here the velocity profile at the distance of 13.6 ft. downstream of the jet (y = 4) most closely resembles the experimental data. Over the entire range of the experimental data GOTHIC's velocity profile at y = 4 mimics that of the experiment. The profiles given by y = 2 and y = 3 also give accurate representations of the velocity up to the jet half-width, but diverge from the experimental data beyond this point. Overall, GOTHIC predicts a reasonable velocity profile considering the coarseness of the subdivided volume.

While the longitudinal velocity profile from the RNG model provides better results than the previous models, the lateral velocity profile does not. Figure 3.18 gives the lateral velocity profile of GOTHIC at several downstream distances and compares it to Wygnanski's experimental data. All of the GOTHIC profiles predict a much lower peak velocity. The profile given at y = 4 does mimic the shape of the experimental data, but all of the data points out to two jet half-widths under predict the velocity. The jet centerline velocity profile given in Figure 3.19 is not in good agreement with the data fit of the experimental data. GOTHIC's prediction with the RNG model gives a slower reduction in the jet centerline velocity than is given by experiment. Thus, the RNG k-ε model in GOTHIC does not provide a good representation of the experimental lateral and centerline velocity profiles.

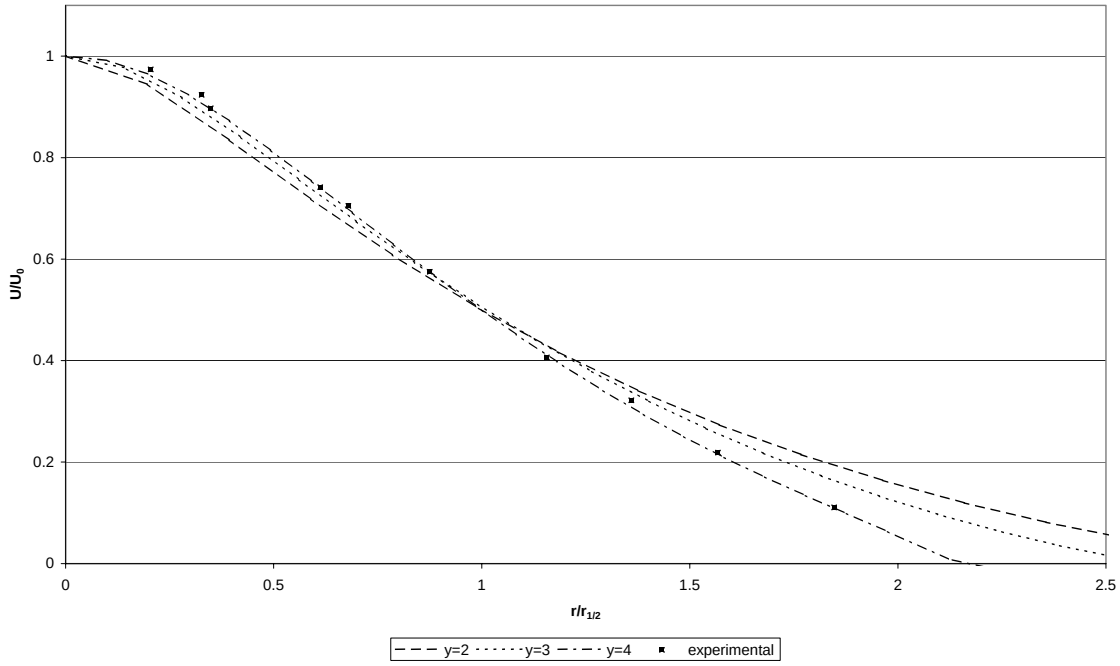

Figure 3.17: Axi-symmetric jet velocity profile at various downstream distances (RNG)

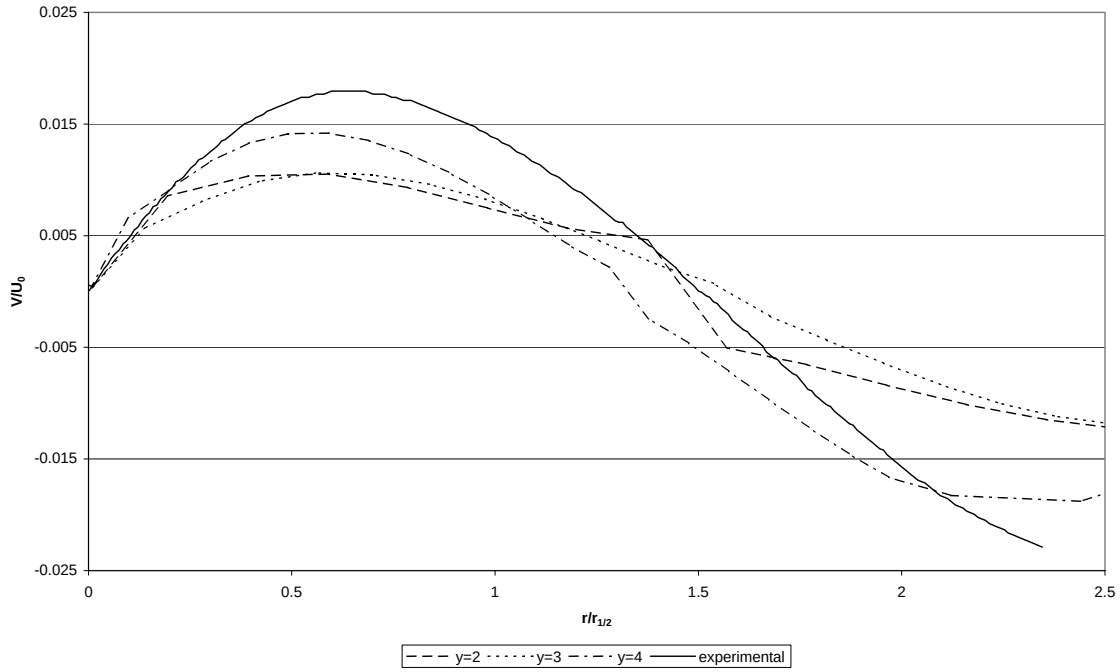

Figure 3.18: Axi-symmetric jet lateral velocity profile at various downstream distances (RNG)

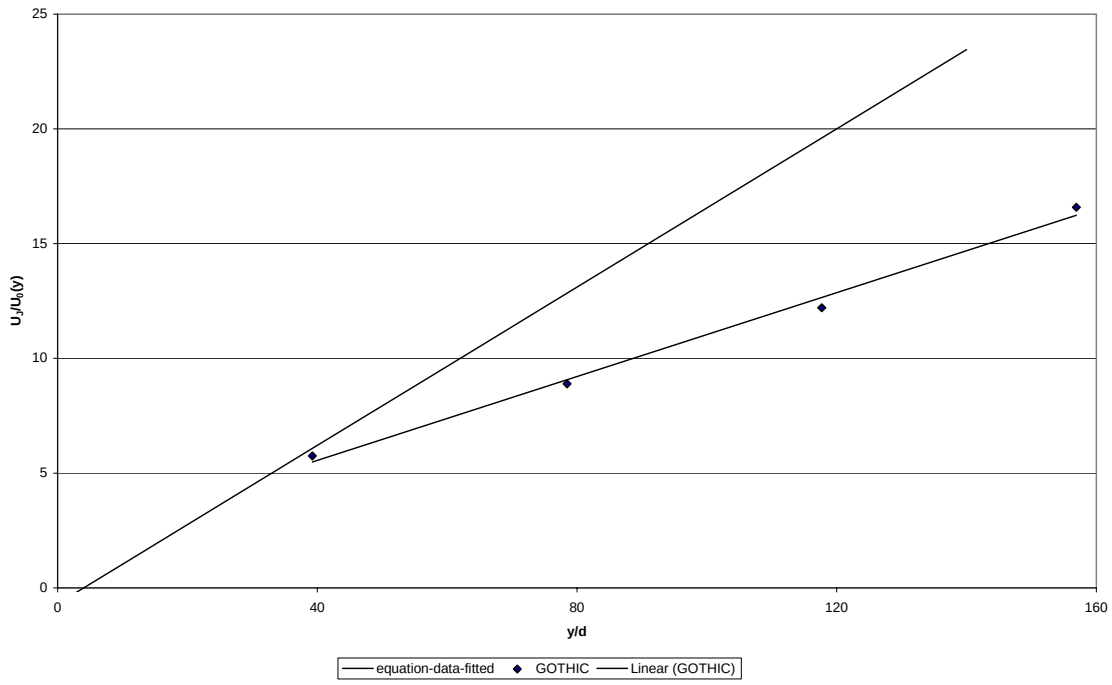

Figure 3.19: Axi-symmetric jet centerline velocities (RNG)

The turbulent kinetic energy of the axi-symmetric jet is shown in Figure 3.20. While the profiles at various downstream distances have the same general shape as the experimental data, the magnitude of the dimensionless energy is significantly lower. While the actual value of the kinetic energy between the standard and RNG k-ε models are similar, the squaring of the nearly twenty percent difference in the centerline velocity (identified in Figure 3.19) results in the magnitude of the scaled kinetic energy being significantly smaller for the RNG model. Thus, the kinetic energy and shape of the profile are similar to the experimental data and the differences between the values in the profile are the result of the differences or inconsistencies in the velocity profile predicted.

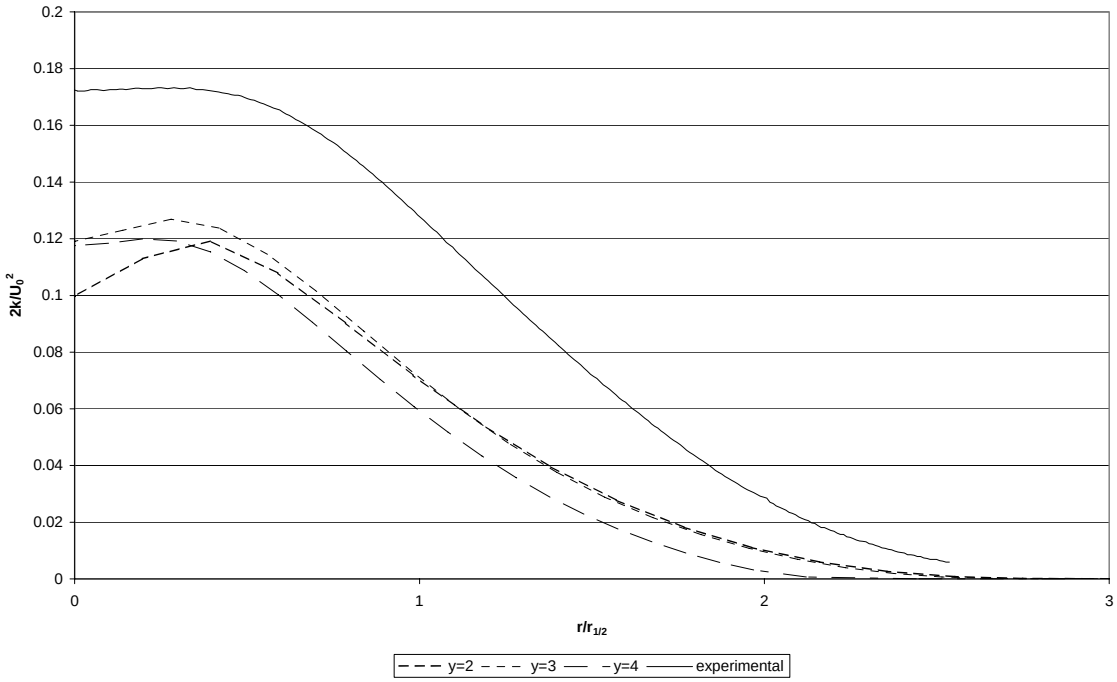

Figure 3.20: Axi-symmetric jet turbulent kinetic energy profile at various downstream distances (RNG)

3.3.4. Comparison between turbulence models

In Sections 3.3.1 through 3.3.3, comparisons of each of the turbulence models were made to experimental data. The figures in these sections showed the flow parameters for different downstream distances of the jet. In this section we will compare the flow properties for each of the models with each other and experimental data. This will allow us to make easier determinations about each model's strengths and weaknesses as they relate to the flow configuration analyzed, the axi-symmetric jet.

The mean velocity profiles for the flow at y = 2, y = 3, and y = 4 are shown in Figure 3.21, Figure 3.22, and Figure 3.23, respectively. As discussed previously, the velocity profiles generated by the mixing length models do not contain a sufficient

number of data points to accurately judge the credibility of the mixing length model. A comparison of the velocity profiles of the k-ε model and the RNG model show that they are in agreement from the jet centerline to approximately one half-width for all downstream distances. From the jet half-width to the outer edge of the jet, the RNG model's velocity profile most closely matches the experimental data. However, for the downstream distance corresponding to y = 4, both models provide a reasonable approximation of the experiment.

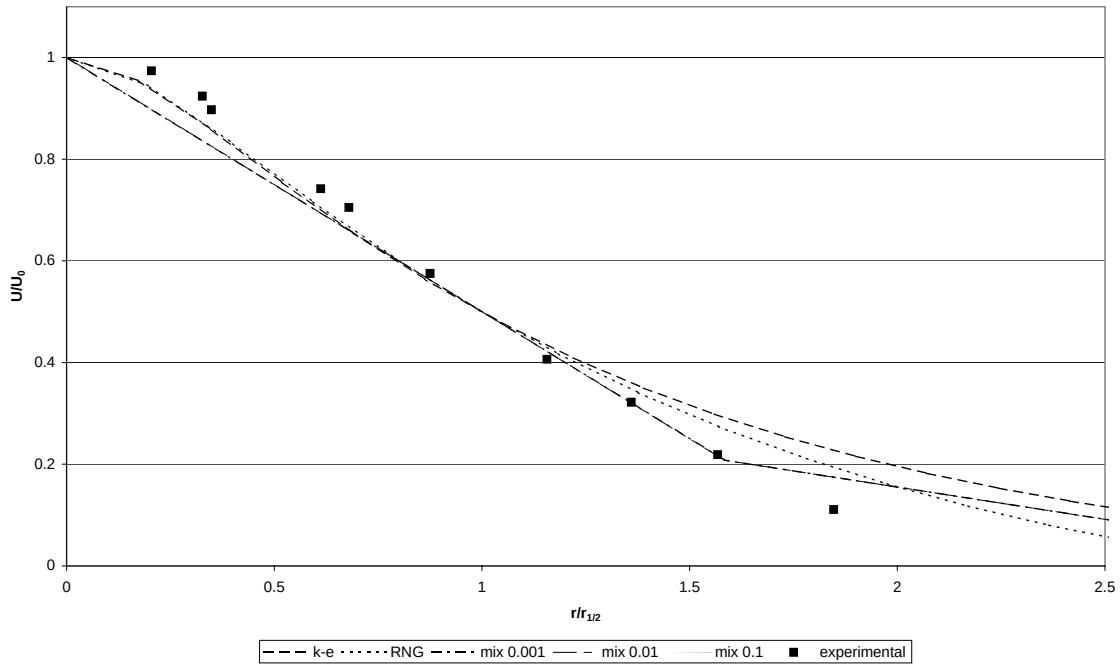

Figure 3.21: Axi-symmetric jet velocity profile comparison (y=2)

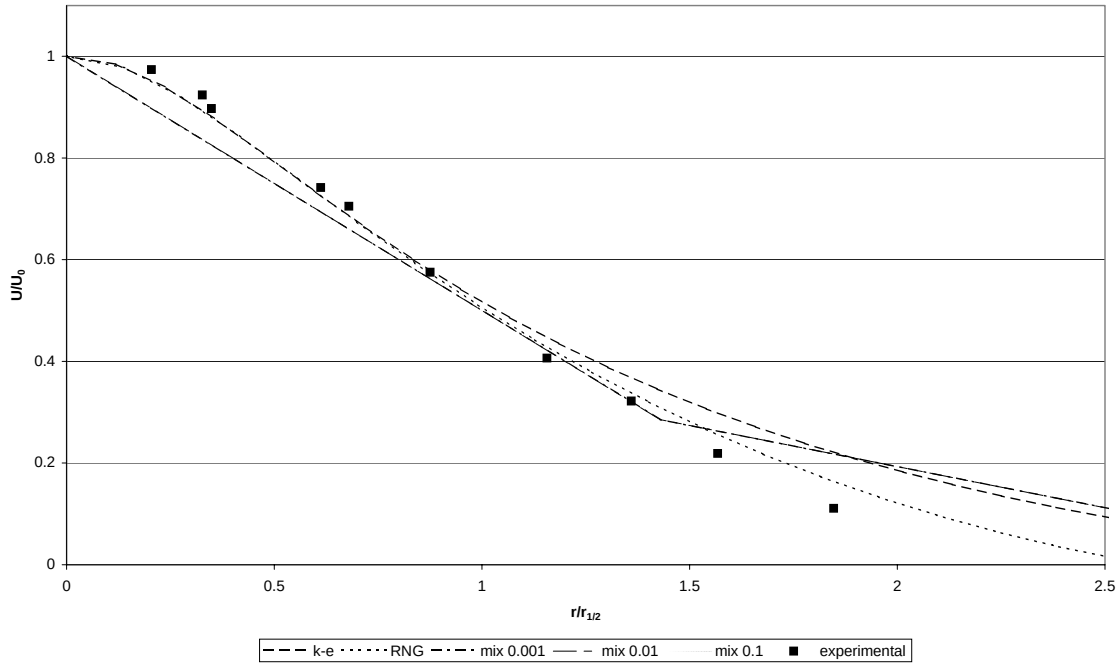

Figure 3.22: Axi-symmetric jet velocity profile comparison (y=3)

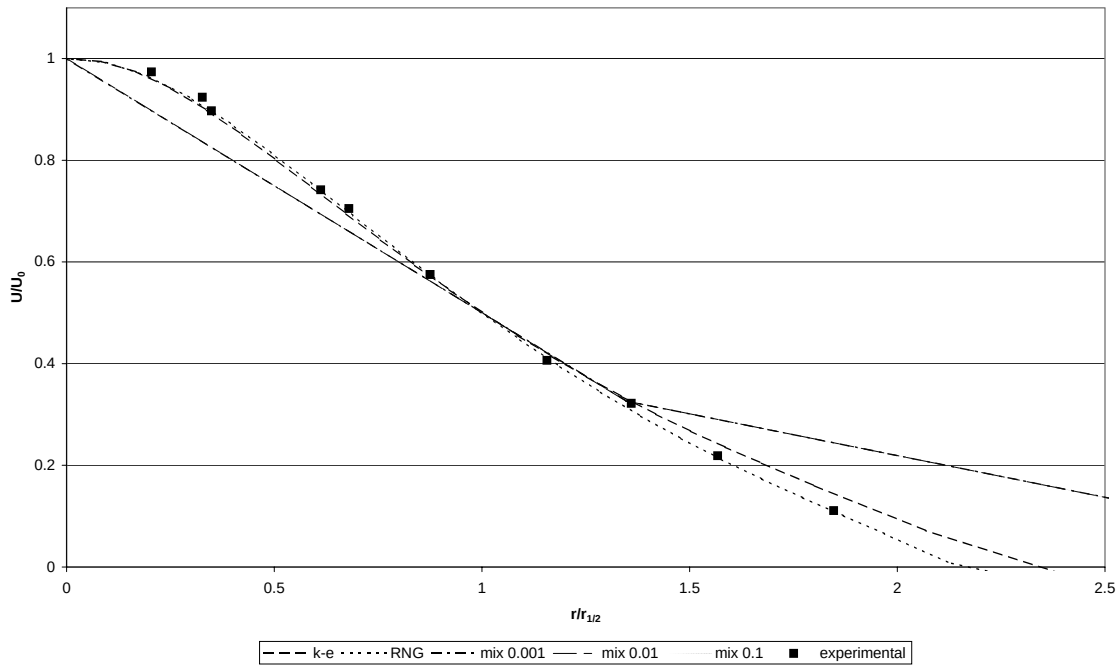

Figure 3.23: Axi-symmetric jet velocity profile comparison (y=4)

Lateral velocity profiles for the jet are given in Figure 3.24 through Figure 3.26. As with the mean flow velocity, the lateral velocity profiles of the mixing length models provide a poor representation of the experimental flow data for all three profiles. From the jet centerline to 1.5 half-widths, the k-ε model provides a more accurate velocity magnitude than the RNG model. However, the RNG model most closely matches the shape of the experimental data in this range. Beyond 1.5 half-widths, both models greatly under predict the velocity of the entrained (stagnant) air for y = 2 and y =3. For the profile at y = 4, the RNG model comes much closer to predicting the velocity of the entrained air on the edge of the jet. Overall, the RNG model provides a better representation of the physics of the lateral velocity flow, since its shape most closely resembles the experimental data. However, the standard k-ε model more accurately predicts the magnitude of the lateral velocity. Despite this, it is concluded that the RNG model provides a better representation of the axi-symmetric jet for predicting the lateral velocity profile.

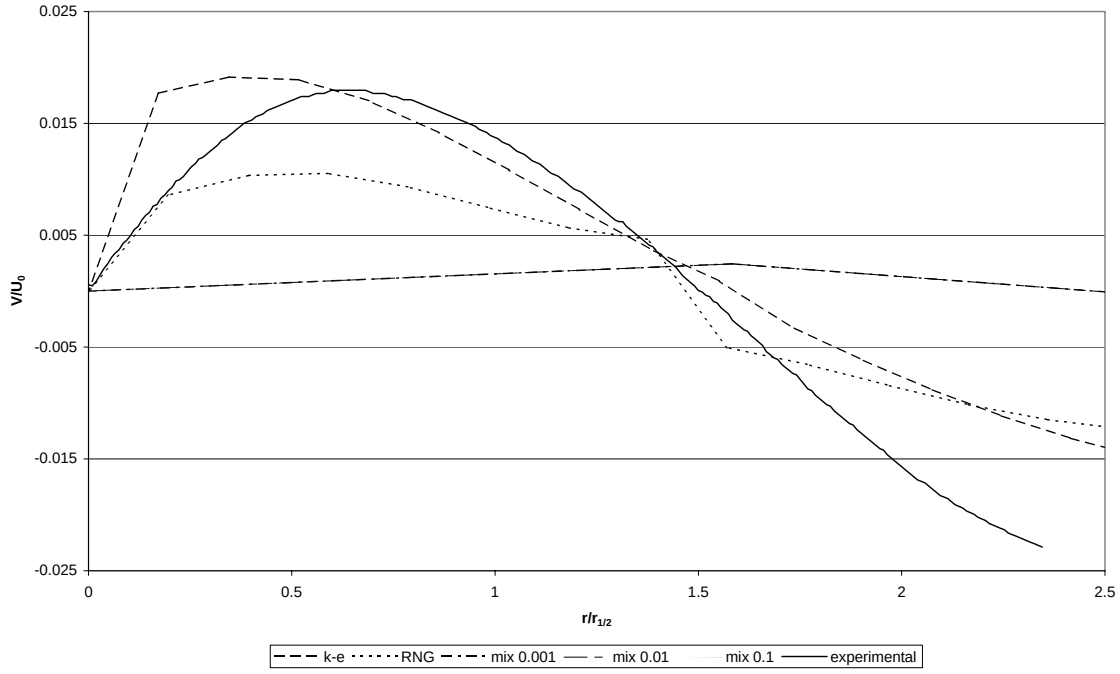

Figure 3.24: Axi-symmetric jet lateral velocity profile comparison (y=2)

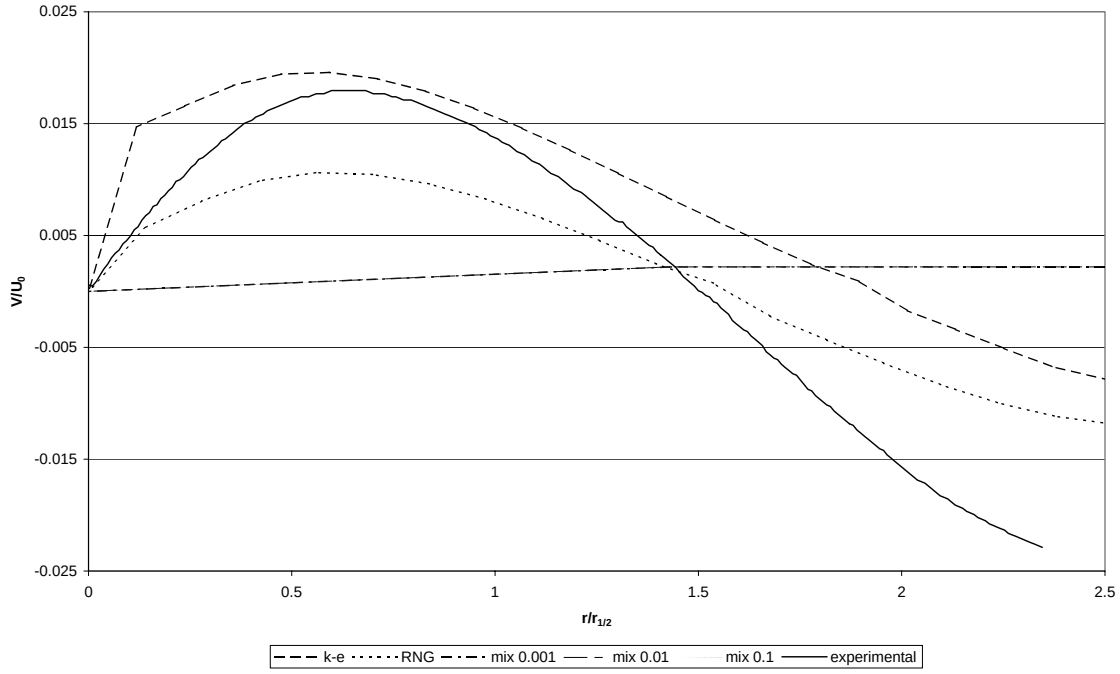

Figure 3.25: Axi-symmetric jet lateral velocity profile comparison (y=3)

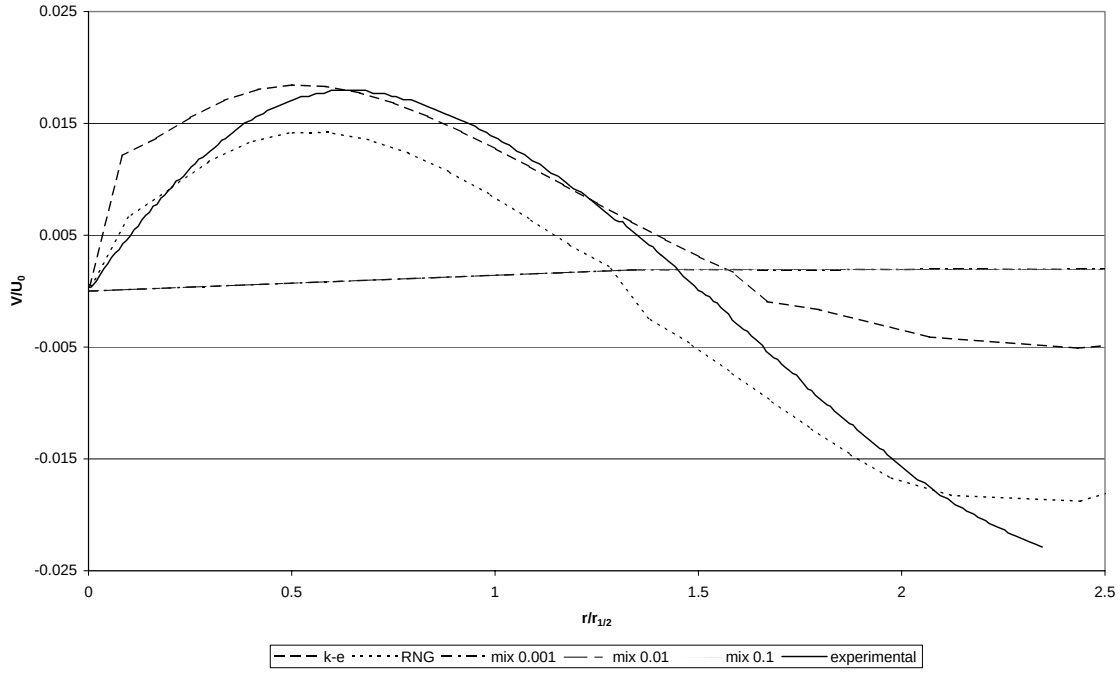

Figure 3.26: Axi-symmetric jet lateral velocity profile comparison (y=4)

The normalized turbulent kinetic energy of the jet is given in Figure 3.27, Figure 3.28, and Figure 3.29. As described in the sections above, the turbulent kinetic energy of the mixing length models produce horizontal lines across the jet, as the energy is constant. This is a poor approximation which is obviously invalid and will not be discussed further. At each of the profiles given, the RNG model shape is consistent with experiment and could likely be scaled to match the experimental data. However, the magnitude of the RNG kinetic energy is significantly lower than in the experiment. The k-ε model shape shows the kinetic energy profile is compressed toward the jet centerline. Over most of the range of the experimental data, the k-ε model over predicts the turbulent kinetic energy. These observations are consistent with the velocity profiles discussed previously since the turbulent eddies that produce the turbulence kinetic energy obtain their energy from the mean flow. Based on the

fact that the RNG model shape is most similar to the experimental data, it is concluded that it produces the best result for the turbulent kinetic energy.

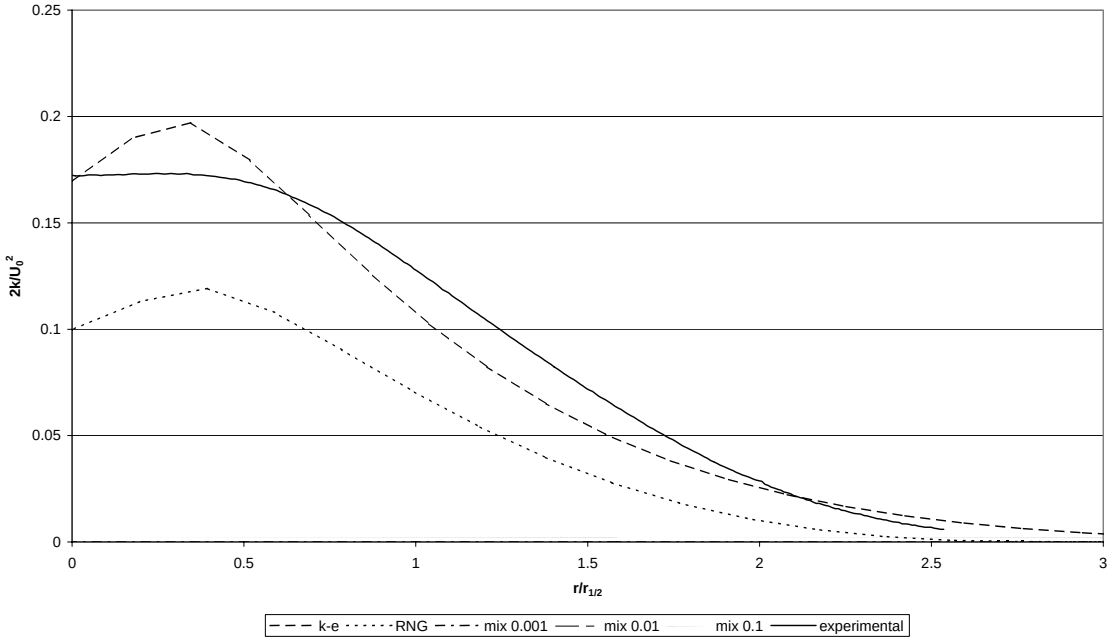

Figure 3.27: Axi-symmetric jet turbulent kinetic energy profile comparison (y=2)

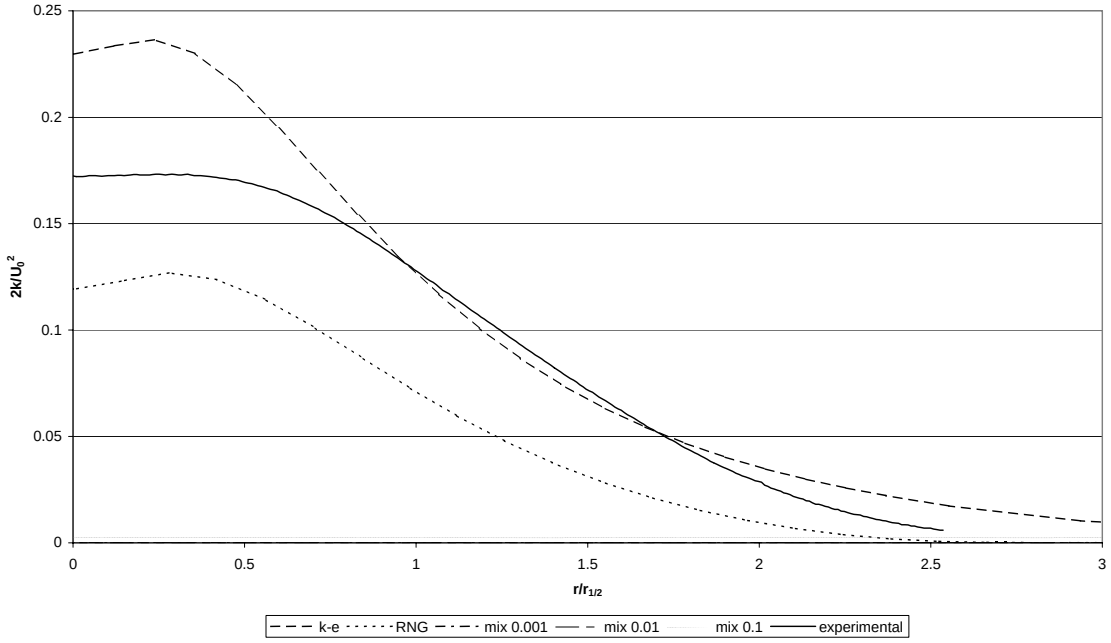

Figure 3.28: Axi-symmetric jet turbulent kinetic energy profile comparison (y=3)

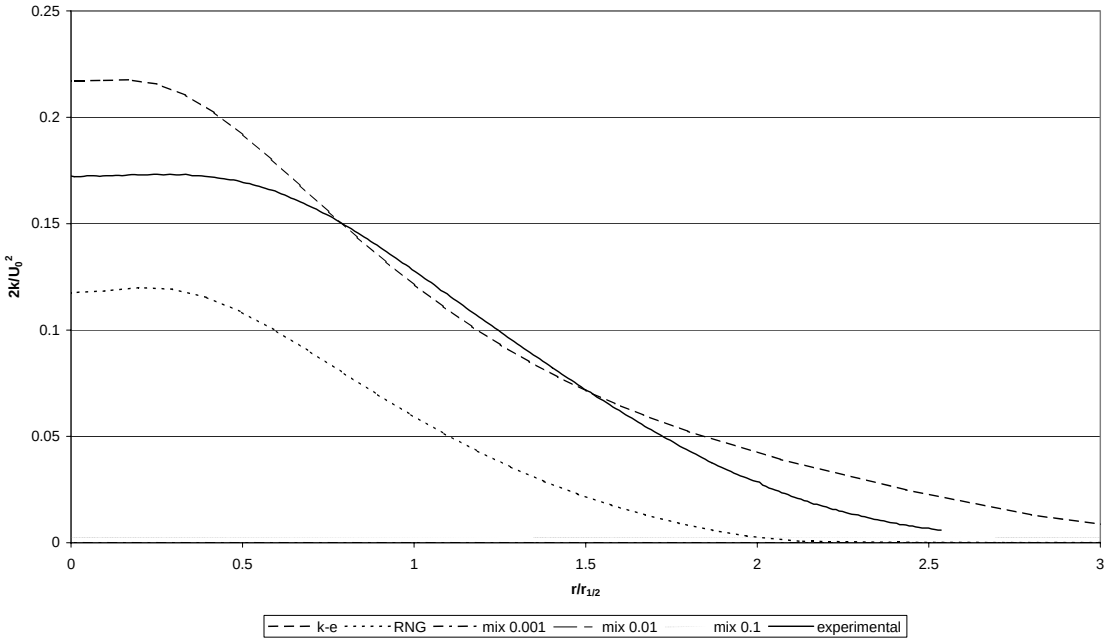

Figure 3.29: Axi-symmetric jet turbulent kinetic energy profile comparison (y=4)

Figure 3.30, below, compares the predicted centerline velocities for each of the turbulence models. Each of the mixing length models provides results that are similar to each other but invalid. The downward slope of these lines would indicate that the jet centerline velocity is increasing as one moves downstream. This is obviously incorrect, as there is no mechanism for acceleration of the flow downstream of the jet entrance. Each of the remaining models predicts a deceleration in the centerline velocity, although both do not dissipate it as rapidly as shown by experiment. A comparison of the two-equation models shows that the standard k-ε model most closely models the deceleration of the axi-symmetric jet. Thus, the k-ε model provides the most accurate modeling of deceleration of the jet.

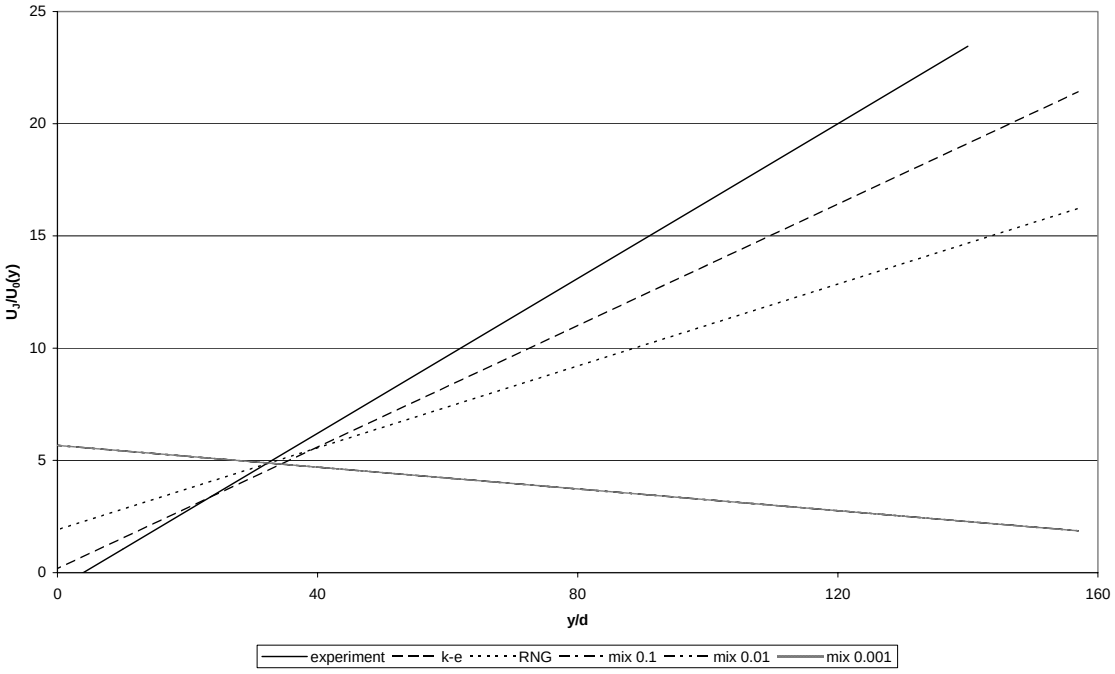

Figure 3.30: Axi-symmetric jet centerline velocity profile comparison

4. Channel Flow Model

Rather than model a physical experiment for the channel flow, data from a numerical simulation performed by Kim, Moin, and Moser at the NASA Ames Research Center [13] is primarily used as the basis for comparison to GOTHIC's results. Additionally, experiments performed by Eckelmann [9] and Kreplin and Eckelmann [14], which Kim, et. al. reference, are also compared with GOTHIC results. The following sections explain the setup of the computational grid, explain how it is modeled in GOTHIC, and provides a comparison of GOTHIC's results with the computational and experimental data.

4.1. Experimental setup from literature

Kim, et. al. selected a computational grid that was fine enough to resolve all of the turbulence scales seen at a Reynolds number of 3,300 (based on the centerline velocity and channel half-width) [13]. Such a grid was found to exist with a resolution of 192 x 129 x 160 grid points in the x, y, and z directions, respectively, giving a total of 3,962,880 grid points. The coordinate system utilized makes the x-axis the direction of the mean flow with y being the vertical direction and z the cross-stream direction. The subdivisions in the x and z directions are equally divided along their entire distances. For the y direction, in which the velocity profile will primarily form, the mesh fineness varies from $y^+ = 0.05$ near the wall to $y^+ = 4.4$ at the centerline. The quantity 'y^+' is a scaled distance from the wall calculated with the density, kinematic viscosity, and the wall shear stress which is defined in Section 4.3 (**Note: The z^+ quantity defined in Section 4.3 is based on the coordinate system utilized in the GOTHIC model. This quantity is equivalent to the y^+ value described above.**). The sufficiency of the grid to resolve the

turbulence scales was verified after the computation was finished. Using the grid described above, Kim, et. al. produced computational results for the turbulent channel and compared them with data from Eckelmann [9] and Kreplin and Eckelmann [14].

4.2. GOTHIC model

The GOTHIC model replicating the simulation of Kim, et. al. is modeled with control volumes, 3-D connectors, flow paths, and boundary conditions. Figure 4.1 gives the noding diagram used to replicate the simulation. Volume 1s is a subdivided control volume representing the channel. Volumes 2 and 3 represent the inlet and outlet of the channel, respectively. These intermediate volumes must be used in the model because 3-D connectors can only be used to connect two control volumes, as detailed in Section 2.1.4. A flow boundary condition supplies air to the inlet volume (Volume 2) that connects to the inlet of the subdivided volume representing the channel. In order to model the assumed uniform velocity profile at the inlet, a 3-D connector is used for transferring the supplied inlet velocity from the inlet volume to the channel. A 3-D connector is also used to connect the outlet of the channel to the control volume that connects to the pressure boundary condition that acts as a sink for the fluid.

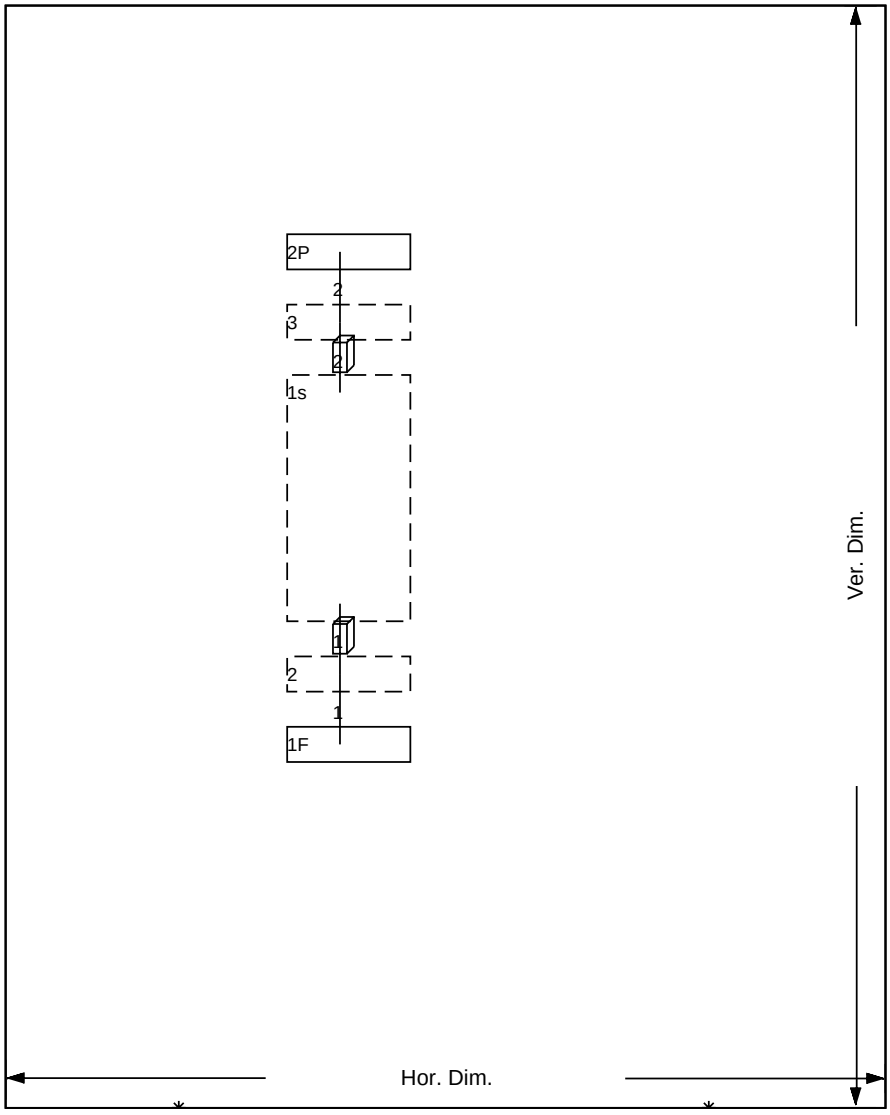

Figure 4.1: Channel GOTHIC noding diagram

The subdivided mesh of Volume 1s is shown in Figure 4.2. In the x-direction, the length of 0.4 m. is not subdivided. Rather, slip boundary conditions are applied to these surfaces to eliminate their effect on the flow. This effectively ensures that there are no wall effects in this direction on the fluid. The 10 m. length in the y-direction, which is the direction of the mean flow, is uniformly divided into six cells with lengths of 1.667 m. each. The total height modeled in the z-direction is two cm. This distance is

subdivided using the logarithmic and linear subdivision schemes in GOTHIC. Rather than model the entire channel, we can take advantage of the symmetry seen about the channel centerline and only model half of the channel. Setting the top face of the volume to a slip condition replicates this by eliminating any wall shear stress on the cells adjacent to this plane. From the channel centerline (i.e., the top of the volume) to a distance of 1.4 cm., the volume is subdivided using GOTHIC's logarithmic grid scheme with 12 cells within this domain. From 1.4 cm. to the wall (2 cm.) the domain is modeled with 12 grid cells of equal length. The 3-D connectors discussed earlier are attached at the front and end of the channel volume. For the inlet, this corresponds with the 3-D connector spanning across the coordinates from (1, 1, 1) to (1, 1, 24). For the exit, the 3-D connector is attached from (1, 6, 1) to (1, 6, 24). Using this setup, the turbulent channel flow computation is replicated in GOTHIC.

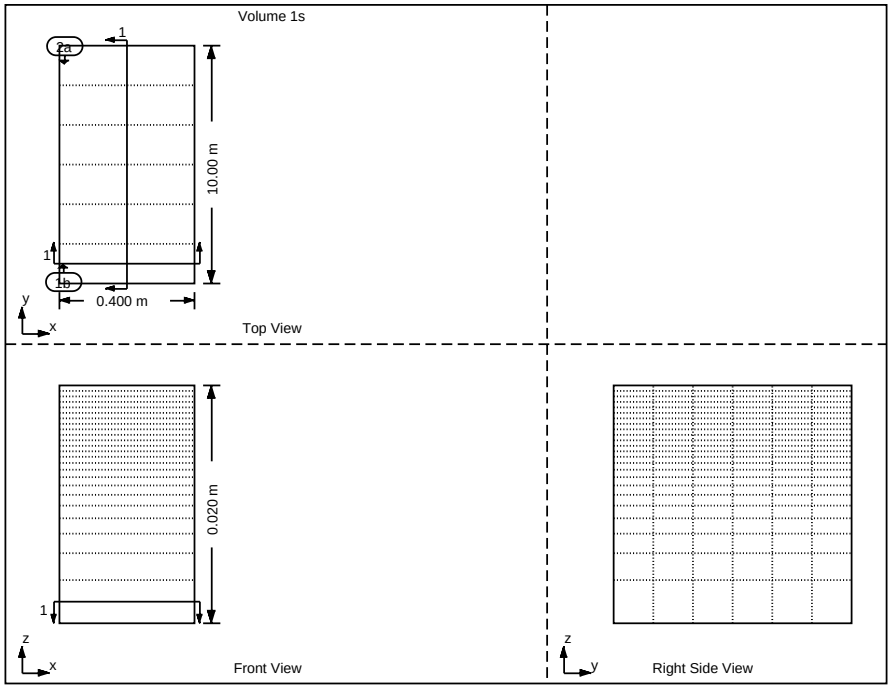

Figure 4.2: 3-D mesh of channel

4.3. Results

The following sections provide the results for each of the turbulence models analyzed. The ability of each model to predict experimental data is evaluated in the first three sections. The final section compares the computational results for each of the models against both the experimental data and the other models. The following definitions are used for producing non-dimensional values which allow comparison of the GOTHIC and experimental data.

U_m	Average entrance velocity
U_0	Mean centerline velocity
U	Mean velocity in primary flow direction (y-axis)
V	Mean lateral velocity
τ_w	Wall shear stress
ρ	Fluid density
$u_\tau = \sqrt{\frac{\tau_w}{\rho}}$	Friction velocity
$k = \frac{1}{2}\overline{u_i' u_i'}$	Turbulent kinetic energy
δ	Channel half thickness
$z^+ = z\frac{u_\tau}{\upsilon}$	Scaled distance from wall
$u^+ = \frac{U}{u_\tau}$	Scaled mean velocity

4.3.1. Mixing length models

The mixing length model results for the channel flow with lengths of 0.1, 0.01, and 0.001 m. are presented below. For a transient time of 10 seconds, each of the mixing length models required 0.16 hours of computational time. Figure 4.3 shows the scaled velocity profile, u^+, of the 0.1 m. mixing length model at several distances downstream of the entrance. The same figure also gives the DNS data of Kim, et. al. [13] and the experimental data of Eckelmann [9]. The profiles at y = 2, y = 3, and y = 4 are located at distances from the channel entrance of 3.33 m., 5.00 m., and 6.67 m., respectively. As the figure shows, each of the profiles has approximately the same shape over the entire width of the channel. The profile for y = 3 most closely predicts the channel centerline velocities given by DNS and experiment, herein simply referred to as experimental data. The other profiles given predict centerline velocities that are slightly higher than both the y = 2 profile and the experimental data. With the exception of the centerline velocities, the mixing length velocity profiles predicted differ significantly from the experimental data, especially from $\delta/2$ (the mid point distance from the wall and the centerline) to the wall. This is further emphasized in Figure 4.4, which shows the same GOTHIC and experimental data as Figure 4.3, but provides it with linear scaling on the abscissa. This shows that the 0.1 m. mixing length model predicts a much slower increase in the velocity profile as one moves toward the channel centerline. From the wall to $z^+ = 30$, the average GOTHIC velocity is less than half of that predicted by experiment for all the profiles. Based on the profile at y = 3 most accurately predicting the mean centerline velocity, and none

of the velocity profiles resembling the experimental data, it is concluded that this profile is most representative of experiment.

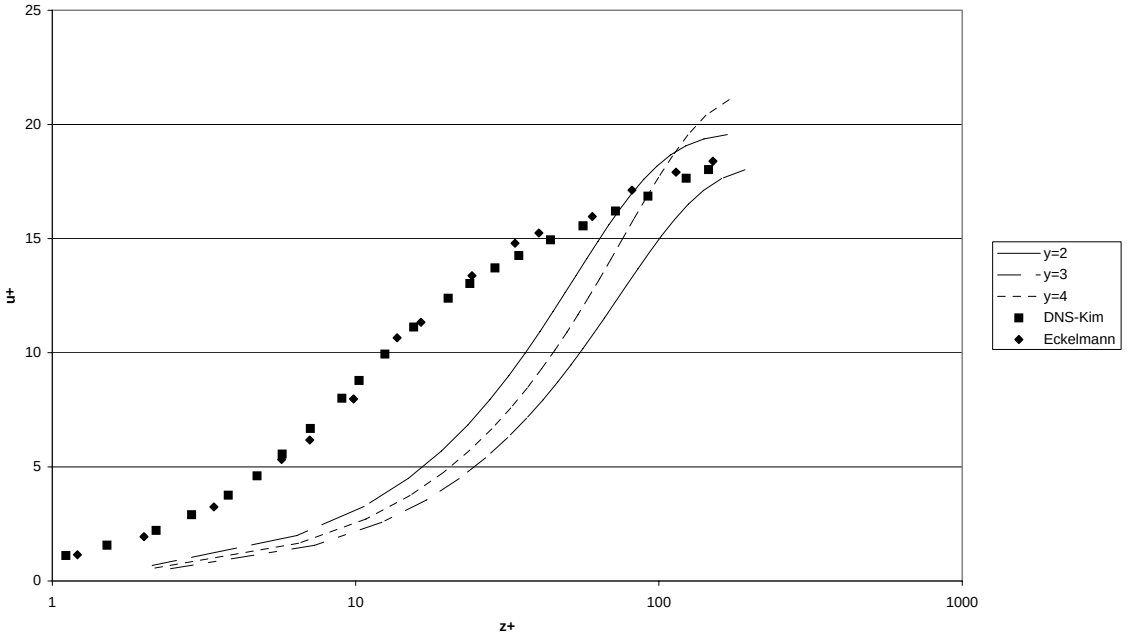

Figure 4.3: Velocity normalized by friction velocity over entire channel (mix 0.1)

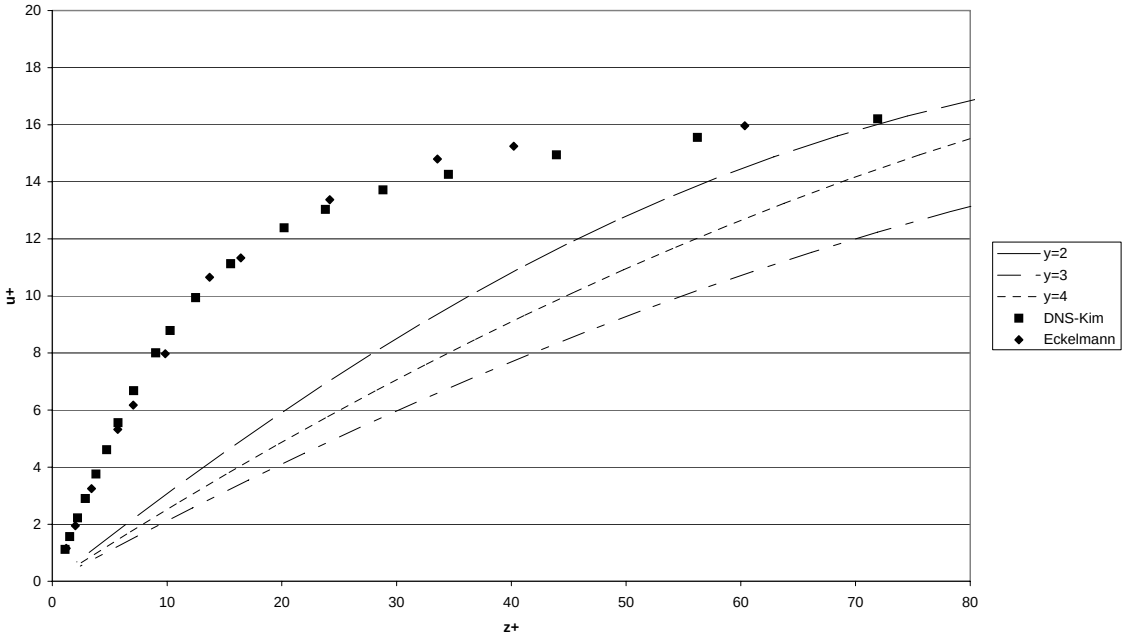

Figure 4.4: Mean velocity profile of channel close to wall (mix 0.1)

Another method of scaling the velocity is to divide it by the average velocity across the channel, U_m. This scaling is used for the velocity profiles given in Figure 4.5. Such data is not provided by Eckelmann's paper but is given by Kim, et. al. [13] and is presented in this same figure. As discussed previously, the profile is shallower in the near wall region for each of the profiles than is given by experiment. At a z/δ value of 0.37, the GOTHIC 0.1 m. mixing length profile reaches the value given by Kim's DNS. By a z/δ value of 0.6 the GOTHIC profile at y = 2 begins to show a similarity in the rate of velocity increase to that of the DNS. Its final U/U_m value is 1.30, similar to the value of 1.16 given by Kim. The values given by the profiles at y = 3 and y = 4 are significantly higher, giving errors as high as 22%. Another velocity profile that can be examined for the channel flow is the velocity defect, which is defined as the difference between the velocity at a given point in the flow and the centerline velocity. When the velocity defect is scaled by the friction velocity, the flow simply becomes a function of z/δ. The velocity defect for the GOTHIC 0.1 m. mixing length model is given in Figure 4.6. While the profiles given by GOTHIC are significantly higher than the DNS data, the general shape of the curves does match. Of these profiles, the defect velocity at y = 2 gives values that most closely approach the DNS data. Based on these observations of Figure 4.5 and Figure 4.6, the profile at y = 2 gives the best approximation of the DNS data for the GOTHIC 0.1 m. mixing length model.

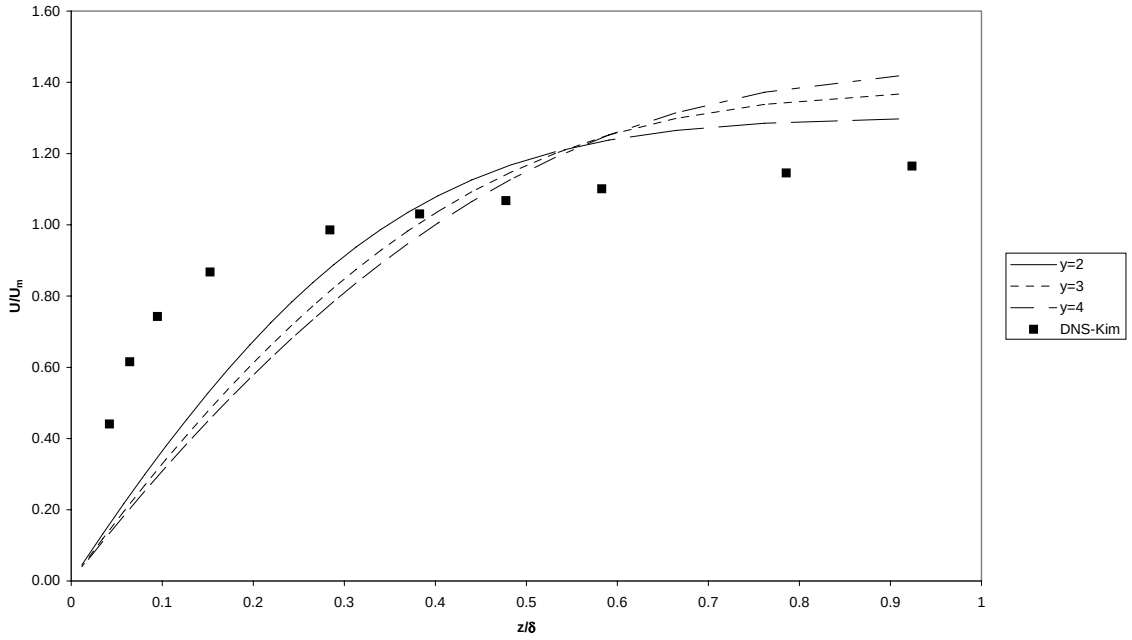

Figure 4.5: Velocity profile normalized by channel mean velocity (mix 0.1)

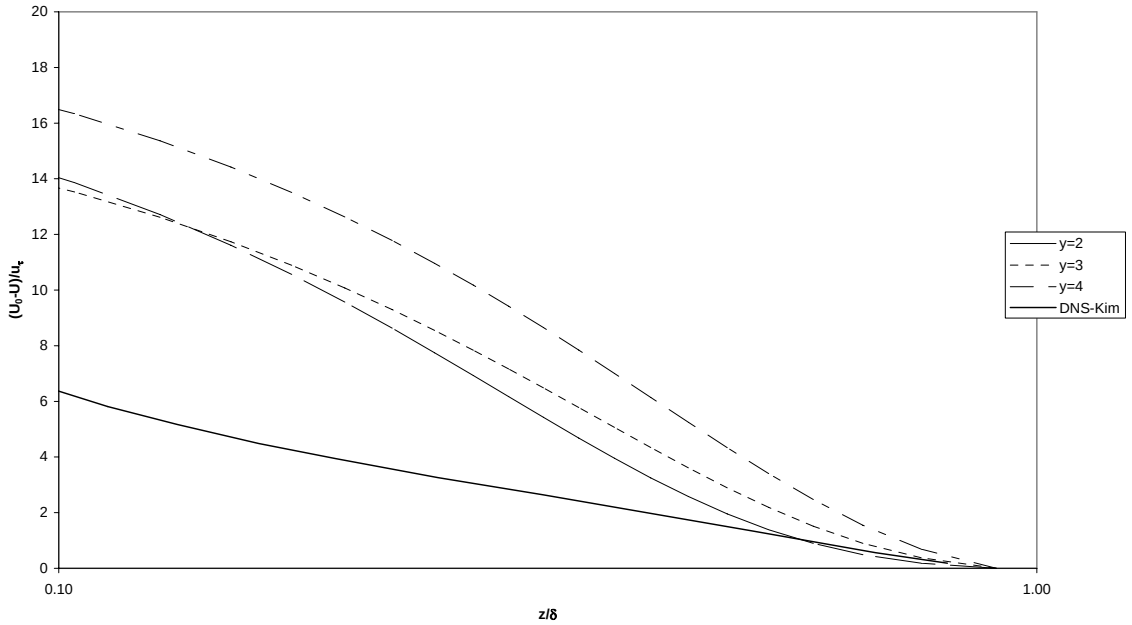

Figure 4.6: Mean velocity defect across channel (mix 0.1)

As has been shown in the previous section for the axi-symmetric jet flow, the mixing length models do not provide a good representation of the turbulent kinetic

energy of the geometries they are modeling. Figure 4.7 shows the GOTHIC normalized turbulent kinetic energy profiles for the channel along with the DNS data of Kim [13] and experimental data of Kreplin and Eckelmann [14]. As the figure shows, the kinetic energy predicted by GOTHIC is essentially not a function of the cross-stream coordinate, z^+. While there are slight variations between the different profiles, none provide a reasonable estimate of the magnitude or profile of the turbulent kinetic energy given by experiment. Thus, the GOTHIC 0.1 m. mixing length model does not provide a realistic assessment of the turbulent kinetic energy of the channel flow.

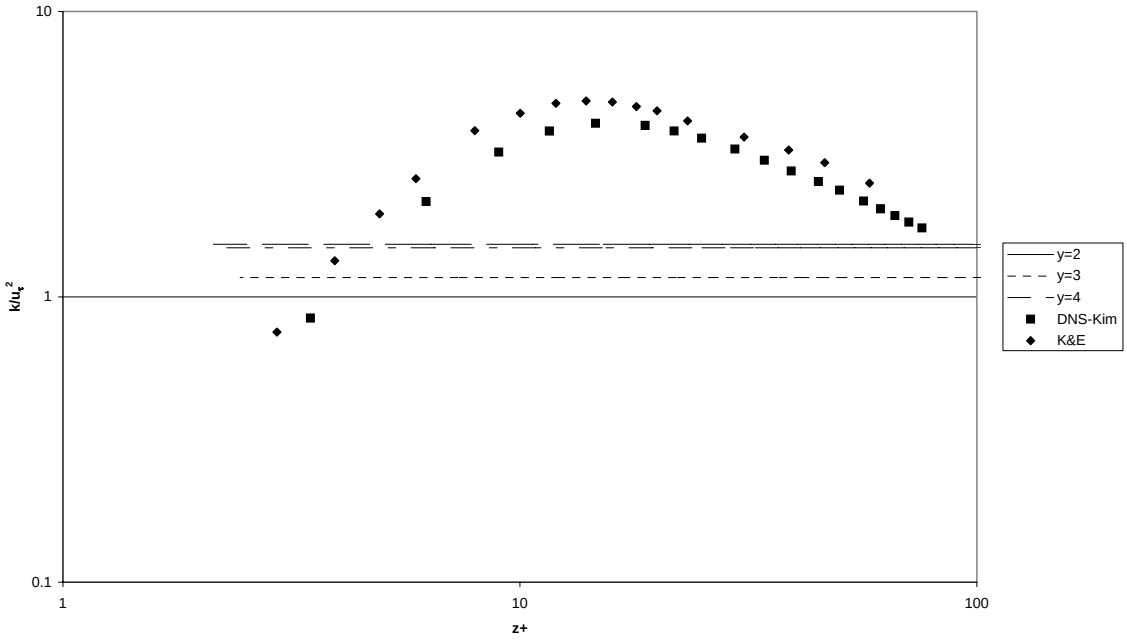

Figure 4.7: Turbulent kinetic energy normalized by the friction velocity (mix 0.1)

Figure 4.8 through Figure 4.17 gives the same velocity, velocity defect, and kinetic energy profiles for the 0.01 and 0.001 m. mixing length models as presented in Figure 4.3 through Figure 4.7 for the 0.1 m. mixing length. As will be discussed

later, there is little difference in any of the profiles between different mixing lengths, specifically for the velocity and velocity defect profiles. Thus, the observations made previously for such profiles in the 0.1 m. mixing length model are also applicable to the 0.01 m. and 0.001 m. models. The turbulent kinetic energy predicted for the 0.01 m. and 0.001 m. models are one and two orders of magnitude smaller than for 0.1 m. model, respectively. This is expected since the kinetic energy is a function of the mixing length squared. When the energy is normalized by the square of the friction velocity there is a one-to-one ratio of the normalized energy to the mixing length. While the magnitudes of the kinetic energy change with the different modeled lengths, the observations stated previously hold. The profiles predicted are again invariant with the cross-stream distance. Therefore, there is little difference between the interpretations of the different mixing length models.

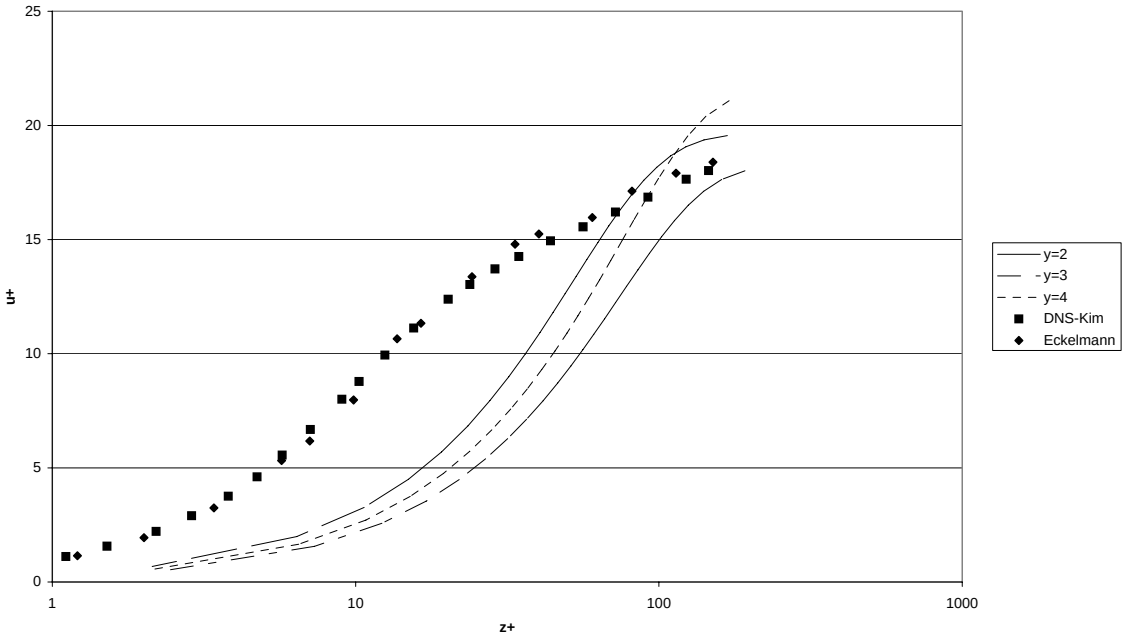

Figure 4.8: Velocity normalized by friction velocity over entire channel (mix 0.01)

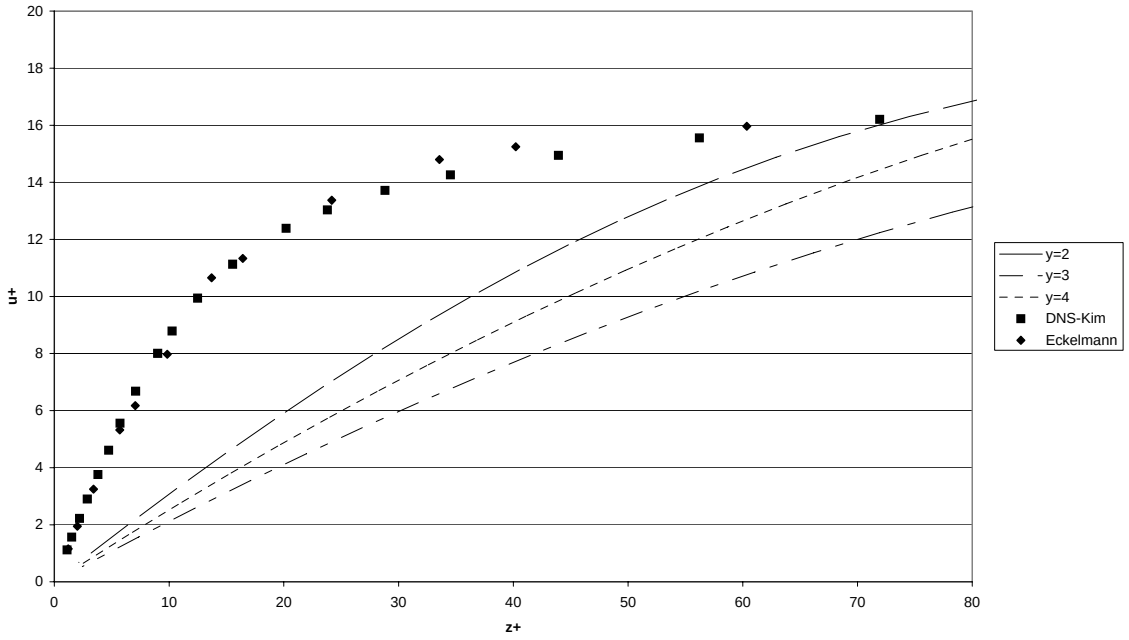

Figure 4.9: Mean velocity profile of channel close to wall (mix 0.01)

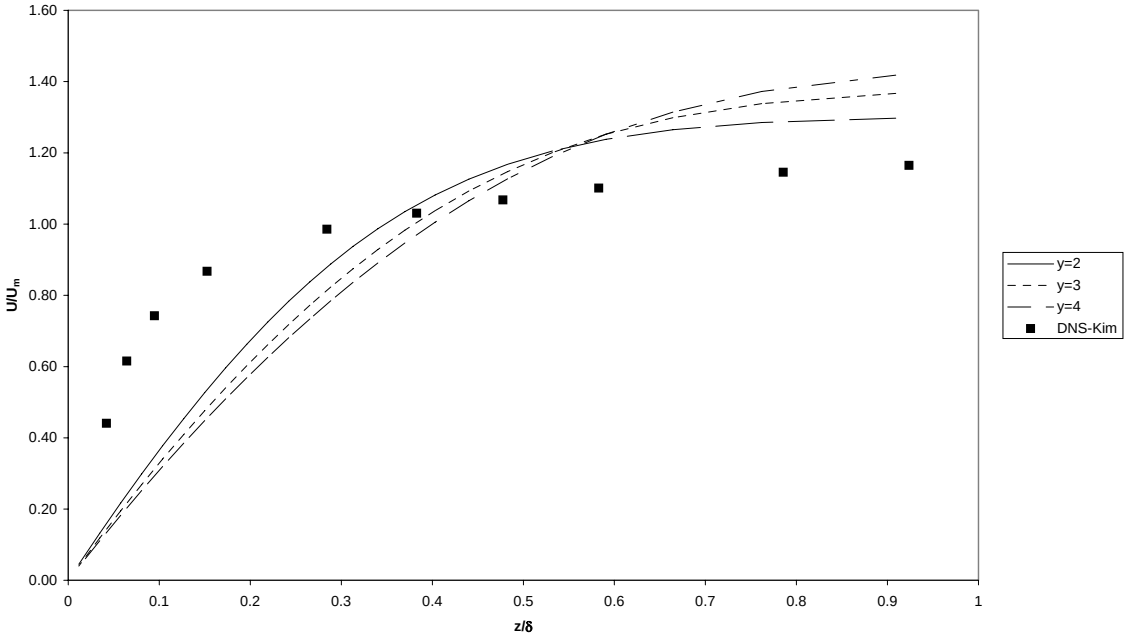

Figure 4.10: Velocity profile normalized by channel mean velocity (mix 0.01)

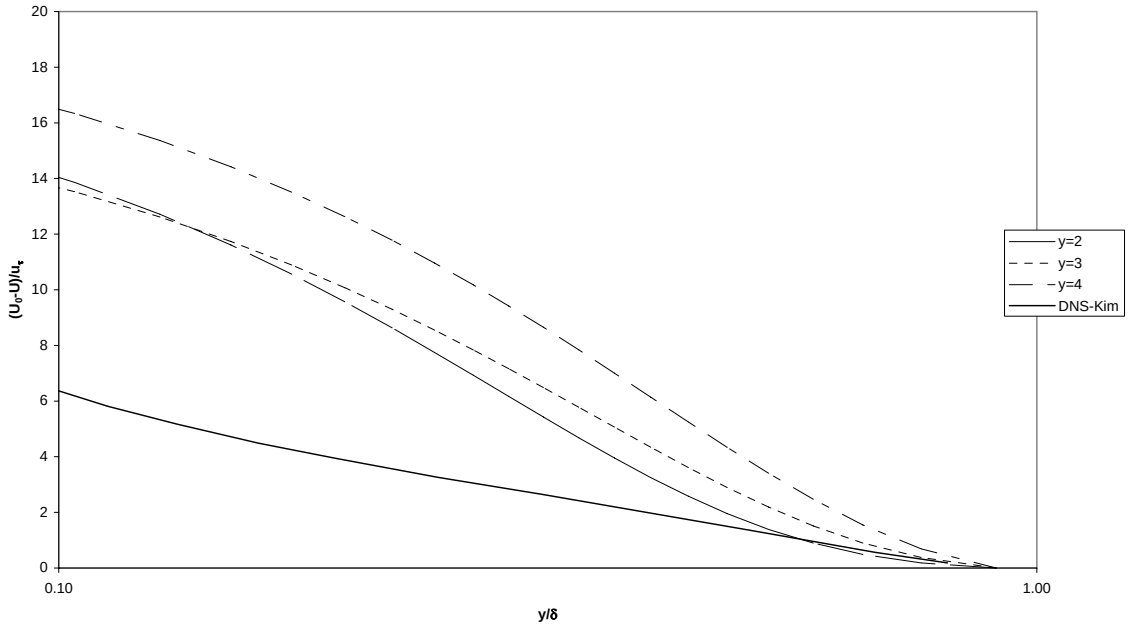

Figure 4.11: Mean velocity defect across channel (mix 0.01)

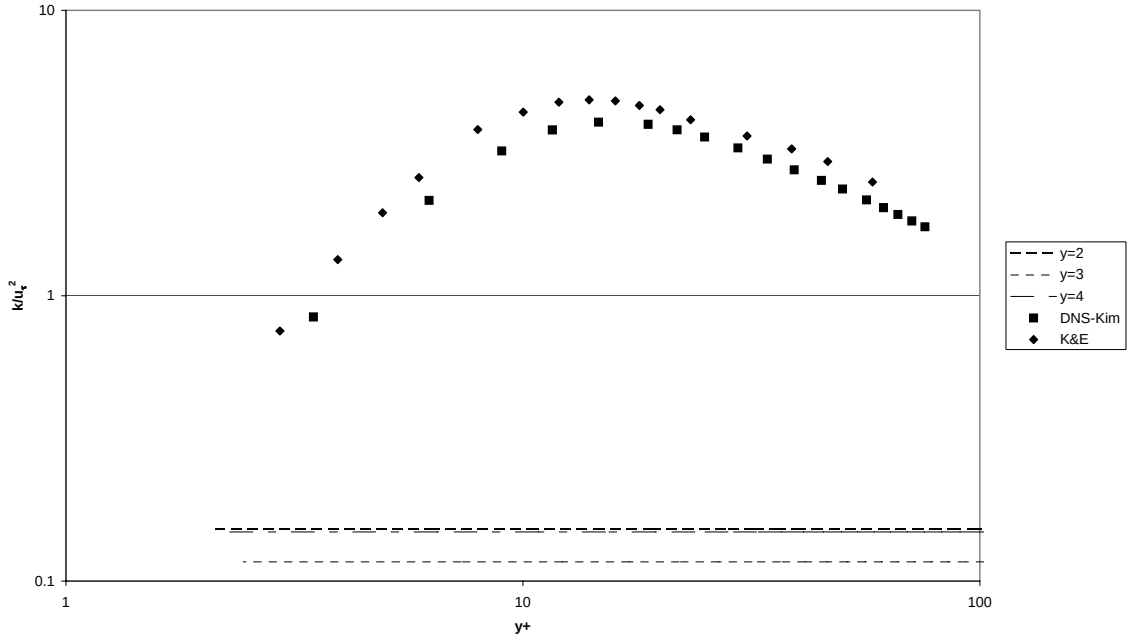

Figure 4.12: Turbulent kinetic energy normalized by the friction velocity (mix 0.01)

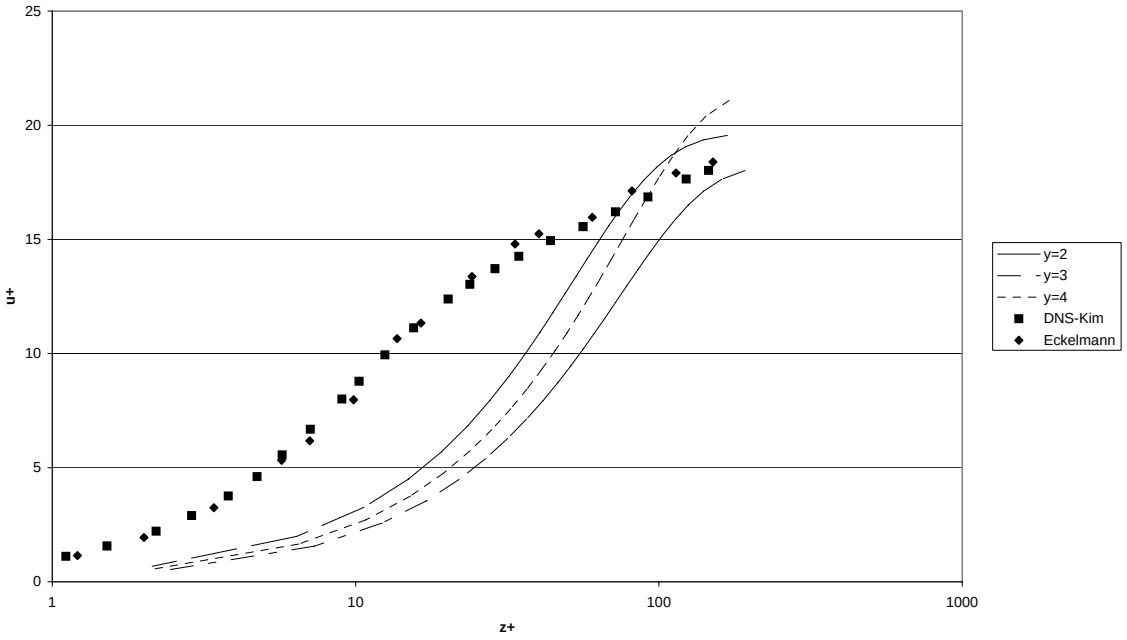

Figure 4.13: Velocity normalized by friction velocity over entire channel (mix 0.001)

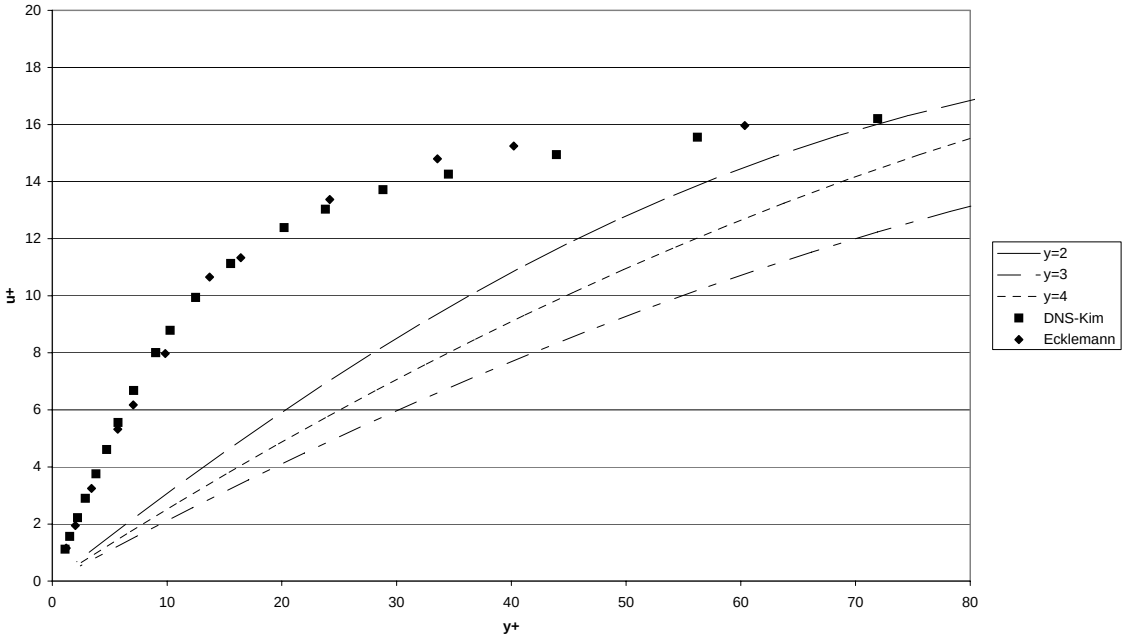

Figure 4.14: Mean velocity profile of channel close to wall (mix 0.001)

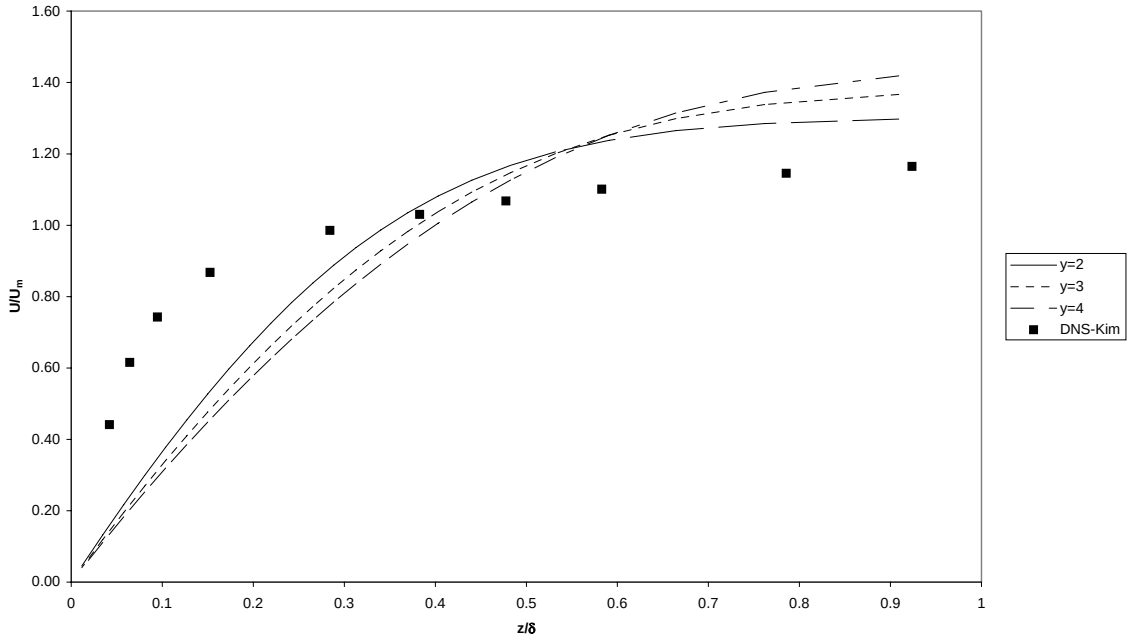

Figure 4.15: Velocity profile normalized by channel mean velocity (mix 0.001)

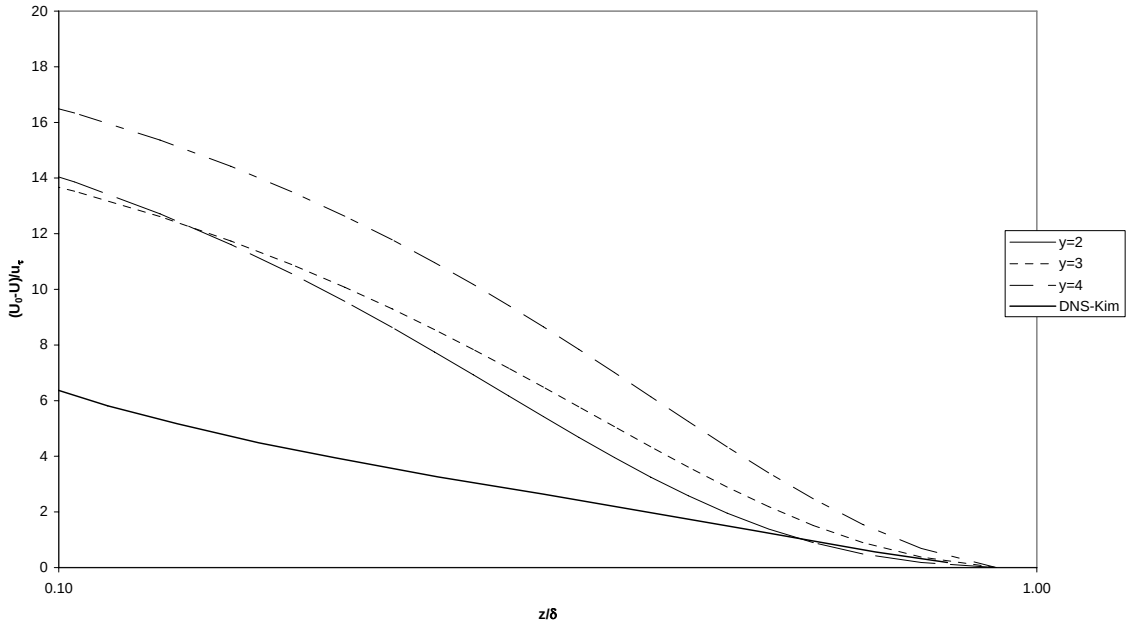

Figure 4.16: Mean velocity defect across channel (mix 0.001)

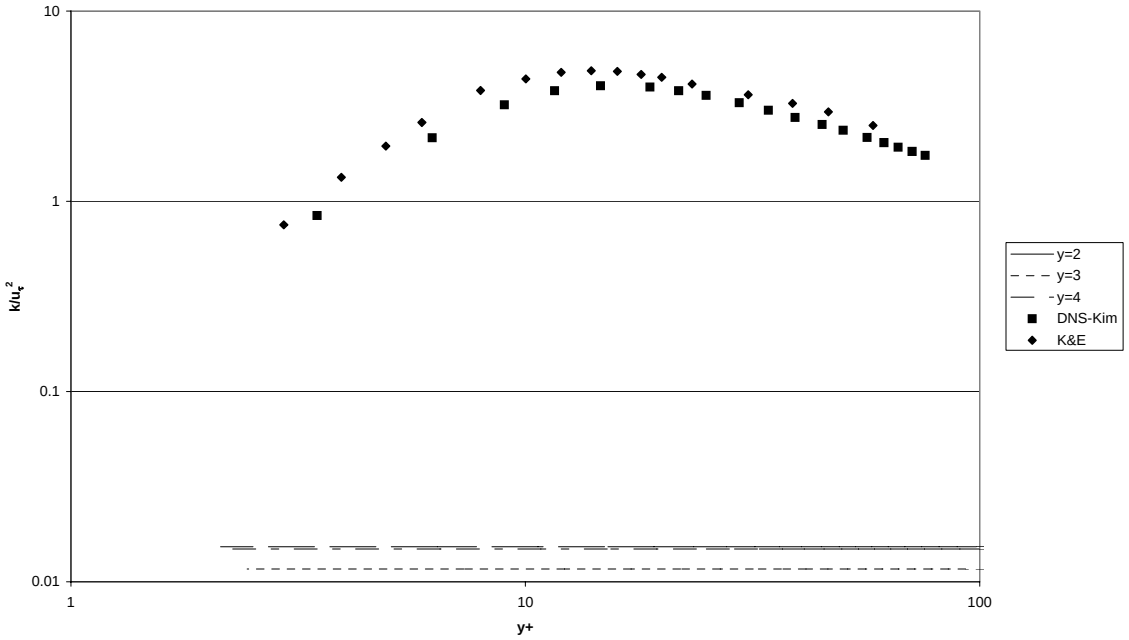

Figure 4.17: Turbulent kinetic energy normalized by the friction velocity (mix 0.001)

4.3.2. Standard k-ε model

GOTHIC results for the k-ε model are significantly better than those presented in the previous section for the mixing length models. As with the axi-symmetric jet, the computational time requirement for the k-ε model is significantly higher than for the mixing length models. For a transient time of 10 seconds, the computational time required for the k-ε model is 18.00 hours. Figure 4.18 gives the normalized velocity profiles for GOTHIC and the experimental and DNS data of Eckelmann and Kim, et. al., respectively. The profiles at y = 2 and y = 4 provide similar representations of the velocity profile. Toward the channel centerline both profiles are similar to that of the experimental data. These profiles also have a shape that is similar to the experimental data. In the near wall region, the experimental velocity profiles are concave with an inflexion point near a z^+ value of 10, with the curves becoming convex from this

point to the channel centerline. A similar feature is also seen in the GOTHIC profiles with the inflexion point near a z^+ value of 30. One significant difference between GOTHIC and experiment is that the GOTHIC velocity profiles appear damped. The GOTHIC data would fall much closer to a straight line (actually a logarithmic line since the abscissa is in logarithmic units) than the experimental data. A comparison of the velocity profiles in the region between the wall and $z^+ = 80$ is given on a linear graph in Figure 4.19. In the near wall region, particularly out to a z^+ value of 10, none of the k-ε model profiles provide a good representation of the experimental data. However, beyond this point the shape of the GOTHIC profiles is very similar to that of experiment. Offsetting the profiles by a u^+ value of approximately three on the ordinate would allow the profiles at $y = 2$ and $y = 4$ to nearly match the experimental data. Thus, while the magnitudes of the GOTHIC velocity predicted do not match the experimental data, the profile shapes are similar.

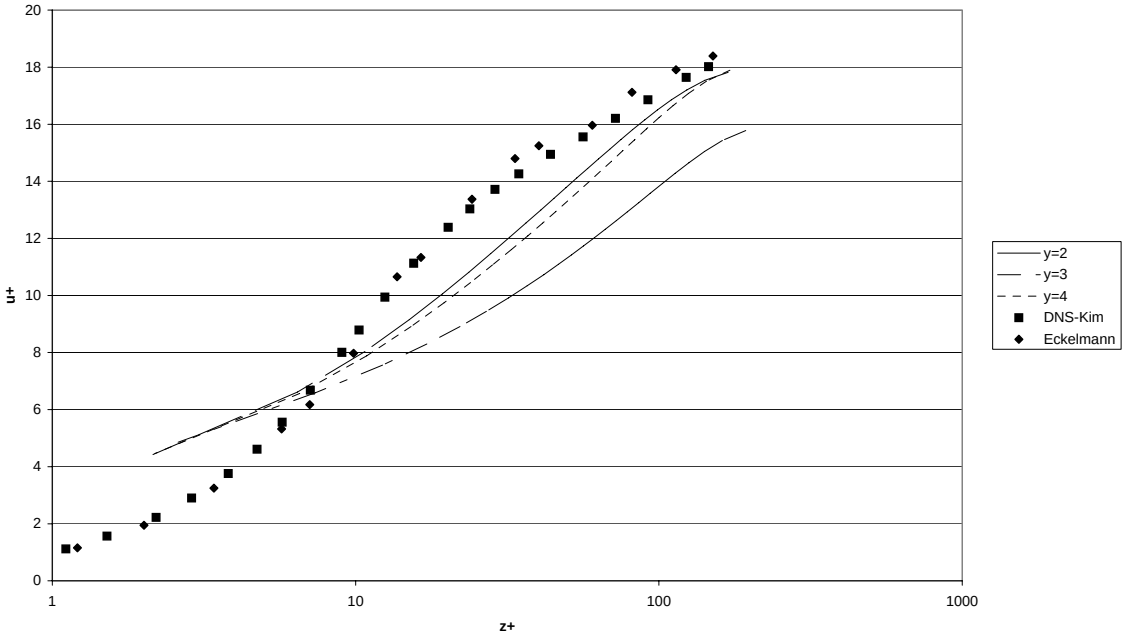

Figure 4.18: Velocity normalized by friction velocity over entire channel (k-ε)

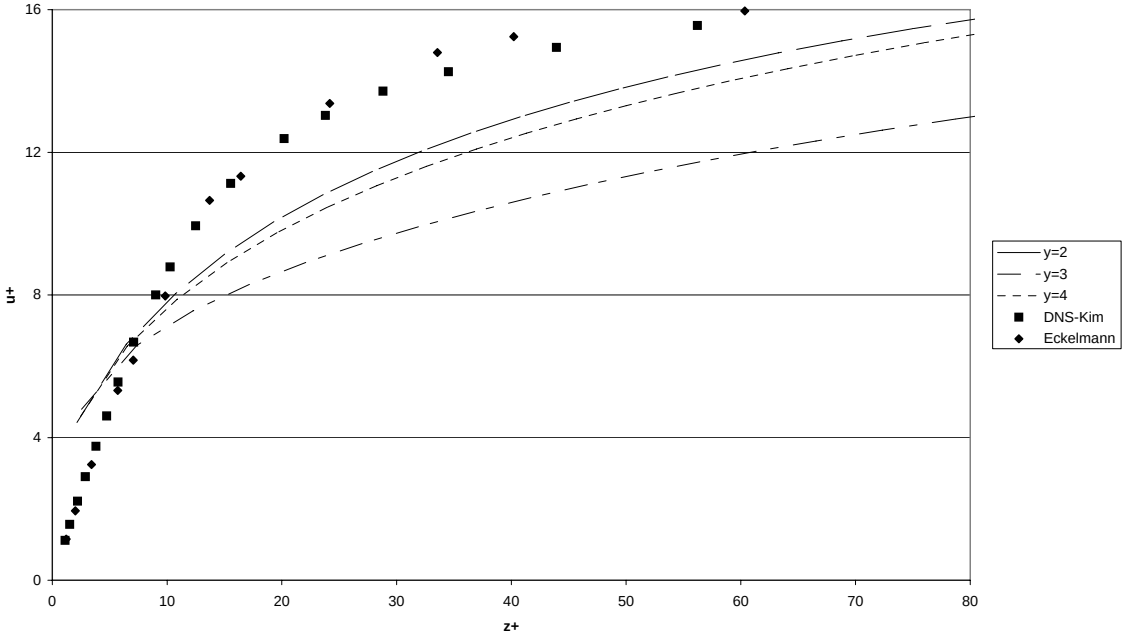

Figure 4.19: Mean velocity profile of channel close to wall (k-ε)

Another method of scaling the velocity is to divide it by the average velocity across the channel, U_m. Figure 4.20 gives the mean velocity scaled with this method. From the channel centerline to a z/δ value of 0.5 all the GOTHIC profiles coincide with the DNS data. At the channel centerline, the DNS predicts a U/U_m value of 1.16, which is consistent with experiment [13]. As one moves closer to the wall, a slow fluid deceleration predicted by GOTHIC flattens the velocity profile compared with the DNS data. This reemphasizes the findings presented in the previous paragraph. The scaled velocity defect profile, given in Figure 4.21, also shows all three GOTHIC profiles predict values similar to the DNS data. These finding support the claim that that GOTHIC's standard k-ε model can properly model the physics of channel flow.

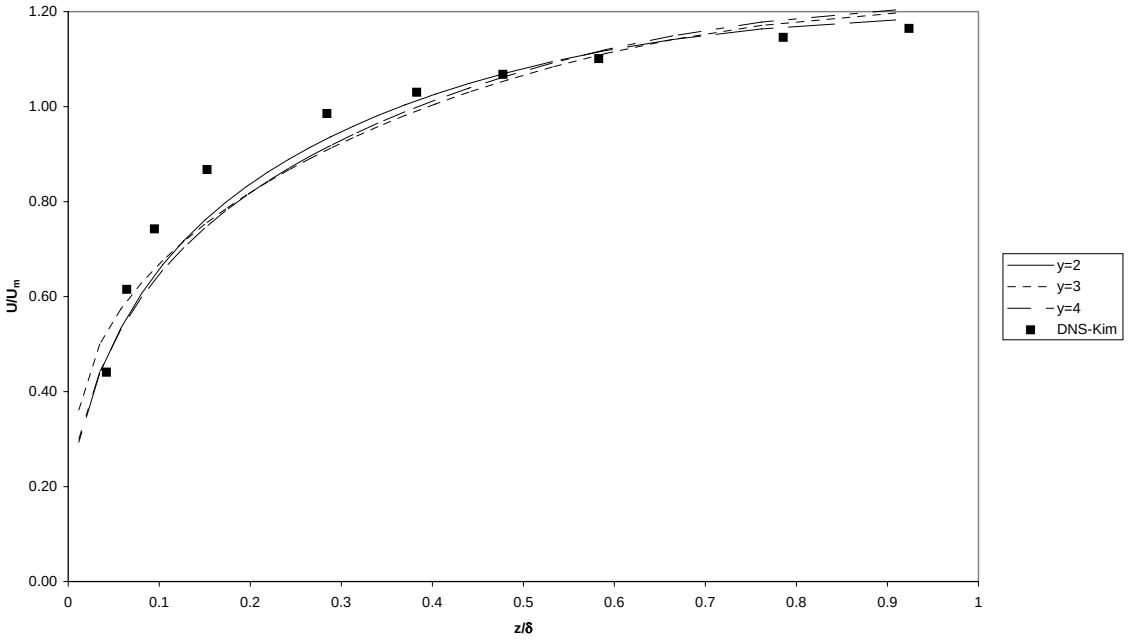

Figure 4.20: Velocity profile normalized by channel mean velocity (k-ε)

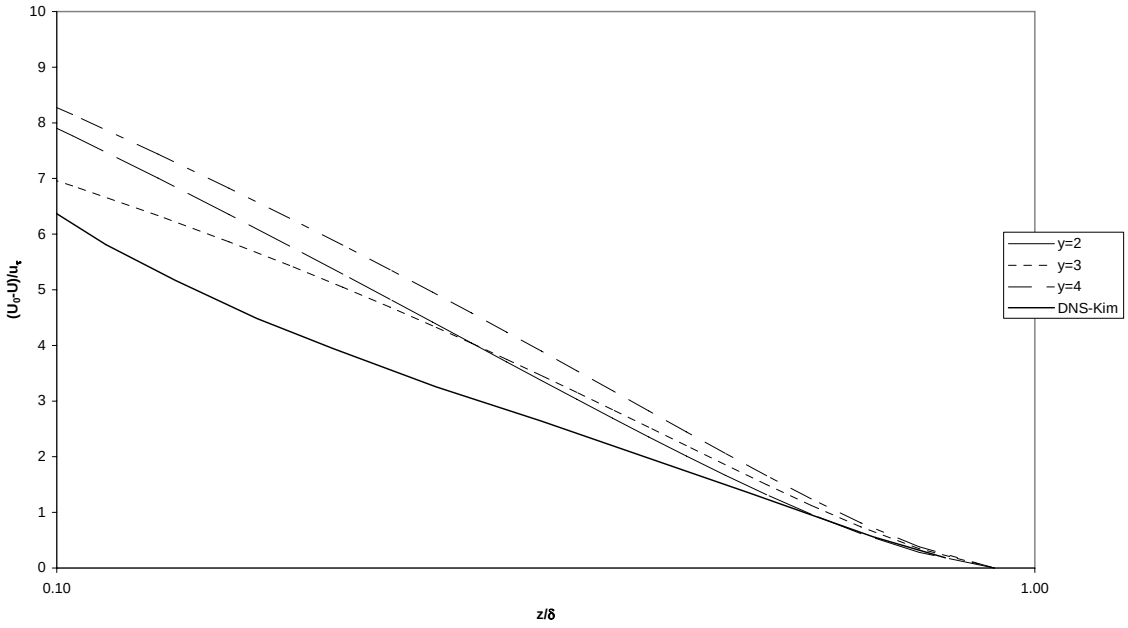

Figure 4.21: Mean velocity defect across channel (k-ε)

The k-ε model also does reasonably well at predicting the kinetic energy of the DNS data [13] and the experimental data of Kreplin and Eckelmann [14]. Figure 4.22 gives the experimental and GOTHIC profiles for the normalized turbulent kinetic energy. Here the DNS and experimental data are not even in good agreement with each other. The profile at y = 4 predicts a significantly larger energy than the y = 3 profile and experiment. The peak energy level predicted by the y = 3 GOTHIC profile is nearly identical to that of the experimental data. Additionally, the shape of the profile is similar to both the experimental and DNS data. The experimental data shows a faster reduction as it moves toward the channel centerline than the GOTHIC profiles. The experimental data also shows a nearly linear profile in the kinetic energy as one moves away from the peak. GOTHIC's k-ε model results show a parabolic shape, especially moving toward the centerline. Overall, however, the k-ε model predicts the experimental data reasonably well.

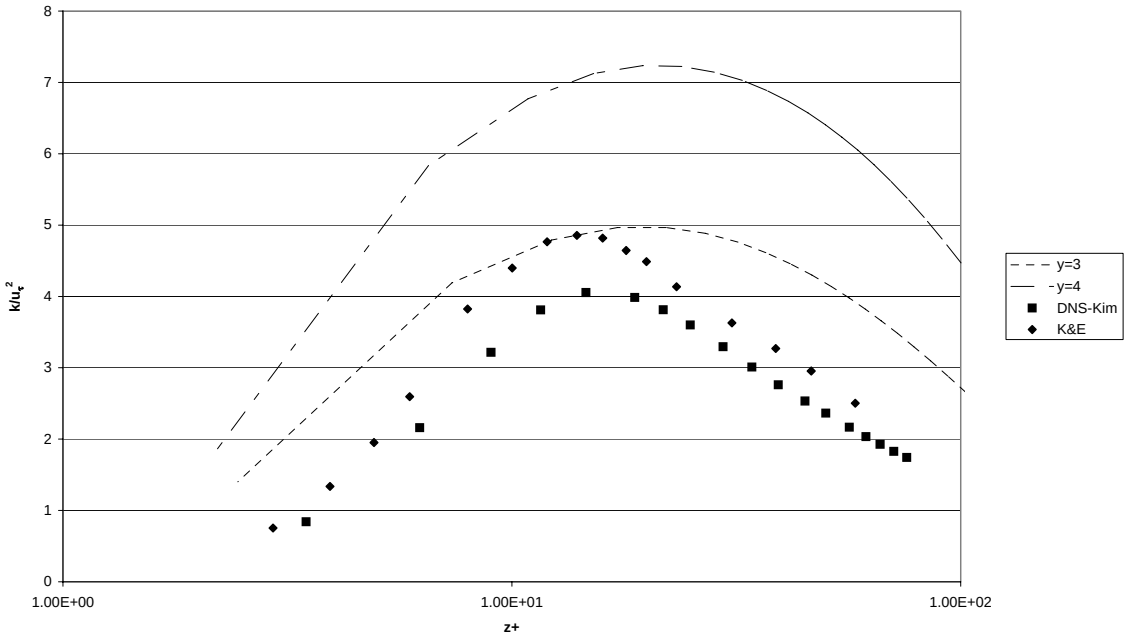

Figure 4.22: Turbulent kinetic energy normalized by the friction velocity (k-ε)

4.3.3. RNG k- ε model

The computational time required for a 10 second transient for the RNG model is 18.67 hours. This model takes the longest time to calculate the solutions of the three turbulence models analyzed here. The scaled velocity profile based on wall units for the entire channel half modeled is given in Figure 4.23. Of the GOTHIC profiles given, the one corresponding to y = 2 gives the best approximation of the experimental and DNS data, hereafter jointly referred to as experimental data except where explicitly discussed separately. Within the buffer region, defined by Pope [17] as $5 < z^+ < 30$, the y = 2 profile matches the experimental data well. Moving into the viscous sublayer near the wall, the GOTHIC profile over predicts the scaled velocity. From the channel centerline to the buffer region, the GOTHIC y = 2 profile also over predicts the velocity. The other GOTHIC profiles also predict scaled centerline and

near wall velocities that are too high. In the regions in between, the y = 3 and y = 4 profiles under predict the experimental velocities. However, neither of these downstream distances provides a profile that is consistent with experiment. However, the y = 2 profile does have a shape that is similar to that of experiment. From the wall to the cross-stream distance of $z^+ = 20$, the velocity profile is concave. From the inflexion point near $z^+ = 20$ to the channel centerline, the profile is convex. The profile shape is consistent with the experimental data, although the experimental inflexion points are near $z^+ = 10$.

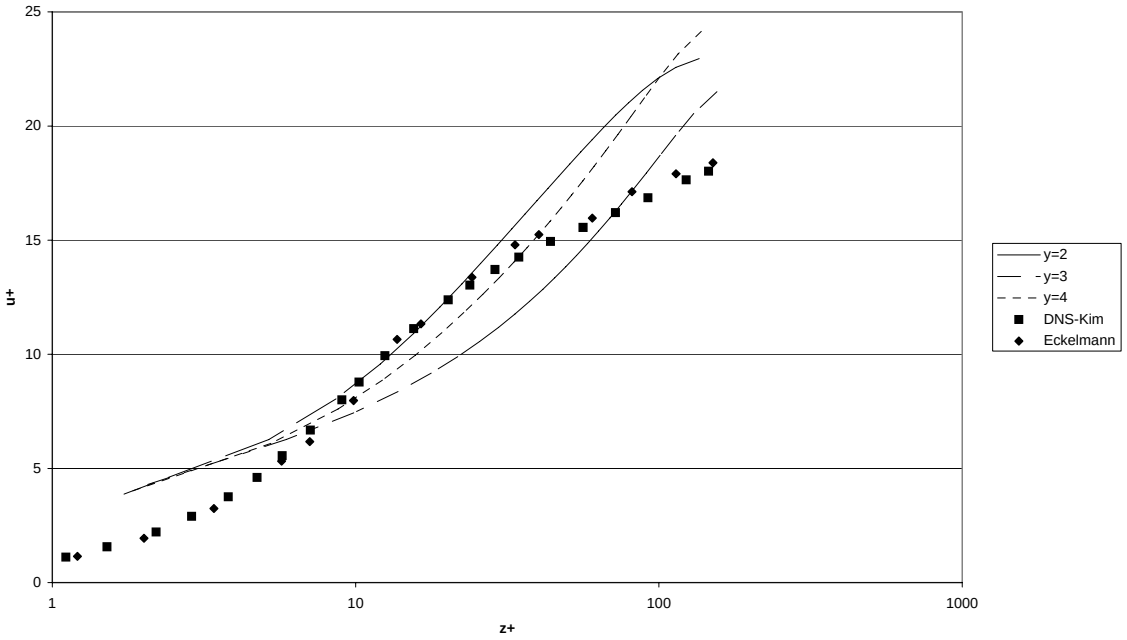

Figure 4.23: Velocity normalized by friction velocity over entire channel (RNG)

The same velocity profiles are plotted on a linear abscissa in Figure 4.24. As documented above, the y = 2 profile gives the best approximation of the experimental data. The slope of the velocity profile, particularly from the wall to $z^+ = 20$, is predicted reasonably well by the GOTHIC RNG model. Beyond this point, the slope

of the experimental data is much shallower than predicted by GOTHIC. The other cross-stream profiles at y = 3 and y = 4 give velocity profiles that are much flatter than experiment and the y = 2 profile. Thus, of the three cross-stream profiles given for the GOTHIC RNG model, the y = 2 profile is most consistent with the experimental and DNS data.

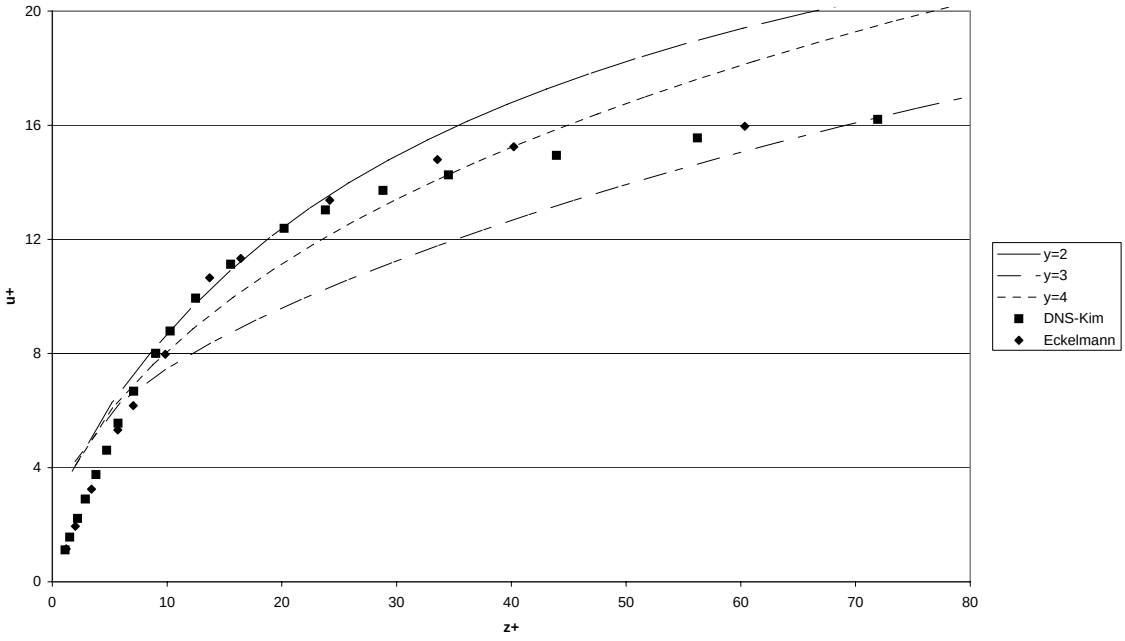

Figure 4.24: Mean velocity profile of channel close to wall (RNG)

As previously documented for the mixing length and k-ε models, rescaling the velocity profile with the average channel velocity for the RNG model also gives further insight into the accuracy of the model. These rescaled velocity profiles are given in Figure 4.25. The cross-stream profile at y = 2 gives the closest approximation to the experimental data. However, all of the GOTHIC profiles predict sharper increases in velocity from $z/\delta = 0.5$ to the channel centerline. From $z/\delta = 0.5$ to the wall, the GOTHIC profiles are much shallower than the experimental

data. A review of the scaled velocity defect (Figure 4.26) profiles shows a significant variation in the GOTHIC and experimental data. The GOTHIC and experimental profiles all show the same intersection on the x-axis. However, as one moves toward the wall, a noticeable difference in the GOTHIC profiles' magnitudes and shapes, as compared to each other and the experimental data, is apparent.

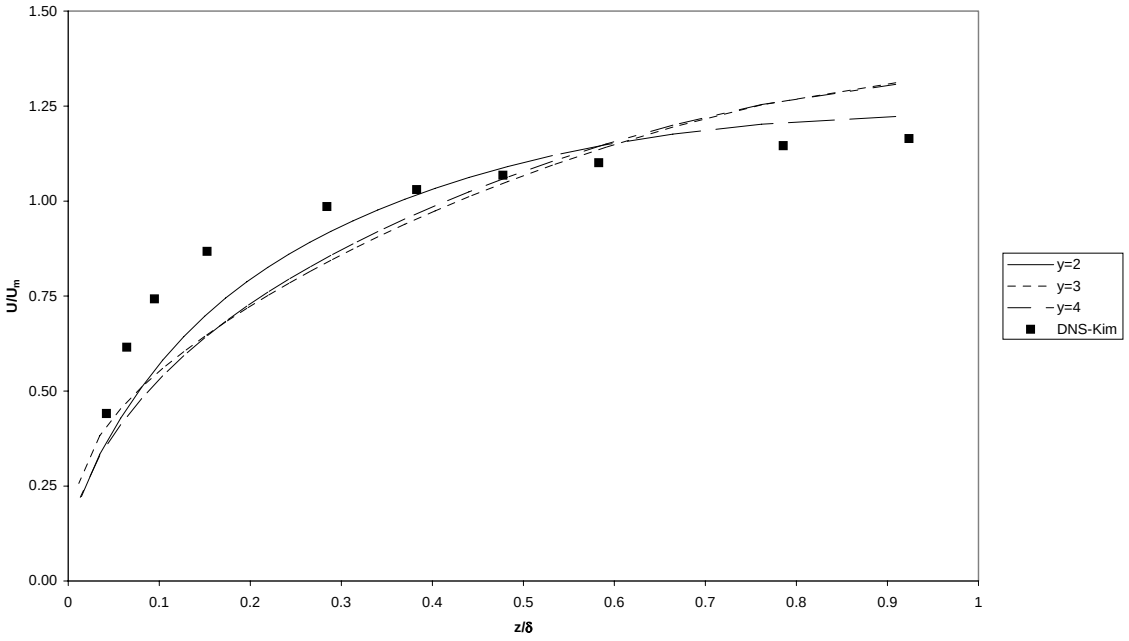

Figure 4.25: Velocity profile normalized by channel mean velocity (RNG)

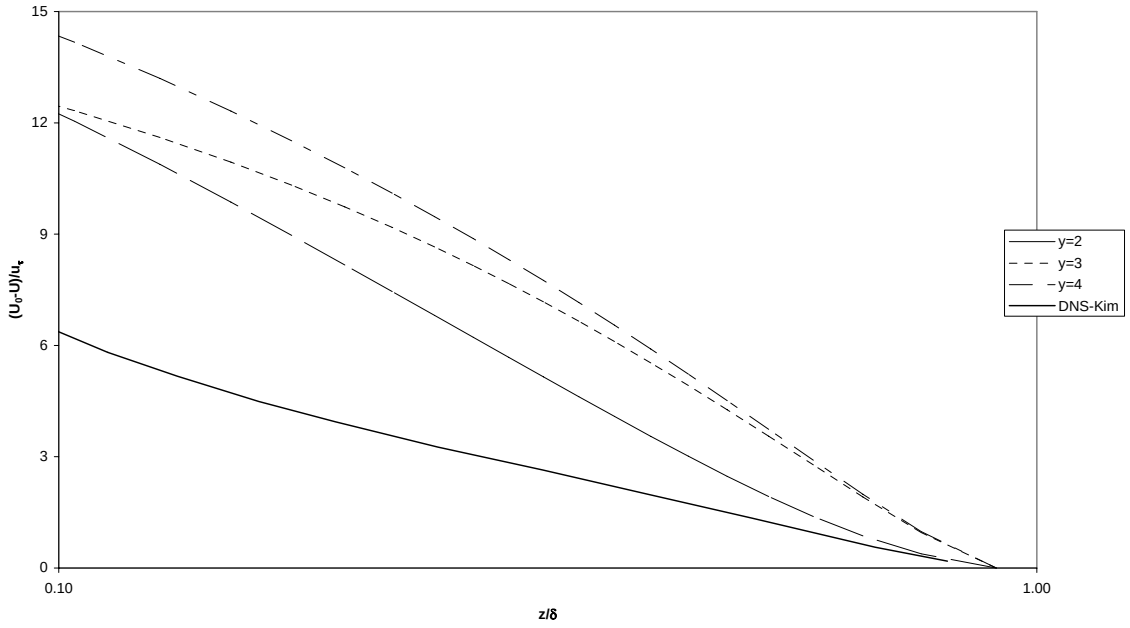

Figure 4.26: Mean velocity defect across channel (RNG)

The RNG model does reasonably well at predicting the kinetic energy of the DNS data [13] and experimental data of Kreplin and Eckelmann [14]. Figure 4.27 gives the experimental and GOTHIC profiles for the normalized turbulent kinetic energy. The profile at y = 4 predicts a significantly larger energy than the y = 3 profile and experiment, as the k-ε model also did. The peak energy level predicted by the y = 3 GOTHIC cross-stream profile is very close to the experimental data. The shape of the profile is also similar to that of the experimental data, although GOTHIC predicts a slower reduction in the kinetic energy as one progresses away from the peak energy level in both directions. Overall, however, the RNG model predicts the experimental data reasonably well.

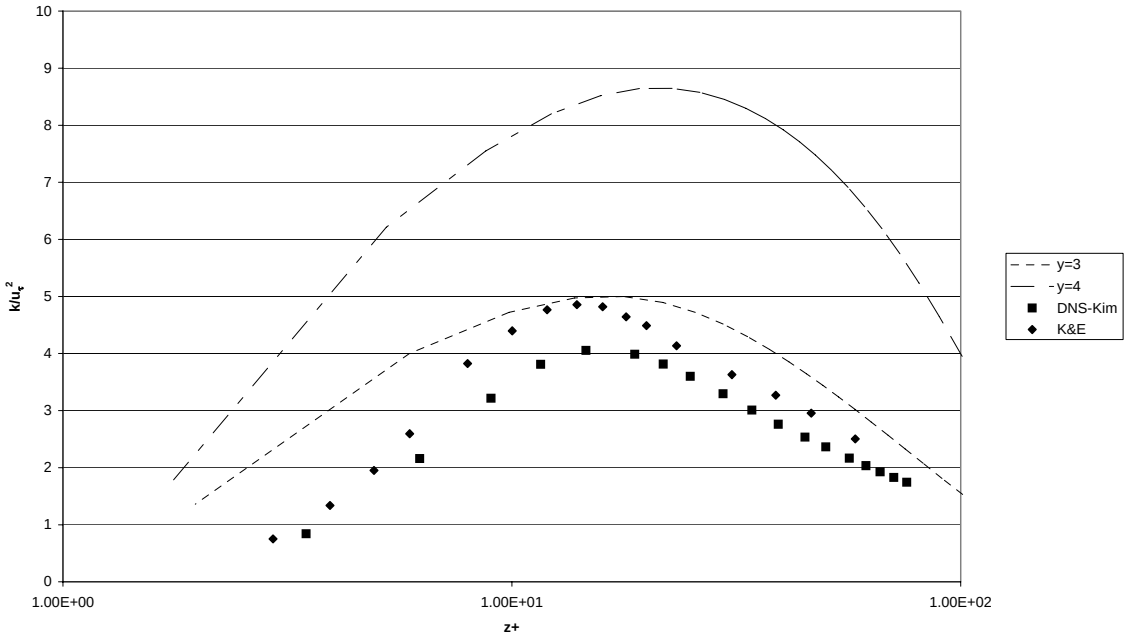

Figure 4.27: Turbulent kinetic energy normalized by the friction velocity (RNG)

4.3.4. Comparison between turbulence models

In Sections 4.3.1 through 4.3.3, comparisons of each of the turbulence models were made to experimental data for the channel flow. The figures in these sections showed various cross-stream velocity and turbulent kinetic energy profiles for different downstream distances from the channel entrance. In this section we will compare the flow properties for each of the models with each other and experimental data. This will allow us to make easier determinations about each model's strengths and weaknesses as they relate to the modeling of the channel flow.

Figure 4.28 gives the cross-stream scaled velocity profile for the downstream distance at y = 2. As was detailed in Section 4.3.1, there is little variation in the profiles produced by the three different mixing lengths. This is evidenced in the figure below in that the three mixing length profiles essentially lie on top of each

other. Despite the simplistic modeling for the mixing length models, the predicted centerline velocity of the mixing length models nearly matches the experimental/DNS data. This is not surprising since the mixing length model was developed for modeling flow over a flat plate [20]. However, for the downstream distance of y = 2, the profile predicted by the standard k-ε model most closely matches the experimental data. From the wall until $z^+ \sim 8$, the RNG and k-ε models give the same velocity. Beyond this point, they diverge considerably with the RNG model predicting a much higher velocity than the other models and experiments. For the downstream profiles at y = 4 (Figure 4.30), the same general observations noted above for y = 2 also hold. The exception to this is that the centerline velocities predicted by the mixing length models now diverge significantly from experiment. Figure 4.29 gives the velocity profiles for the cross-stream profiles at y = 3. At this distance, none of the models give a good representation of the experimental/DNS data although the mixing length centerline velocity closely matches the experimental centerline velocity. An overall comparison of the three downstream distances shows that the standard k-ε model provides the best prediction of the experimental and DNS data velocity profiles for the channel flow.

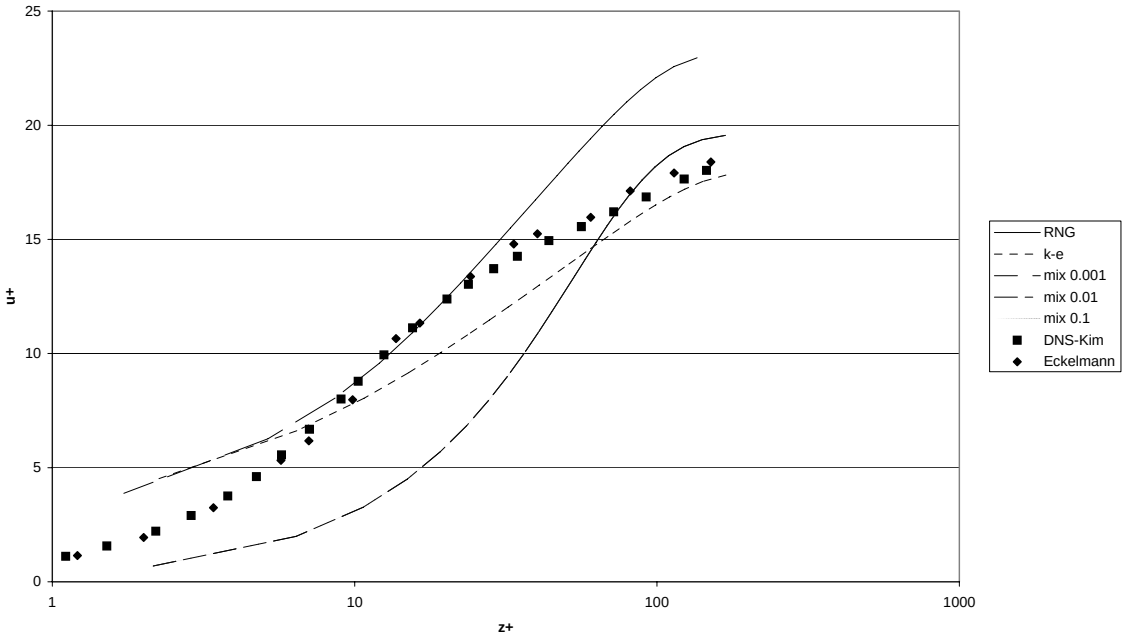

Figure 4.28: Comparison of normalized velocity for different models (y=2)

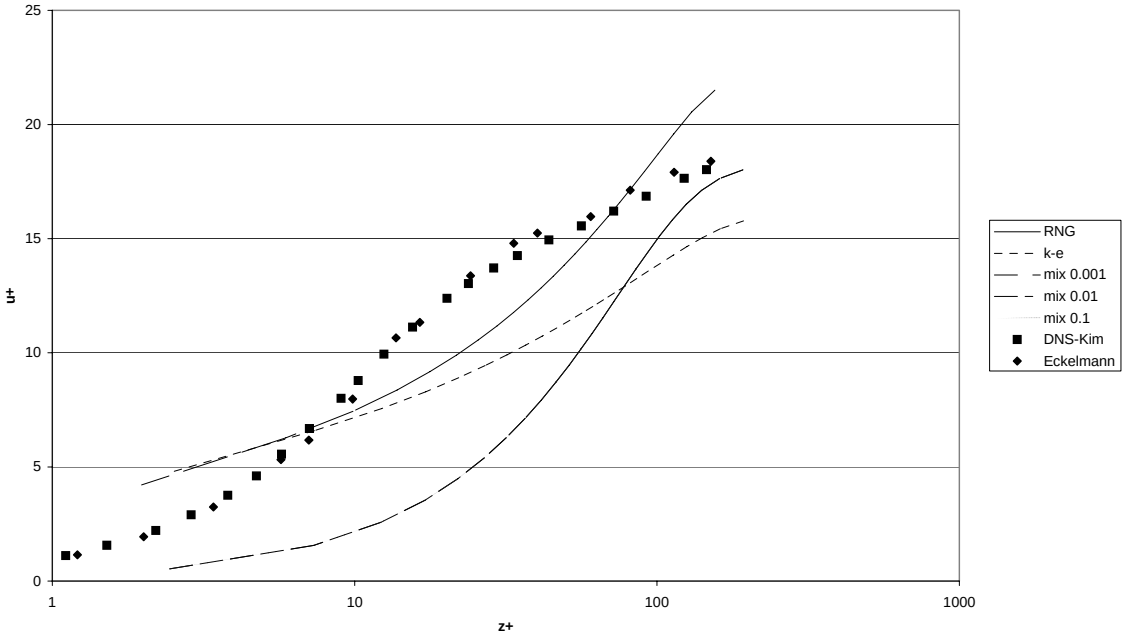

Figure 4.29: Comparison of normalized velocity for different models (y=3)

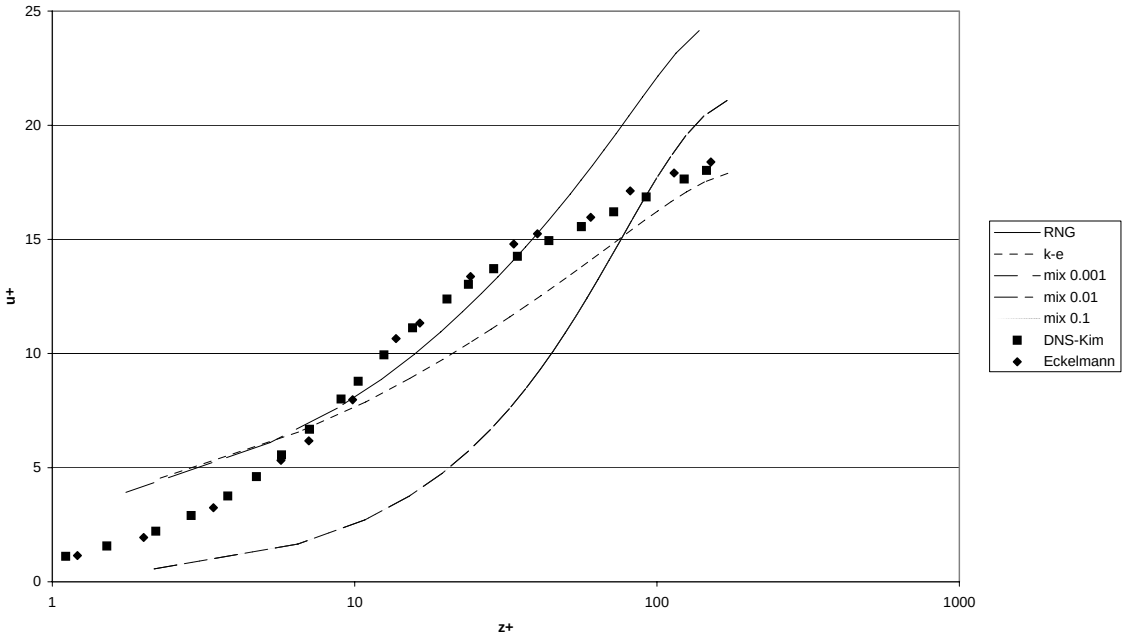

Figure 4.30: Comparison of normalized velocity for different models (y=4)

Figure 4.31, Figure 4.32, and Figure 4.33 give the velocity profiles closer to the wall for the downstream distances at y = 2, y = 3, and y = 4, respectively. In the buffer layer, the RNG model provides the best representation of the experimental and DNS data based on a review of these graphs. Over the range of z^+ values of 30 to 80, the standard k-ε model gives the most accurate shape and magnitude when compared with experiment. In this region, none of the mixing length models give a realistic calculation of the velocity profile. The velocities predicted by these models are significantly smaller over much of the range presented and the shape of the curve differs significantly from experiment. The results presented by these figures provide two conclusions: 1) the RNG model gives the most accurate velocity profile in the buffer layer, and 2) the k-ε model provides the best velocity representation from the buffer layer to the channel centerline.

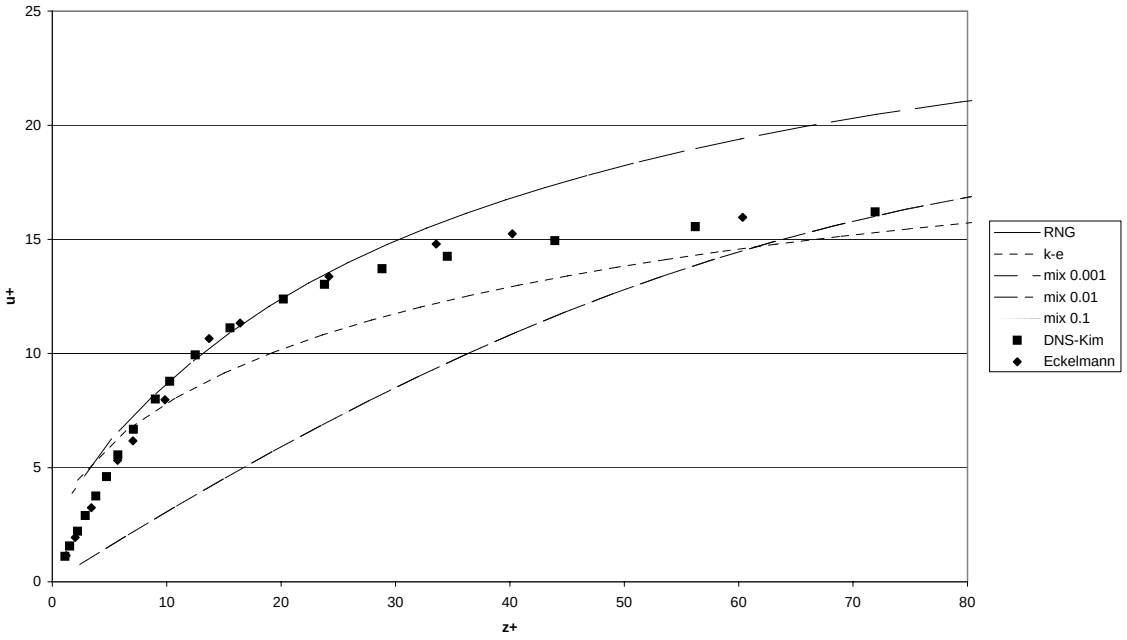

Figure 4.31: Comparison of normalized velocity (near wall) for different models (y=2)

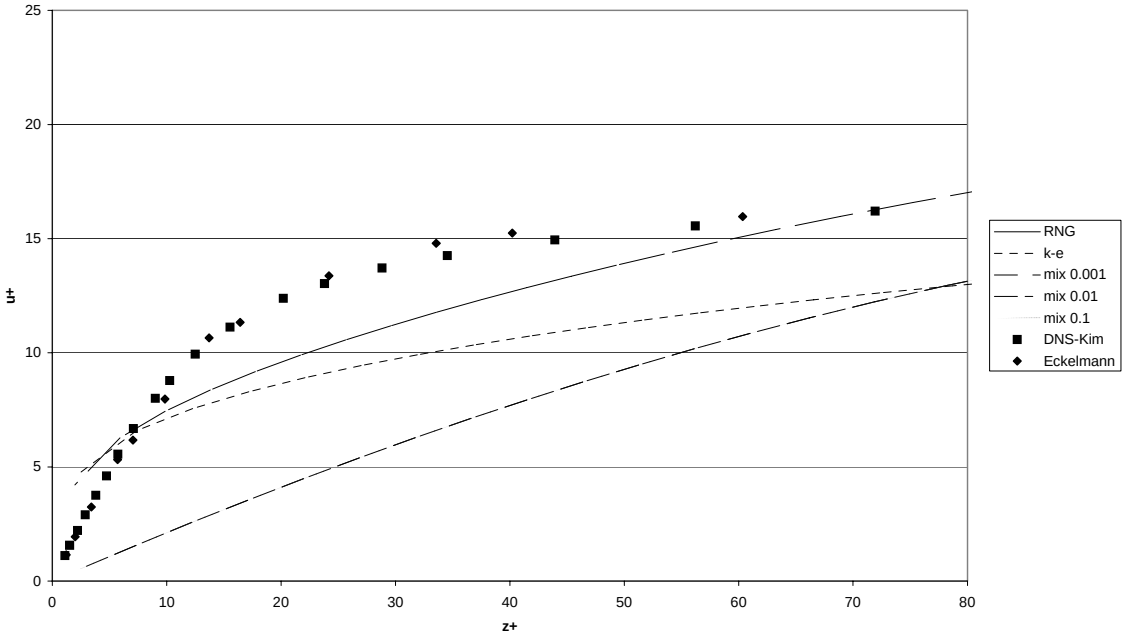

Figure 4.32: Comparison of normalized velocity (near wall) for different models (y=3)

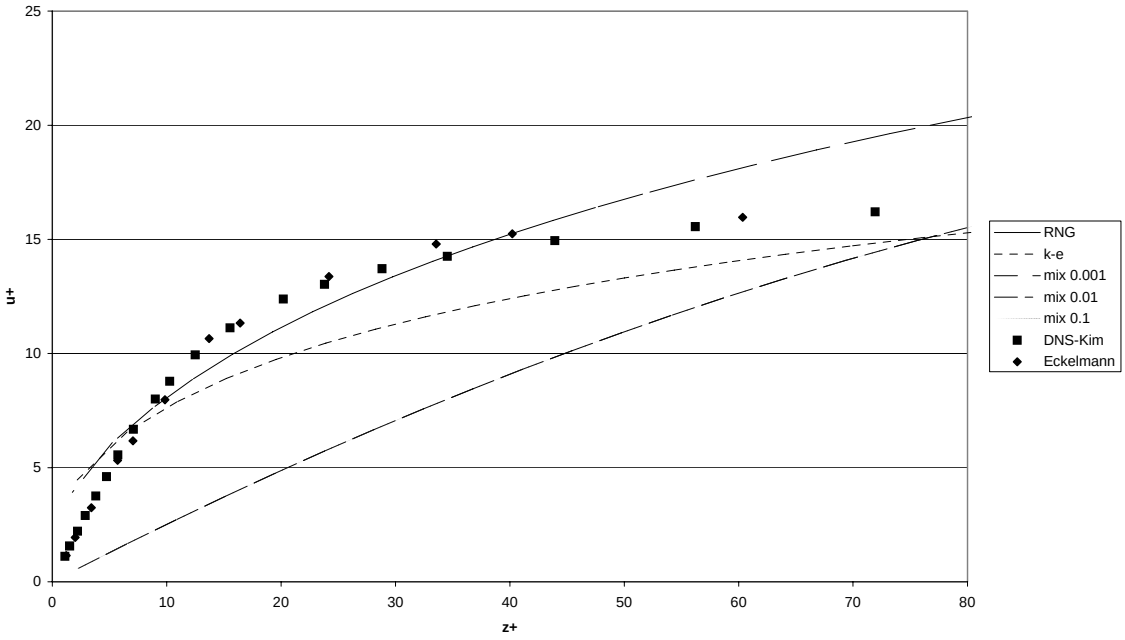

Figure 4.33: Comparison of normalized velocity (near wall) for different models (y=4)

As was done previously for each of the individual turbulence models in the prior sections, the average channel velocity is used to normalize the cross-stream velocities at various downstream distances. Figure 4.34 through Figure 4.36 give these velocity profiles for downstream distances at y = 2, 3, and 4. From z/δ at 0.35 to the centerline, the mixing length models over predict the velocity while significantly under predicting the velocity closer to the wall. The same can be stated for the RNG model except that the intersection point of the experimental and GOTHIC data occurs closer to a z/δ of 0.50. Over the majority of the channel, the k-ε model predicts a slightly smaller velocity than experiment. However, the magnitude and shape of the k-ε profile is very close to that of experiment, particularly toward the channel centerline. Thus, using this normalization of the velocity profile, the k-ε model most accurately predicts the channel velocity profile for all downstream distances.

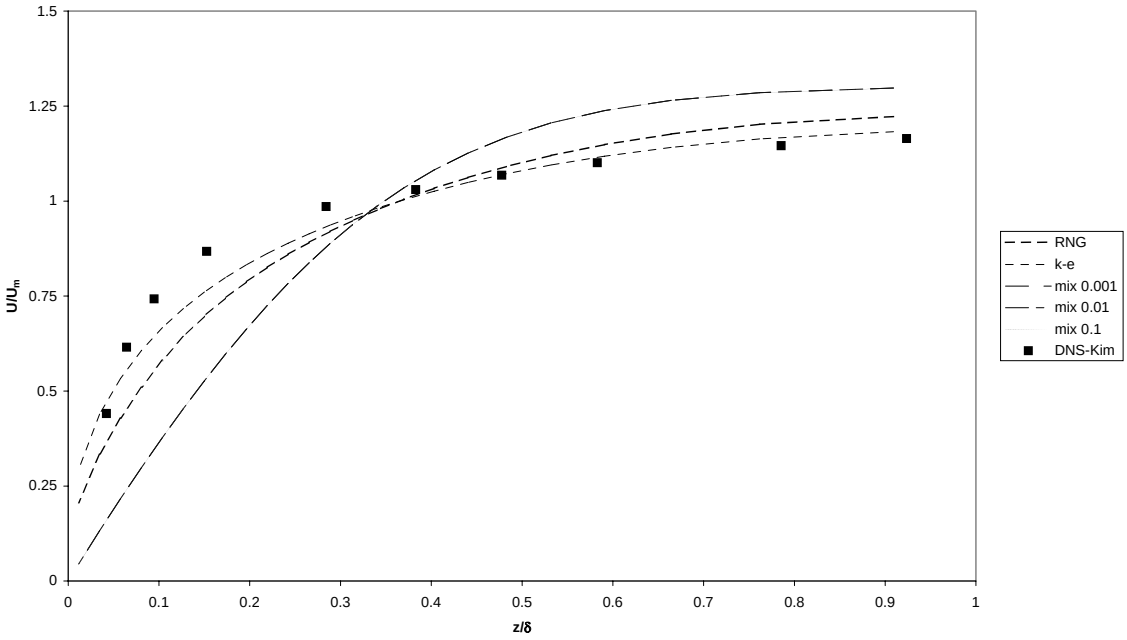

Figure 4.34: Comparison of velocity profiles normalized by channel mean velocity for different models (y=2)

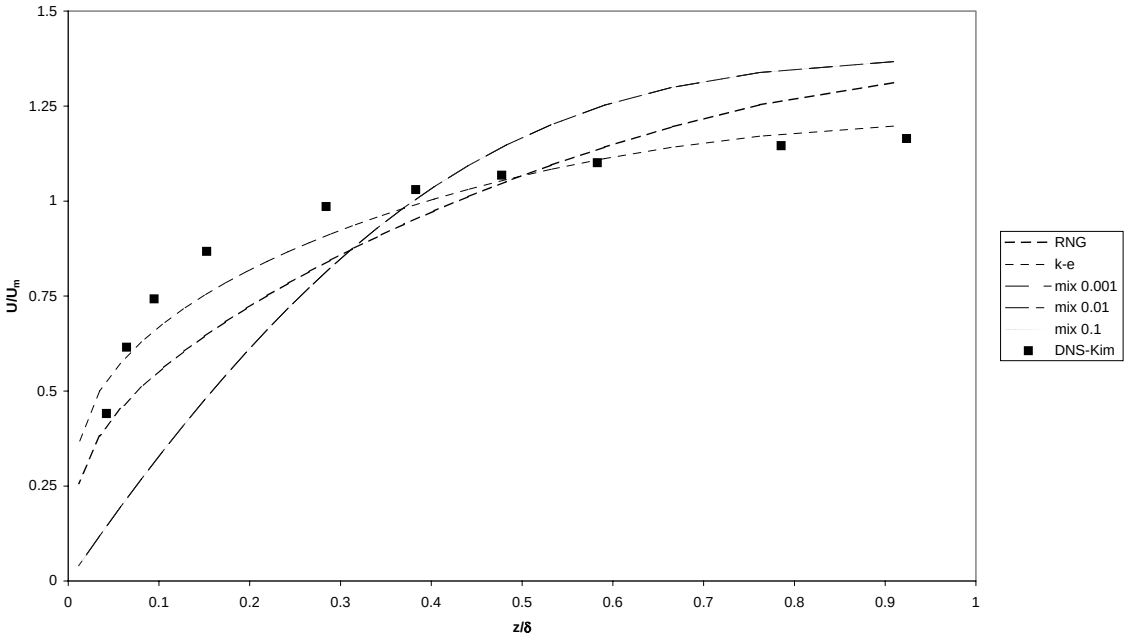

Figure 4.35: Comparison of velocity profiles normalized by channel mean velocity for different models (y=3)

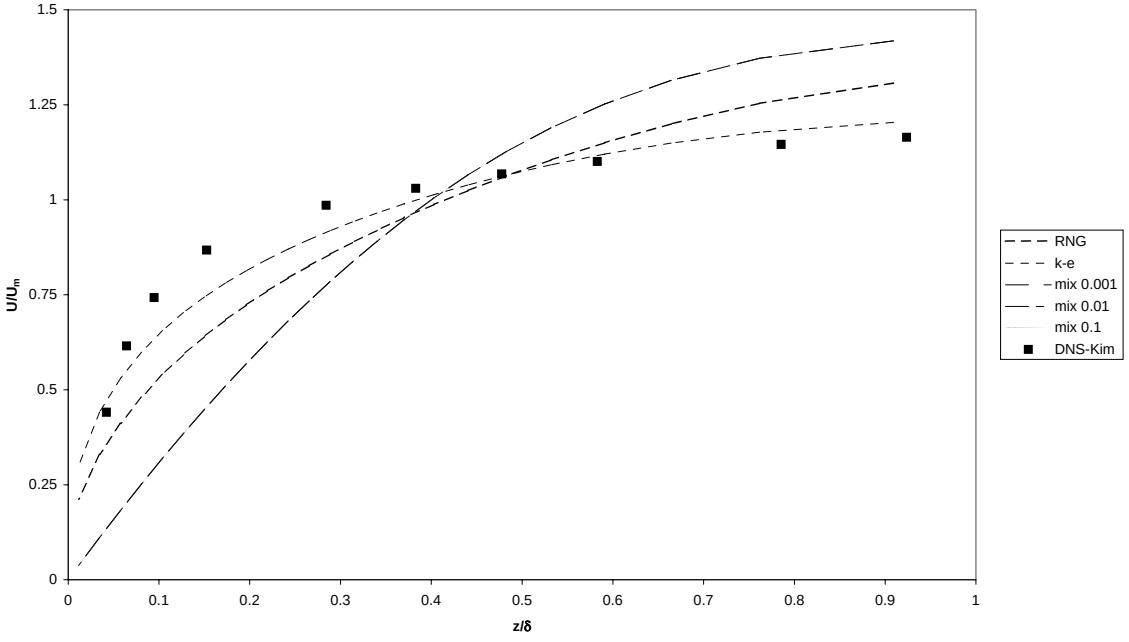

Figure 4.36: Comparison of velocity profiles normalized by channel mean velocity for different models (y=4)

Comparisons of the normalized velocity defects are given in Figure 4.37, Figure 4.38, and Figure 4.39. A significant difference between the data provided in these figures and those provided previously in Section 4.3.1 thorough 4.3.3 is that these graphs give profiles from z/δ values of 0.01 to 1.0 whereas the previous figures only provided data from 0.1 to 1.0. As with the other data given for the mixing length models, the profiles for each of the mixing lengths are nearly identical. For the profiles at $y = 2$ and $y = 4$, the standard k-ε model gives the best representation of the experimental data magnitudes. A review of all the GOTHIC profiles given in Figure 4.37 through Figure 4.39 shows that none of them reproduces the shape of the experimental data. Moving from the centerline toward the wall, the experimental profile starts with a convex shape with an inflexion point near $z/\delta = 0.05$. From this point to the wall, the velocity defect is concave. Of the 15 profiles given in the referenced figures, only four have even have an inflexion point. Most of the profiles are concave in shape and those that have an inflexion point show it being much closer to the centerline than the DNS data. Thus, while the k-ε model most accurately duplicates the magnitude of the velocity defect, none of the models accurately predict the shape of the profile.

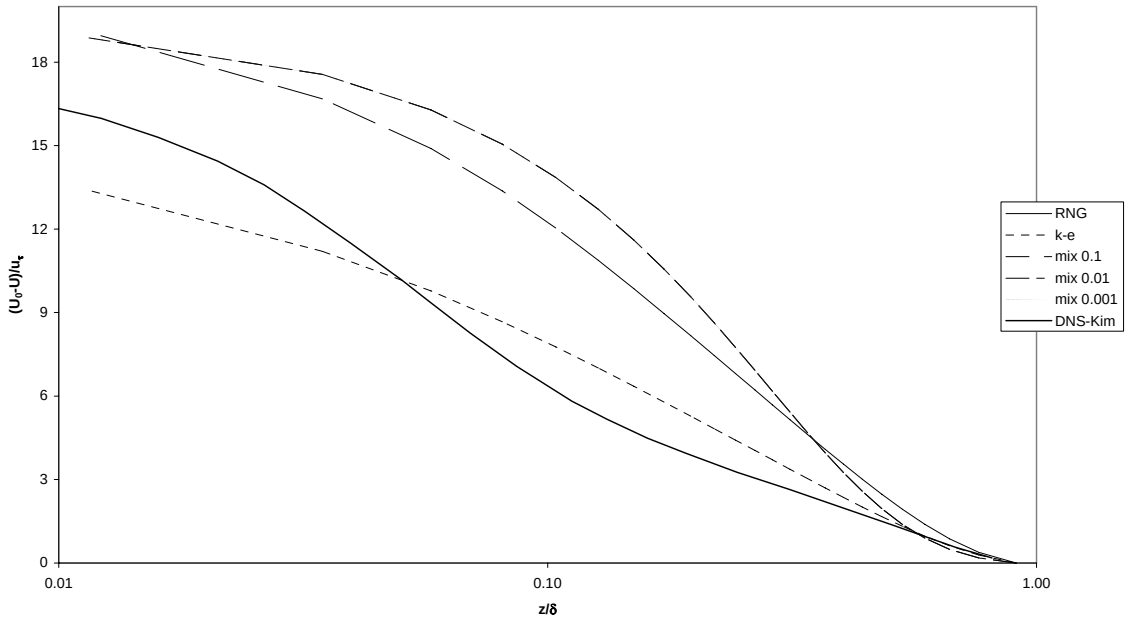

Figure 4.37: Comparison of mean velocity defect across channel for different models (y=2)

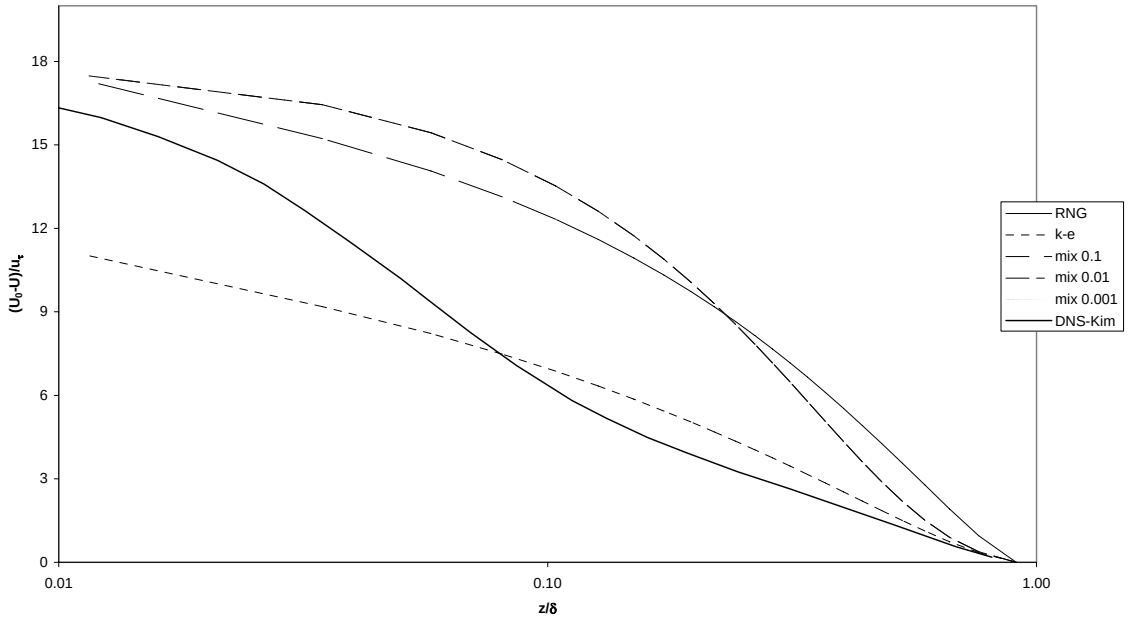

Figure 4.38: Comparison of mean velocity defect across channel for different models (y=3)

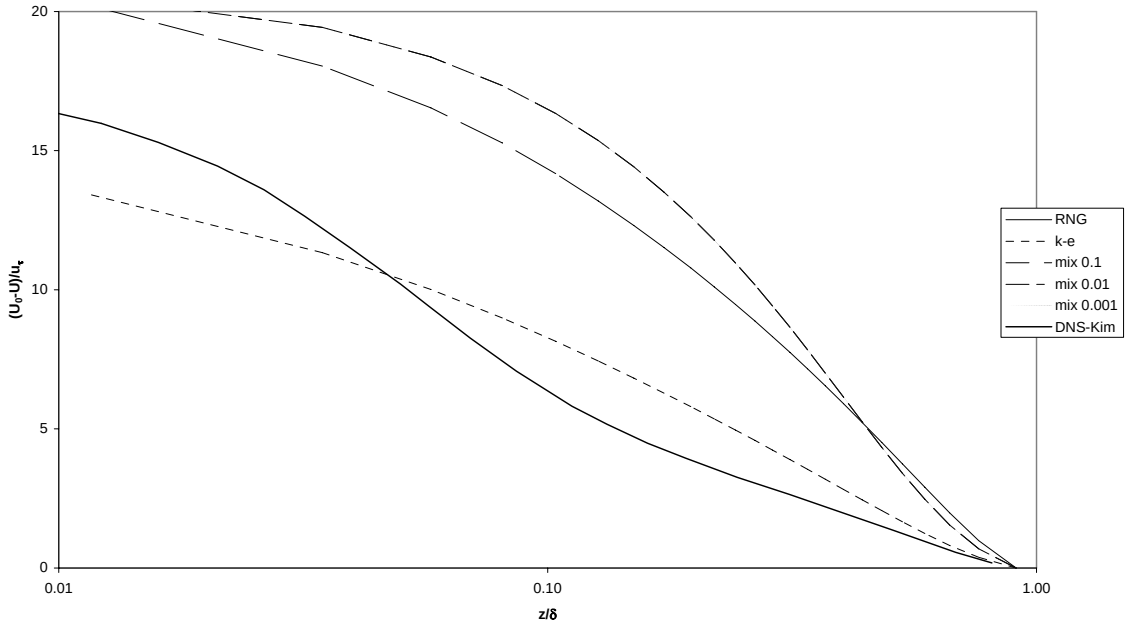

Figure 4.39: Comparison of mean velocity defect across channel for different models (y=4)

The kinetic energy profiles for the GOTHIC and experimental results are given in Figure 4.40 and Figure 4.41, below. As discussed previously, the mixing length models do not give a good representation of the turbulent kinetic energy in the channel flow. The kinetic energy is essentially invariant with the cross-stream profile. The RNG and k-ε model both give good representations of the peak kinetic energy in the profile at y = 3. Overall, the RNG model gives a better representation of the experimental data. From the peak to the channel centerline, the RNG model is closest to the experimental data. From the wall to the peak, the k-ε model most closely matches experiment. For the profile at y = 4, the peak kinetic energy predicted by GOTHIC is almost double the experimental value. The k-ε profile is closest throughout the experimental range for the profile at y = 4. Since the kinetic energy is most closely predicted by the y = 3 profile, it will be used as the basis for

the RNG model most accurately predicting the turbulent kinetic energy of the channel flow.

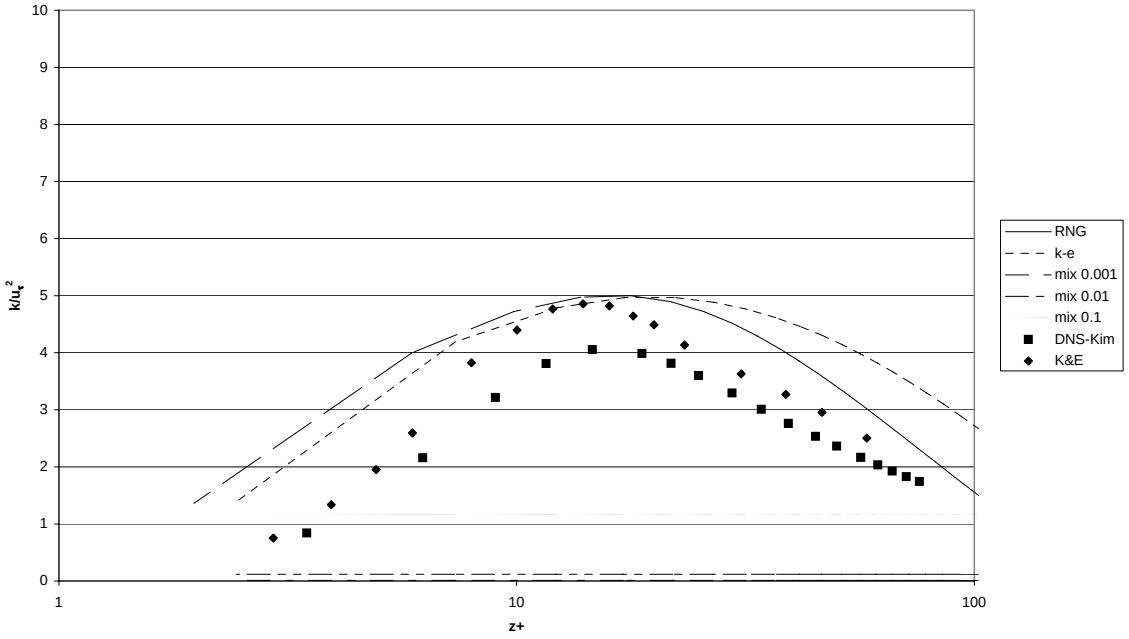

Figure 4.40: Comparison of turbulent kinetic energy normalized by the friction velocity for different models (y=3)

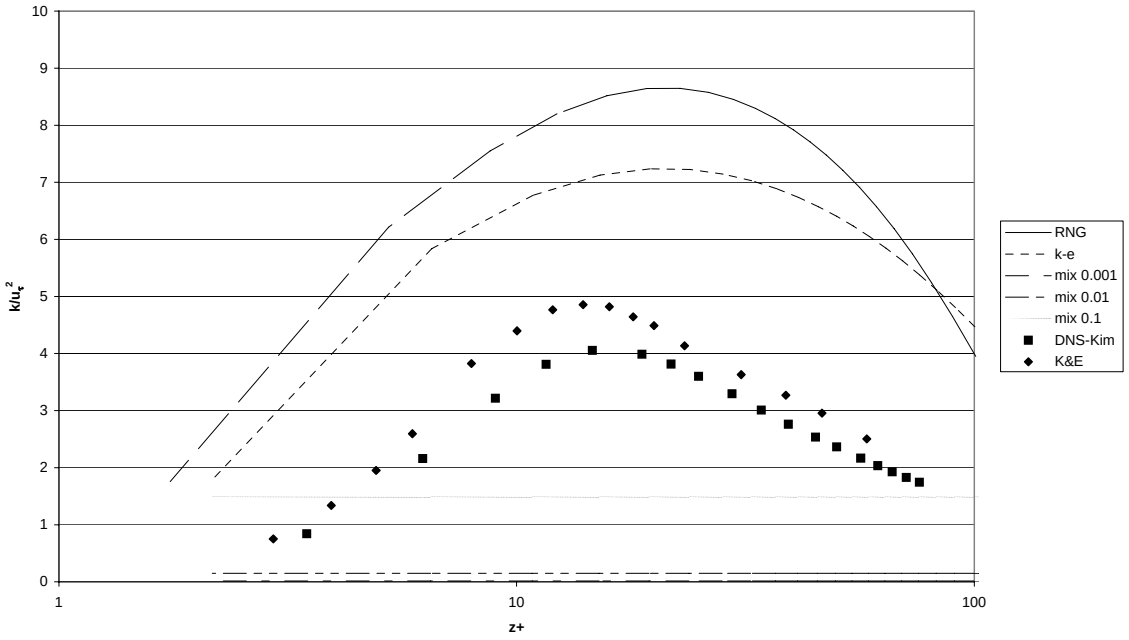

Figure 4.41: Comparison of turbulent kinetic energy normalized by the friction velocity for different models (y=4)

5. Mixing Layer Flow Model

The experiment modeled for the mixing layer flow is the two-dimensional mixing region experiment performed by Champagne, Pao, and Wygnanski in 1974 [8]. This is one of the simplest free shear layer experiments that can provide fundamental verification of GOTHIC's ability to properly calculate the flow properties. The following sections explain the physical setup of the experiment, explain how it is modeled with GOTHIC, and provides a comparison of GOTHIC's results with the experimental data.

5.1. Experimental setup from literature

In order to take measurements of the mixing layer, Champagne, et al., [8] utilized a similar setup to that utilized by Wygnanski and Fiedler (1970) [22] for measuring the axi-symmetric jet. A five hp. blower supplied flow through a diffuser section and plenum chamber. The air is again cleaned with an electrostatic precipitator and the temperature is maintained at ±1°F. The air leaves the plenum chamber through a 17.8 cm. high by 50.8 cm. long opening as shown in Figure 5.1. Air exits the nozzle at a speed of 8 m./s. and mixes with the stagnant air in the chamber. Flow measurements were taken using linearized, constant-temperature hotwire anemometers and the signals were processed using a variety of circuits to sum, multiply, integrate, and differentiate the readings of the hotwires. Using the apparatus described above, experimental flow data was taken and processed.

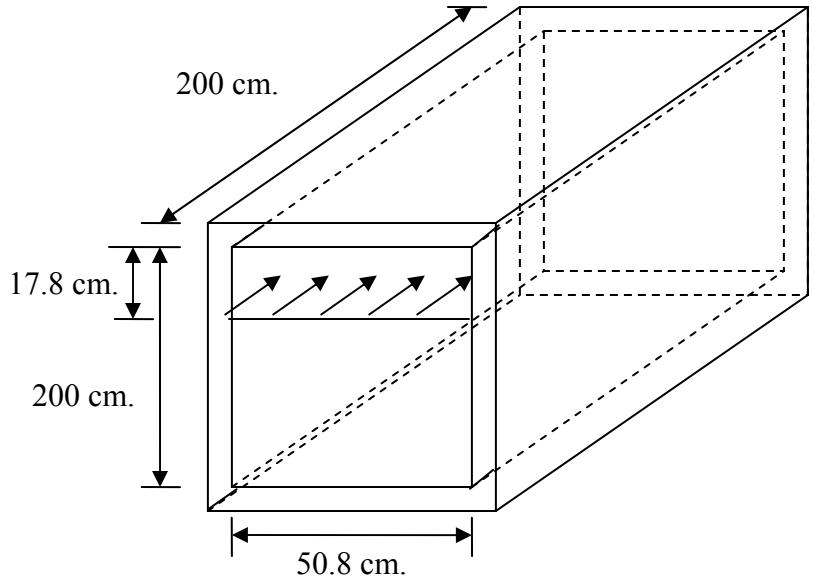

Figure 5.1: Diagram of apparatus for mixing layer experiment

5.2. GOTHIC model

To model the experiment performed by Champagne, et. al., a simple GOTHIC model is created that contains the necessary elements to reproduce the results. Figure 5.2 gives the noding diagram used to replicate the experiment. Volume 1s is a subdivided control volume where the mixing layer will be measured. Volumes 2 and 3 represent the exit atmosphere and plenum chamber, respectively. These intermediate volumes must be used in the model because 3-D connectors can only be used to connect two control volumes, as detailed in Section 2.1.4. In order to model the assumed uniform velocity profile at the inlet, a 3-D connector is used for supplying the mixing velocity. A 3-D connector is also used to model the outlet of facility that goes to the atmosphere.

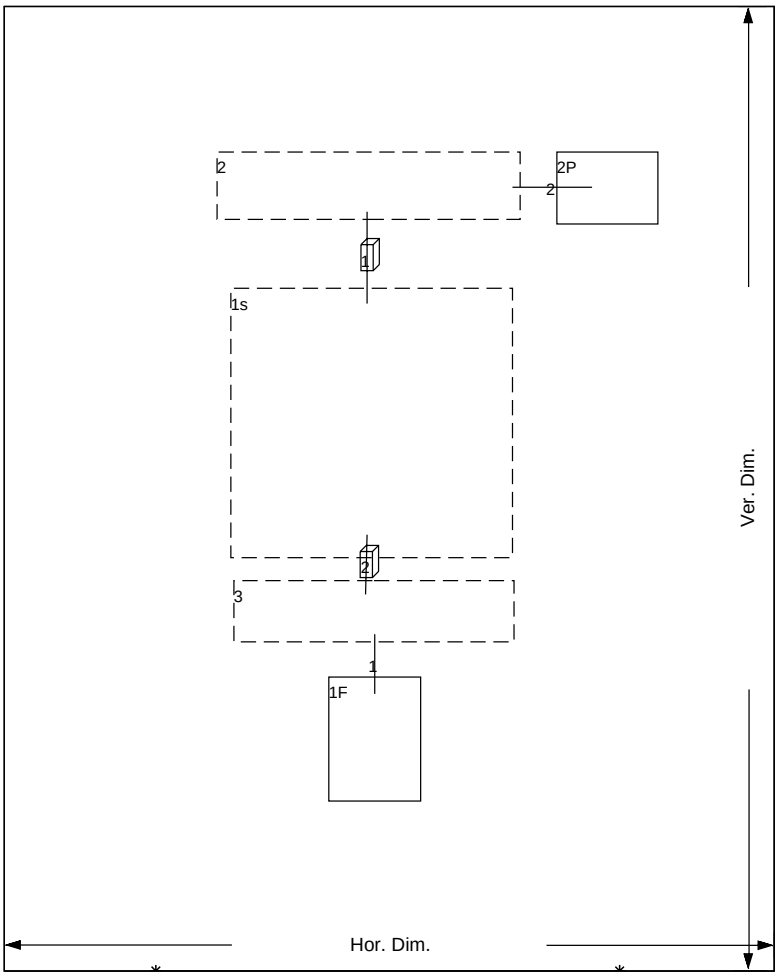

Figure 5.2: Mixing layer GOTHIC noding diagram

The subdivided mesh of Volume 1s is shown in Figure 5.3. In the x-direction, the volume is subdivided into four cells of equal length since the flow properties should have little variation in this direction. The y-axis of the volume is subdivided into five cells. The first three cells in the y-direction are 0.25 m. in length, the fourth is 0.75 m., and the final cell is 0.5 m. The y-direction is subdivided in such a manner so that effects further downstream of the plenum can be measured without significantly increasing the computational time of the code. The z-direction is subdivided into 101 cells of equal length. Since this is the direction in which the mixing region is measured, a large number

of cells are required to obtain a significant number of data points within the region. The 3-D connector used to attach the supply plenum to the mixing layer facility is connected across coordinates (1, 1, 93) to (4, 1, 101). The atmosphere/exhaust region for the flow occurs at the back of the facility and is connected with a 3-D connector across cells (1, 5, 1) through (4, 5, 101). Using this setup, the mixing layer experiment is replicated in GOTHIC.

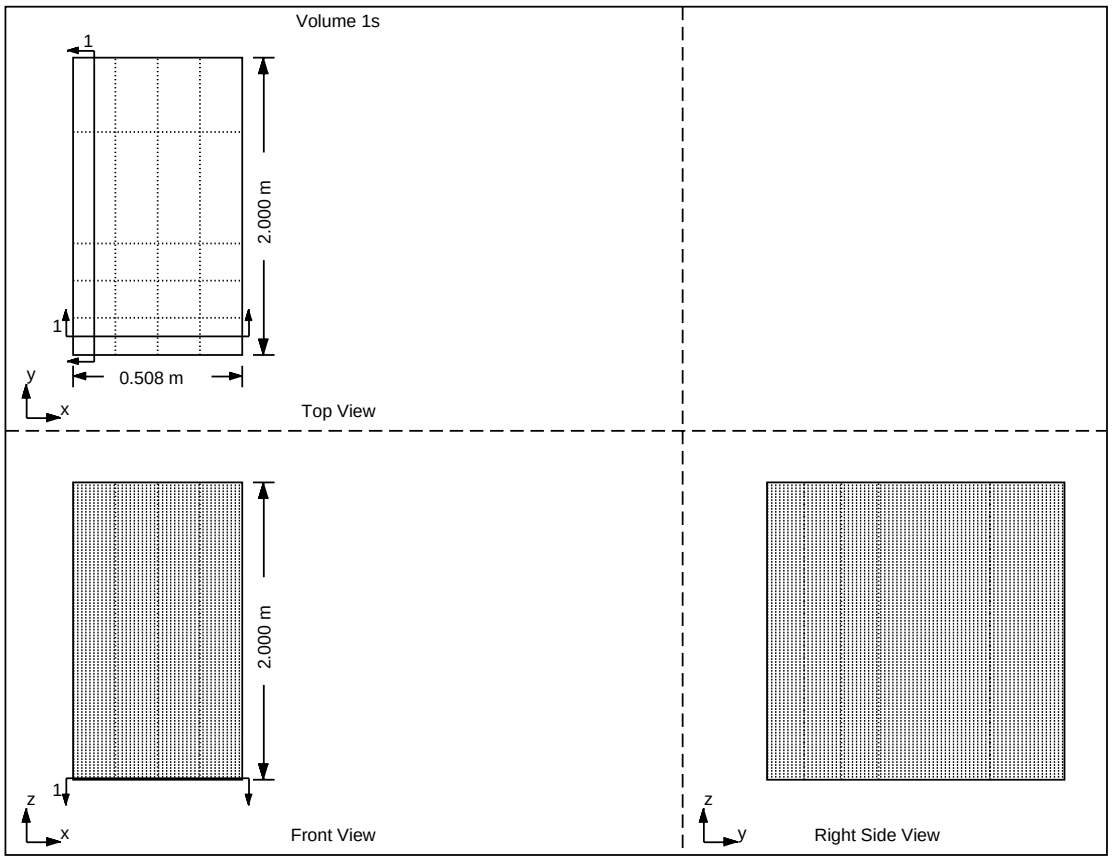

Figure 5.3: 3-D mesh of mixing layer facility

5.3. Results

The following sections provide the results for each of the turbulence models analyzed for the mixing layer model. The ability of each model to predict experimental data is evaluated in the first three sections. The final section compares the computational results for each of the models against each other and the experimental data. The following definitions are used for producing non-dimensional values that allow for comparison of the GOTHIC and experimental data.

U	Mixing layer longitudinal velocity
U_h	Mixing layer longitudinal velocity of injected fluid, 8 m./s.
U_l	Mixing layer longitudinal velocity of stagnant fluid, 0 m./s.
$U_c = \frac{1}{2}(U_h + U_l)$	Mixing layer convection velocity, 4 m./s.
y	Distance downstream of the mixing layer entrance
z	Distance from interface between stagnant and injected fluid
k	Turbulent kinetic energy

For scaling the parameters of the mixing layer, the following terms must be defined. The cross-stream location, z_α, is defined as

$$z_\alpha = z\Big|_{U = U_l + \alpha(U_h - U_l)} \tag{5.1}$$

Using the cross-stream locations of $z_{0.1}$ and $z_{0.9}$, the characteristic width of the flow, δ, is defined by

$$\delta = z_{0.9} - z_{0.1} \tag{5.2}$$

A cross-stream non-dimensional coordinate, ξ, can be defined as

$$\xi = \left[z - \frac{1}{2}\left(z_{0.9} + z_{0.1}\right) \right] \Big/ \delta \tag{5.3}$$

A scaled velocity is also defined as function of the scaled cross-stream velocity as

$$f(\xi) = \left(U - U_c\right)/U_s \tag{5.4}$$

To be consistent with the experimental data provided by Champagne, another scaled cross-stream coordinate, ζ, is defined as

$$\zeta = \left(z - z_{0.5}\right)/\left(y - y_0\right) \tag{5.5}$$

where y_0 is experimentally dependent on the thickness of the boundary layer and the disturbances present [8].

5.3.1. Mixing length models

The results of the mixing length model using various characteristic lengths are given below. The time required to run the models to a transient time of 50 seconds (at which point steady-state profiles are reached) for the 0.001 m., 0.01 m., and 0.1 m. mixing lengths are 1.67, 1.65, and 1.68 hours, respectively. Figure 5.4 gives the mean velocity profile using a mixing length of 0.001 m. As documented in the legend, the profiles generated in GOTHIC corresponding to y = 2, y = 3, and y = 4 are equivalent to downstream distances of 50, 75, 150 cm., respectively. As can be ascertained from the sharp bends in the GOTHIC profiles, the code only produces three data points within the range of the experimental data provided. The profile corresponding to y = 4 matches the experimental data most closely, followed by y = 3 and y = 2. While there are not a large number of data points available, the code does

a reasonable job of predicting the minimum and maximum velocities as well as the overall deceleration of the fluid. In addition, the curves collapse on each other, indicating the profiles are self-similar. Thus, even the simplistic mixing length model with a constant mixing length of 0.001 m. provides a good approximation of the mixing layer velocity profile.

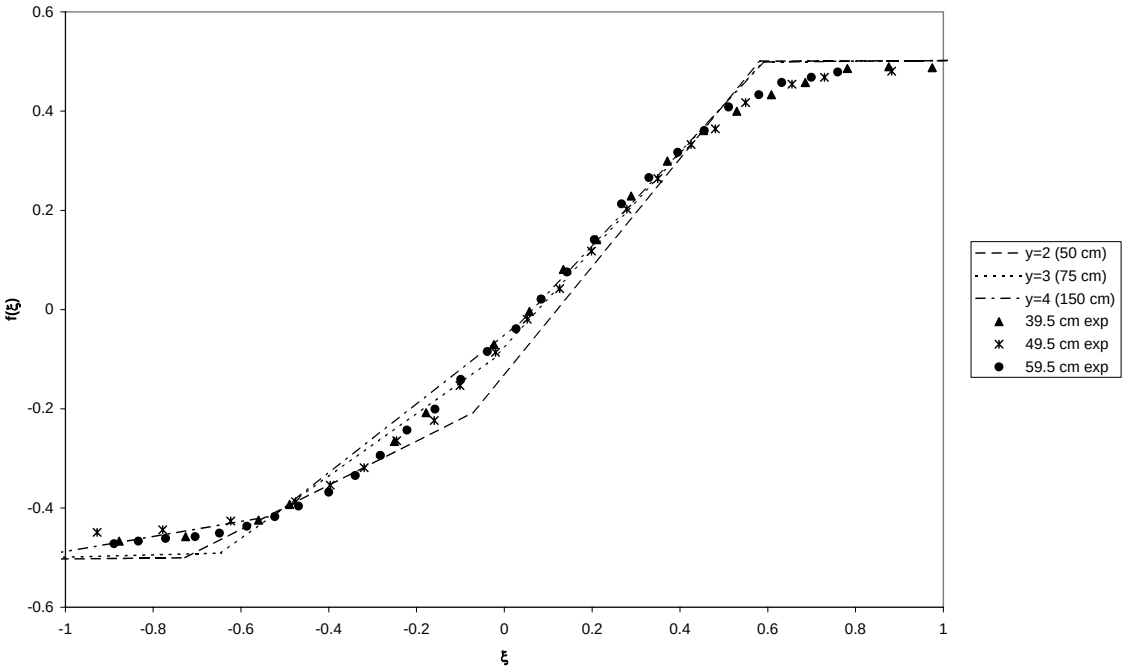

Figure 5.4: Mixing layer velocity profile (0.001 mix)

While the 0.001 m. mixing length model does a reasonable job of predicting the velocity, it does much worse in predicting the growth rate of the mixing region. Figure 5.5 shows the growth rate at $z_{0.1}$, $z_{0.5}$, and $z_{0.95}$ for GOTHIC as well as the experimental data of Champagne, et. al. [8]. The black markers in the figure indicate the experimental data and the GOTHIC values are gray. The regression lines shown are obtained from Microsoft Excel's least squares method for each of the profiles indicated. The mixing length model predicts a much slower growth rate of the

mixing region than given by experiment. In fact, the GOTHIC growth rate is almost non-existent, indicating there is little interaction between the stagnant and injected fluid. Since this is not consistent with experiment, it is concluded that the growth of the mixing region by GOTHIC's 0.001 m. mixing length model is incorrect.

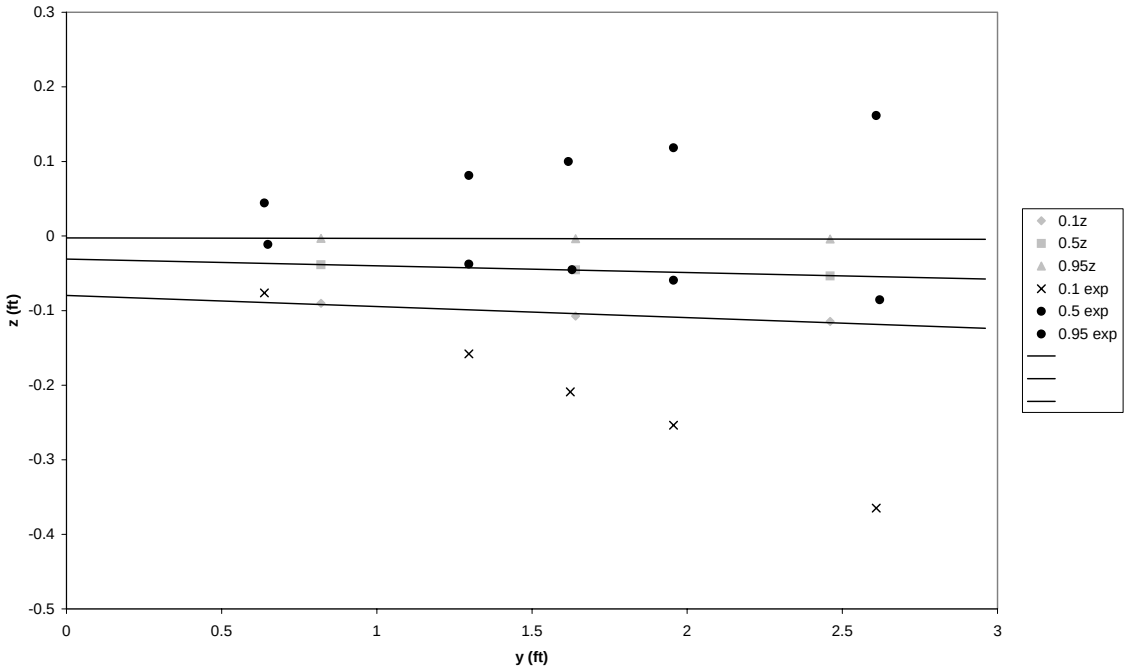

Figure 5.5: Mixing region growth rates (0.001 mix)

The turbulent kinetic energy predicted by the 0.001 m. mixing length model also gives a poor representation of the experimental data. As Figure 5.6 shows, the experimental turbulent kinetic energy provided by Champagne, et. al. [8], Wygnanski and Fiedler [22], and Patel [16] have parabolic profiles. The GOTHIC turbulent kinetic energy shows a linear, unchanging magnitude across the mixing region. This is obviously inconsistent with the experimental data. Thus, it is concluded that turbulent kinetic energy predicted by GOTHIC's mixing length model is unrepresentative of the physical characteristics of the flow.

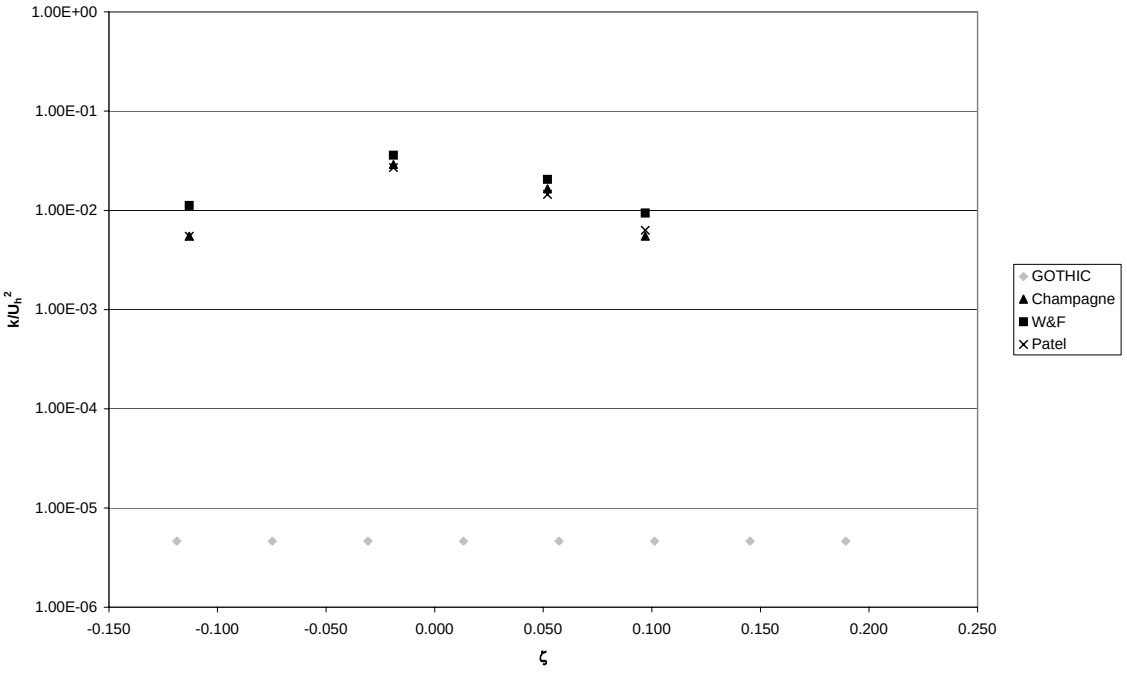

Figure 5.6: Kinetic energy profile of mixing region (0.001 mix)

The flow properties given for the 0.001 m. mixing length model in Figure 5.4 through Figure 5.6 are also given for the 0.01 m. and 0.1 m. mixing length models in Figure 5.7 to Figure 5.12. As will be shown in Section 5.3.4, there is little difference between the flow properties calculated by GOTHIC for each of the three mixing lengths. Thus, the observations detailed above for the 0.001 m. model also apply to the 0.01 and 0.1 m. models. Hence, no further analysis of the flow properties is presented here.

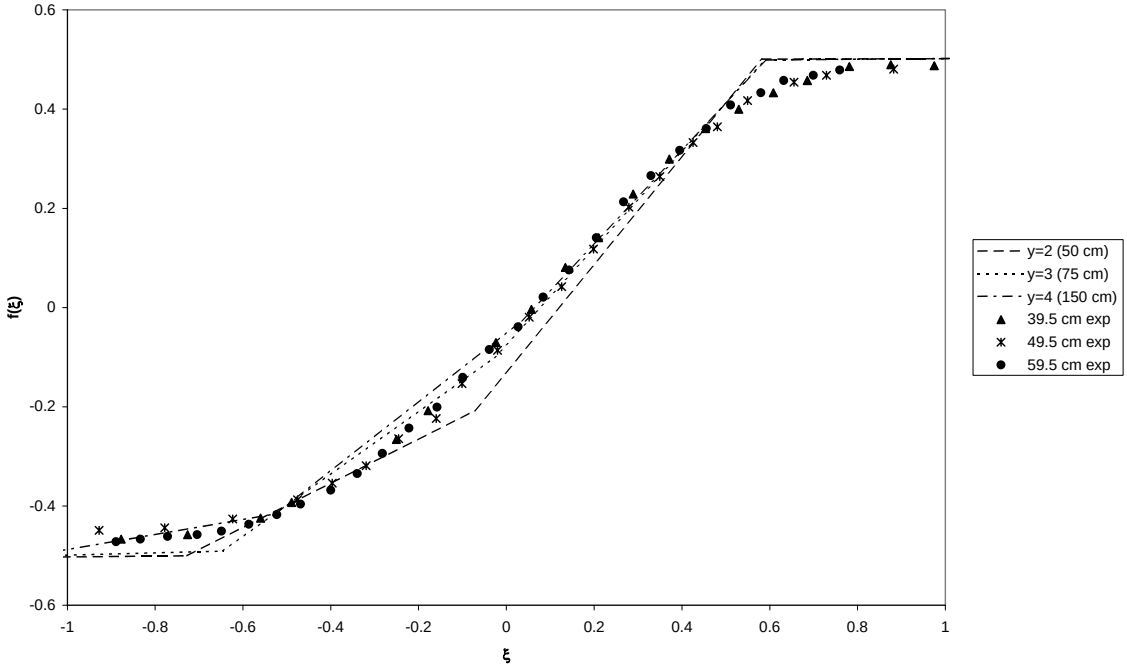

Figure 5.7: Mixing layer velocity profile (0.01 mix)

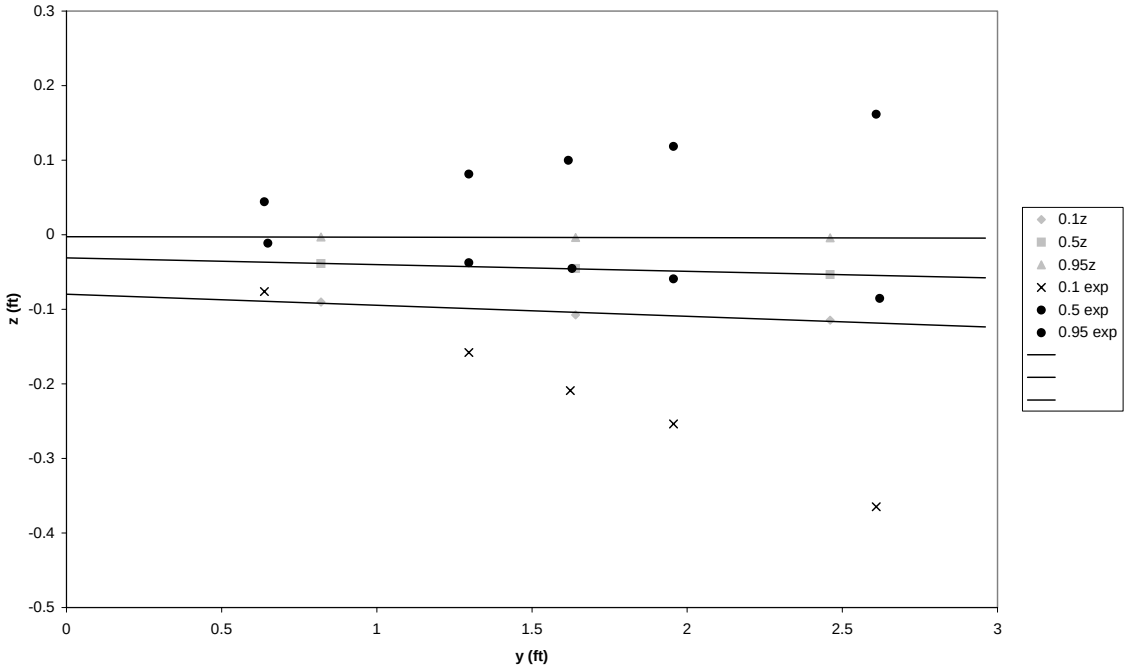

Figure 5.8: Mixing region growth rates (0.01 mix)

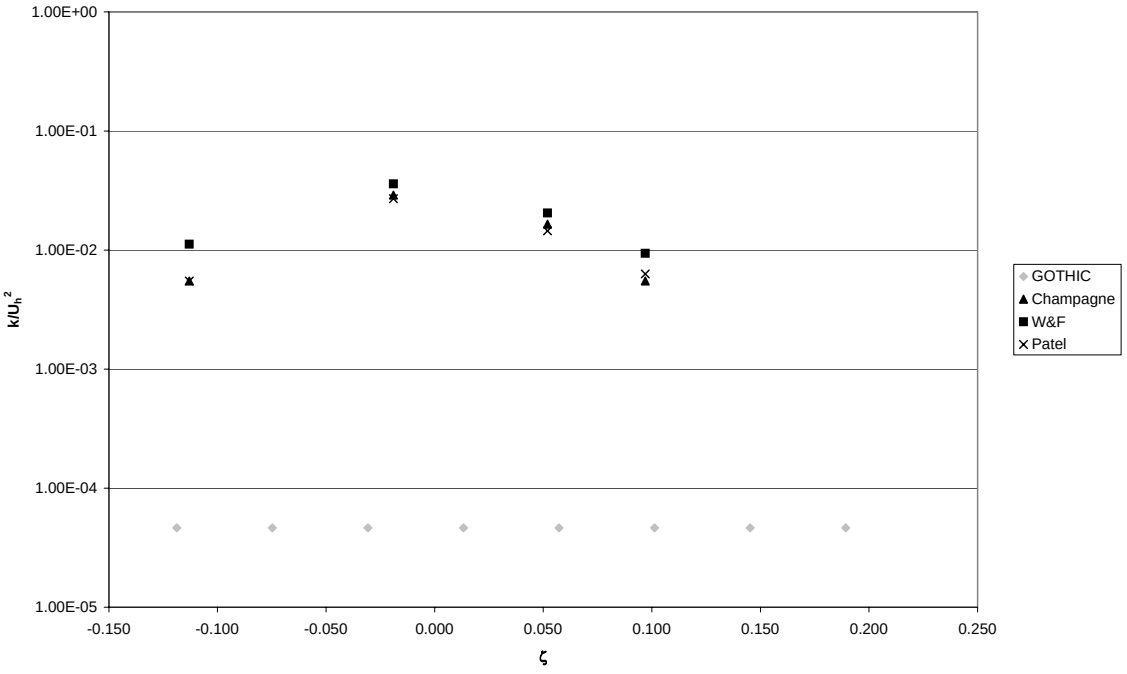

Figure 5.9: Kinetic energy profile of mixing region (0.01 mix)

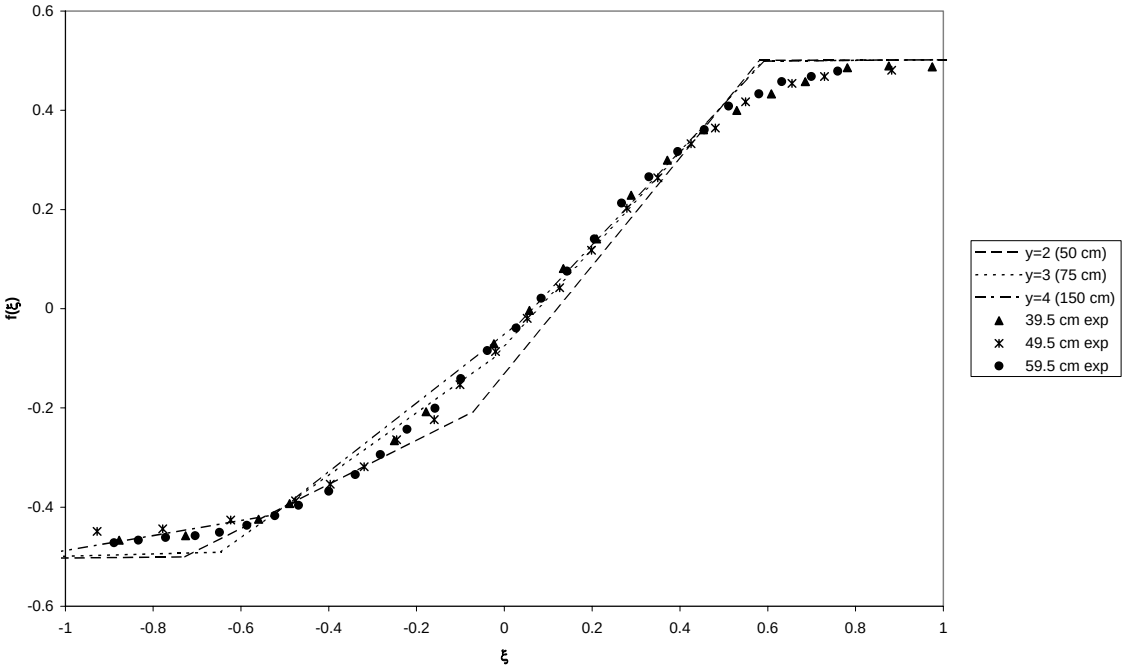

Figure 5.10: Mixing layer velocity profile (0.1 mix)

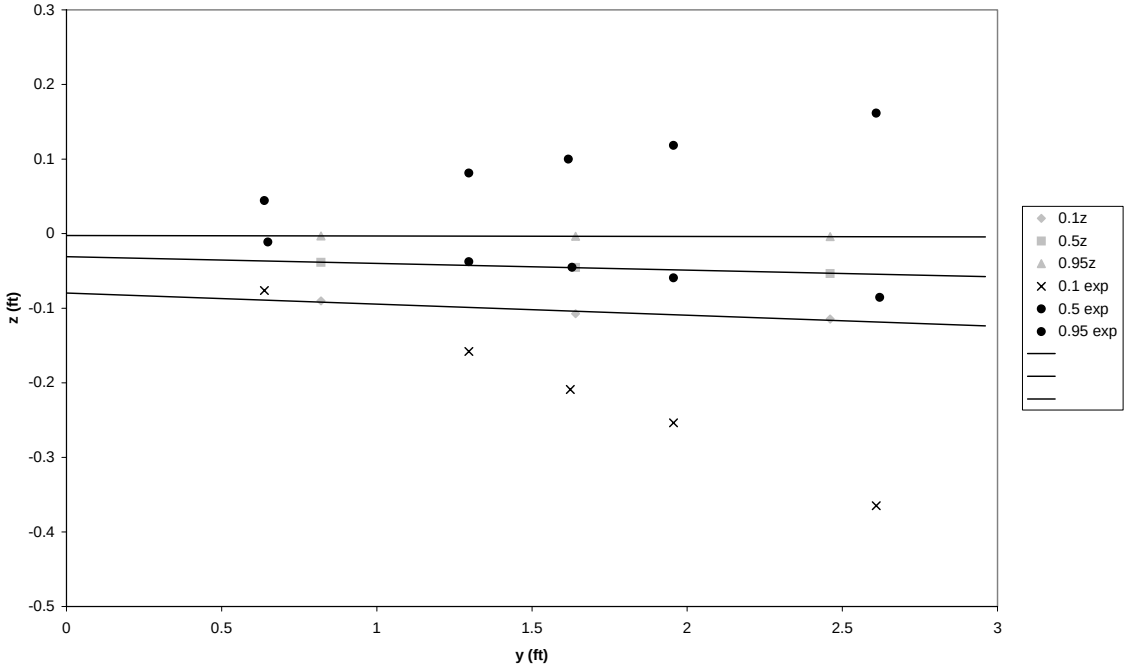

Figure 5.11: Mixing region growth rates (0.1 mix)

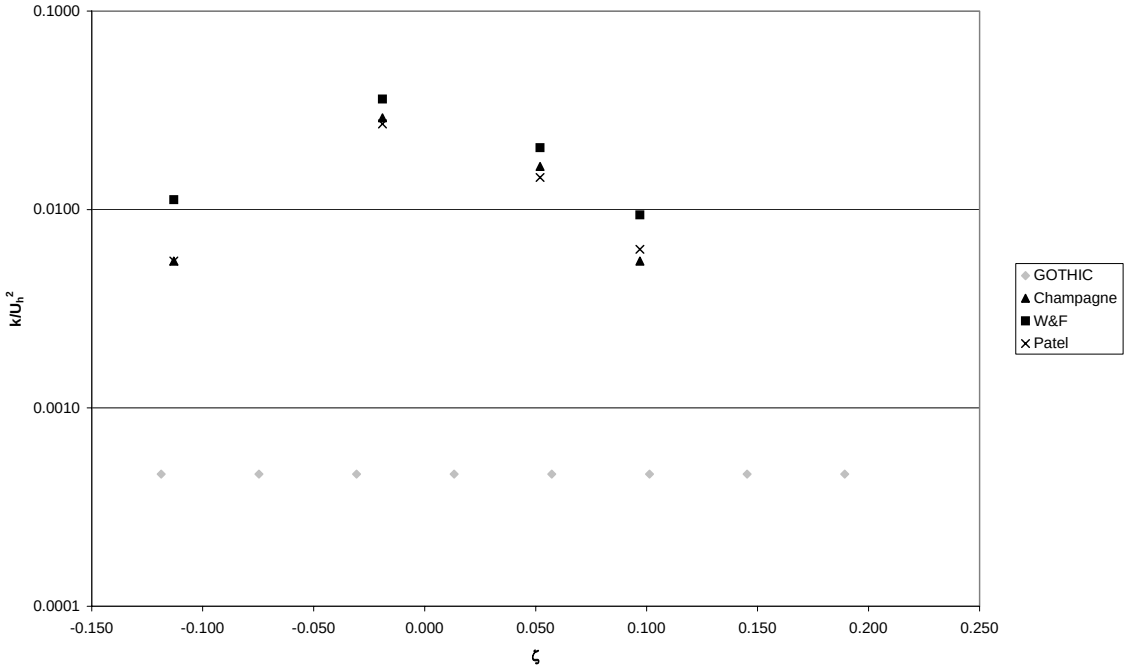

Figure 5.12: Kinetic energy profile of mixing region (0.1 mix)

5.3.2. Standard k-ε model

The standard k-ε model provides excellent agreement with experimental data for the scaled velocity profile of the mixing layer. For a transient time of 50 seconds, the k-ε model requires 31.67 hours of computational time, which is significantly larger than the times required for the mixing length models. Figure 5.13 shows this velocity profile for several different downstream distances for both the GOTHIC and experimental results. As the experimental data shows, the mixing layer is a self-similar flow. GOTHIC also predicts this self-similarity as the profiles collapse on each other over most of the data range provided. This verifies the ability of GOTHIC to correctly predict the physical flow configuration modeled. In addition, the GOTHIC profiles closely follow the experimental data, providing further validation of the standard k-ε turbulence model for this flow geometry.

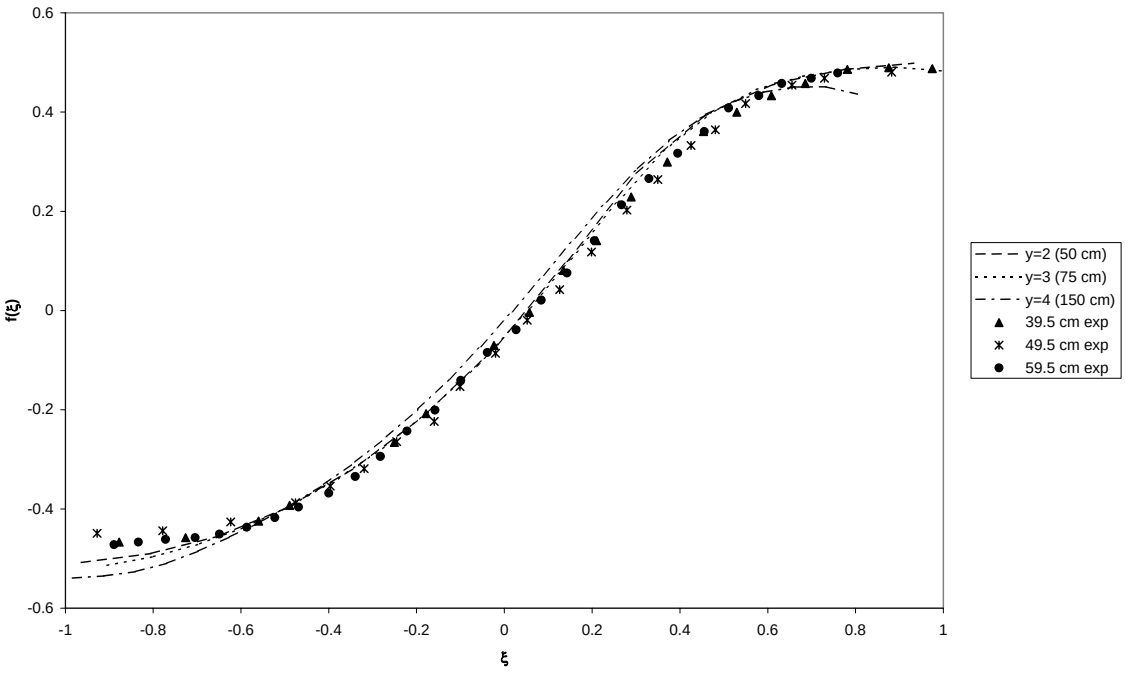

Figure 5.13: Mixing layer velocity profile (k-ε)

The spreading rate of the mixing layer is an additional parameter that can be used when evaluating the turbulence model. Figure 5.14 gives the distance from the interface region between the injected flow and the stagnant to the location of $z_{0.1}$, $z_{0.5}$, and $z_{0.95}$ as defined in Section 5.3. The gray data points in the figure are the predicted values from the standard k-ε model in GOTHIC while the black data points are the experimental data identified in Section 5.3.1. Regression lines for the GOTHIC data points are also given, showing the linearity of the predicted mixing layer. While the data points and regression lines do not coincide directly with the experimental data, the spreading rates are linear in nature as shown by the minimal error in the regression lines. This phenomenon is seen in many mixing layer experiments where the slower fluid is stagnant [16, 22]. GOTHIC's standard k-ε model predicts a faster growth rate of the mixing region than is seen experimentally. This is likely due to the coarseness of the grid required in order to provide reasonable run times. A coarser grid results in faster deceleration of the fluid and a faster spreading rate. Overall, GOTHIC's standard k-ε model represents the physics of the system well.

As the velocity profile and spreading profiles presented above show good agreement with the experimental data, the normalized turbulent kinetic energy from GOTHIC does also. Figure 5.15 gives normalized kinetic energy values generated by GOTHIC along with values from experiment [8, 16, 22]. Near the location of the average velocity of the mixing layer and stagnant fluid (ζ=0), all of the experimental data predicts a significantly higher turbulent kinetic energy than GOTHIC. As one moves away from this point, GOTHIC predicts values that are more consistent with experiment. Thus, while the model has problems predicting the peak turbulent kinetic

energy values near the location of the average velocity fluid, the values fall within the experimental data range given by experiment as one moves closer to the unaffected regions of the mixing layer.

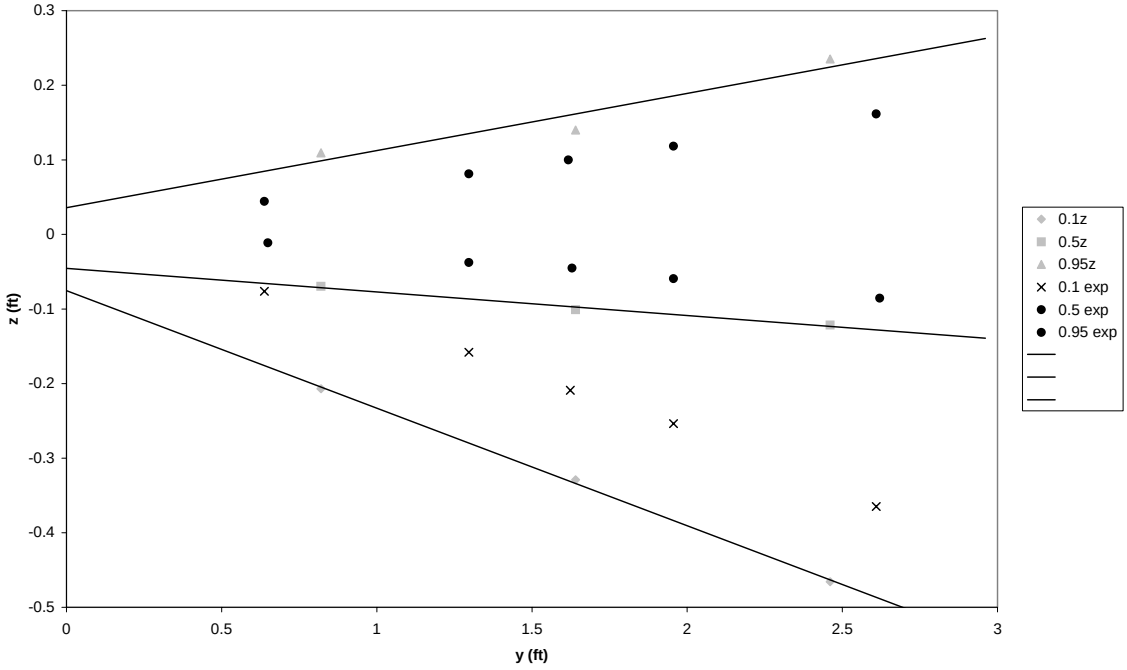

Figure 5.14: Mixing region growth rates (k-ε)

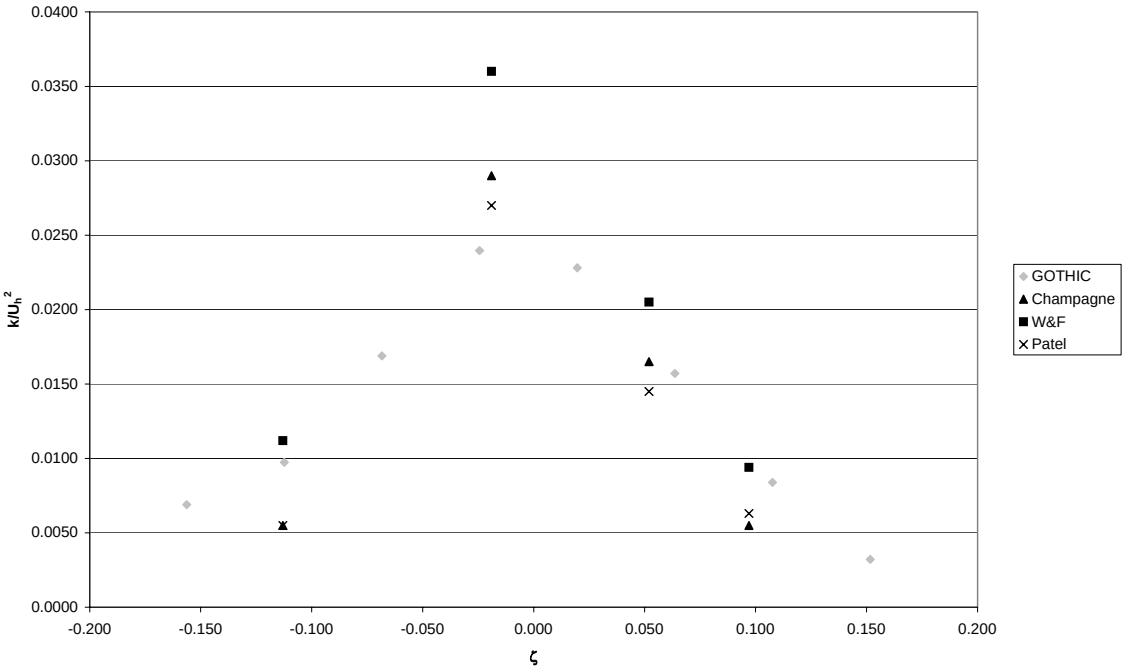

Figure 5.15: Kinetic energy profile of mixing region (k-ε)

5.3.3. RNG k- ε model

The following section provides the results of GOTHIC's simulation of the mixing layer with the RNG k-ε model. The RNG model utilizes the longest computational time, 31.72 hours, of the three models to calculate the transient profile for 50 seconds. Figure 5.16 gives the scaled velocity profile as a function of the scaled cross-stream distance. From cross-stream distances of -0.6 to 0.6, GOTHIC over predicts the velocity of the mixing layer. Both the experimental data and GOTHIC's data in this range are self-similar in that the profiles at various downstream distances collapse on each other. However, the experimental data predicts lower velocities than GOTHIC. For the velocity profiles at distances of 50 cm. and 75 cm. from the mixing layer entrance, the wall friction effects are not significant. However, further downstream at the profile located at 150 cm., the wall effects are observed in the bending of the

velocity profile near $\xi = 0.85$. Thus, the RNG k-ε model in GOTHIC provides acceptable, though not superb, results when compared to the experimental data.

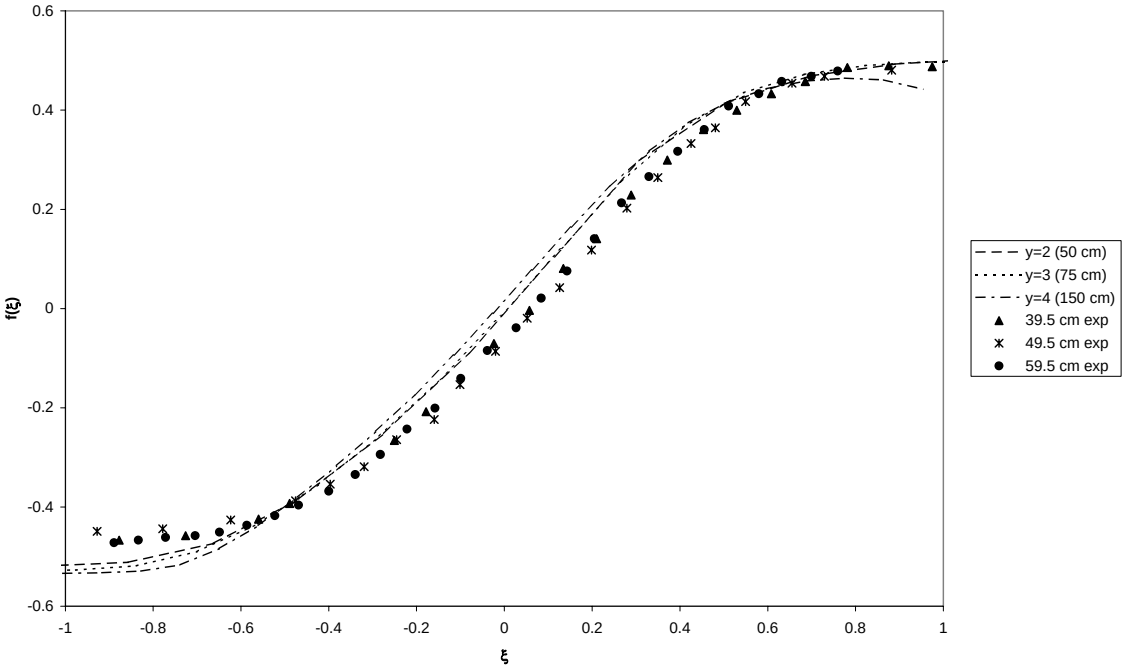

Figure 5.16: Mixing layer velocity profile (RNG)

The spreading rate of the mixing layer for the RNG k-ε model and experimental data are given in Figure 5.17. While the spreading rate predicted (based on the slope of the regression lines for each of the data sets at $z_{0.1}$, $z_{0.5}$, and $z_{0.95}$) appears to be shallower than that given by experiment, the GOTHIC results, specifically at distances of 75 and 150 cm., are very close to the experimental data. GOTHIC's spreading rate at $z_{0.95}$ is significantly affected by the deviation of the data point at 50 cm. This causes the slope of the regression line for the GOTHIC data to diverge from the experimental data. Elimination of this data point results in a spreading rate that is much closer to that of the experimental data. However, a sufficient number of additional data points are not available from the simulation to allow this. An overall

review of the mixing layer growth rate in Figure 5.17 shows that GOTHIC's RNG k-ε model does a reasonable job at predicting the experimental growth rates.

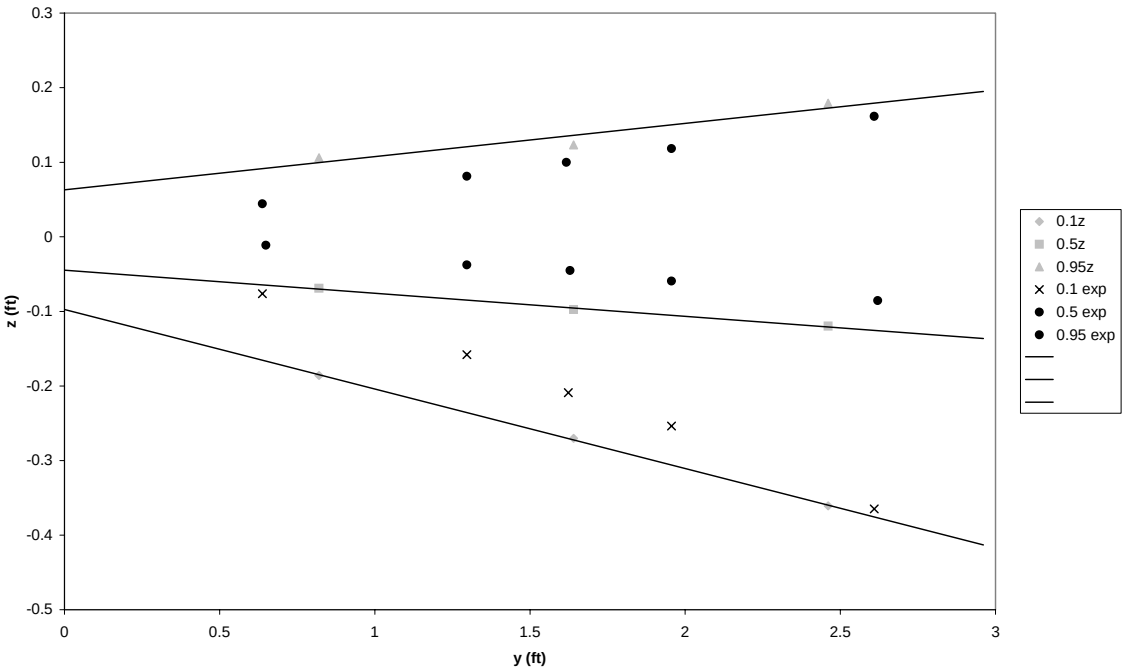

Figure 5.17: Mixing region growth rates (RNG)

The scaled turbulent kinetic energy given by GOTHIC is shown in Figure 5.18 below. A quick comparison of the experimental and GOTHIC values show that the RNG k-ε model greatly under predicts the turbulent kinetic energy of the mixing layer for a significant region of the jet. In fact, only one of the GOTHIC data points falls within the experimental data. Near the interface region of the two fluids, the energy level is under predicted by a factor of two. Further away from this area the energy levels advance closer to the experimental data, although they are still significantly lower. Thus, the RNG k-ε model does poorly at predicting the turbulent kinetic energy of the mixing layer in the region for which experimental data is available.

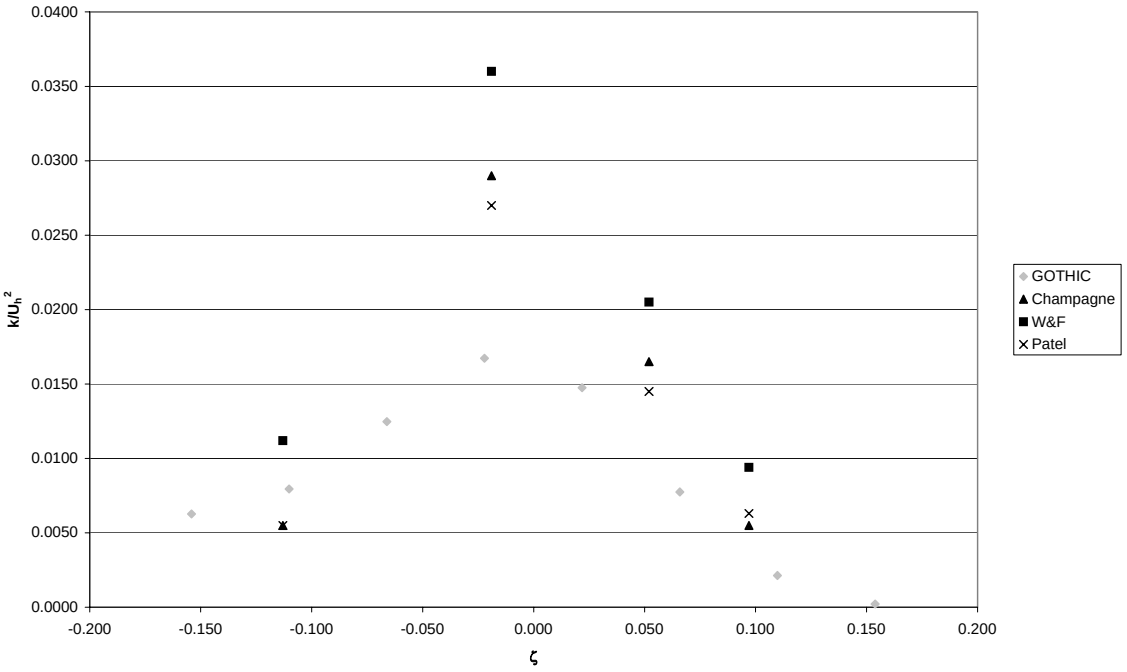

Figure 5.18: Kinetic energy profile of mixing region (RNG)

5.3.4. Comparison between turbulence models

In Sections 5.3.1 through 5.3.3, comparisons of each model and experimental data were made for the mixing layer. The information in these sections showed the velocity, growth rate, and turbulent kinetic energy at different downstream distances. This section will compare the flow properties for each of the turbulence models with each other and experimental data. This allows for an easier determinations about each model's strengths and weaknesses as they relate to the geometric configuration modeled, the mixing layer flow.

A comparison of the velocity profiles at the downstream distance corresponding to y = 2 are given in Figure 5.19. For this distance, the standard k-ε model provides the best replication of the experimental data. The RNG model provides the next closest representation of the experimental data, followed by the mixing length

models. As the figure shows, there is little difference between the three mixing lengths used. These observations also hold for the downstream distances at y = 3 and y = 4. Overall, the models most closely predict the experimental data at a downstream distance of y = 2. Of the three models examined, the standard k-ε model most closely models the experimental results for the mixing layer.

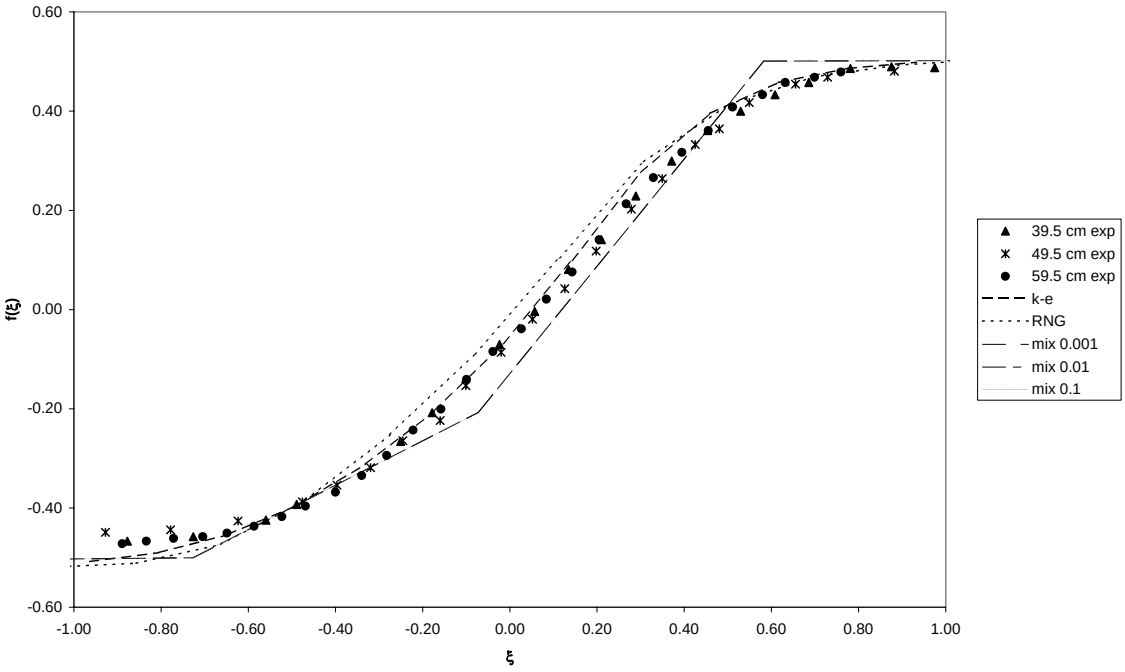

Figure 5.19: Comparison of mixing layer velocity profiles for different models (y=2)

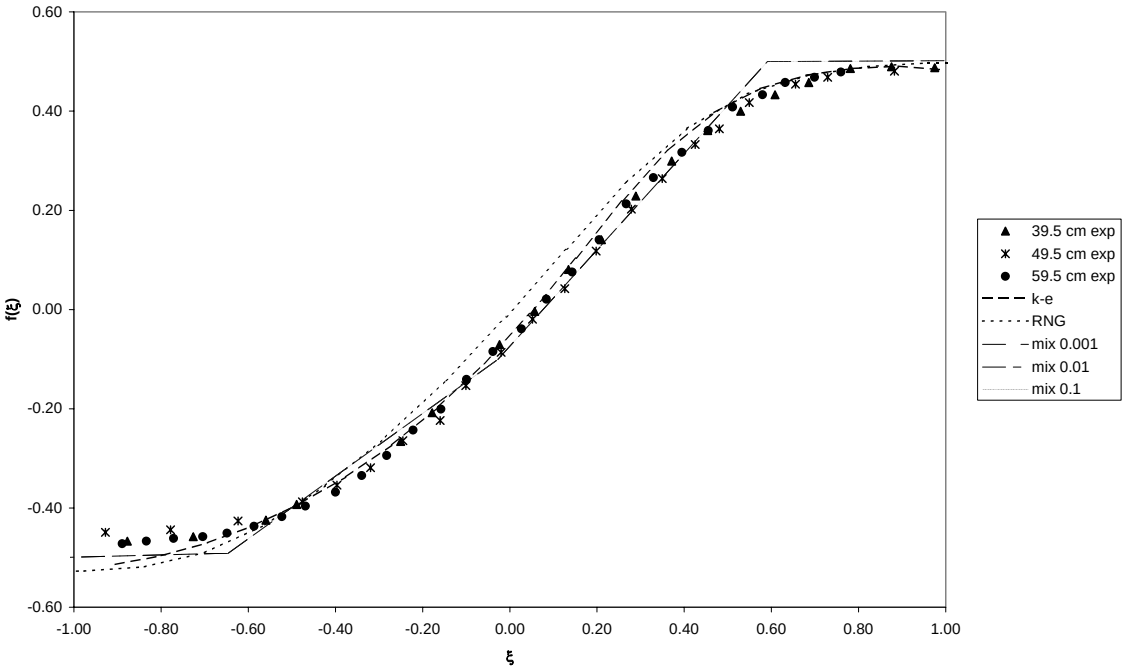

Figure 5.20: Comparison of mixing layer velocity profiles for different models (y=3)

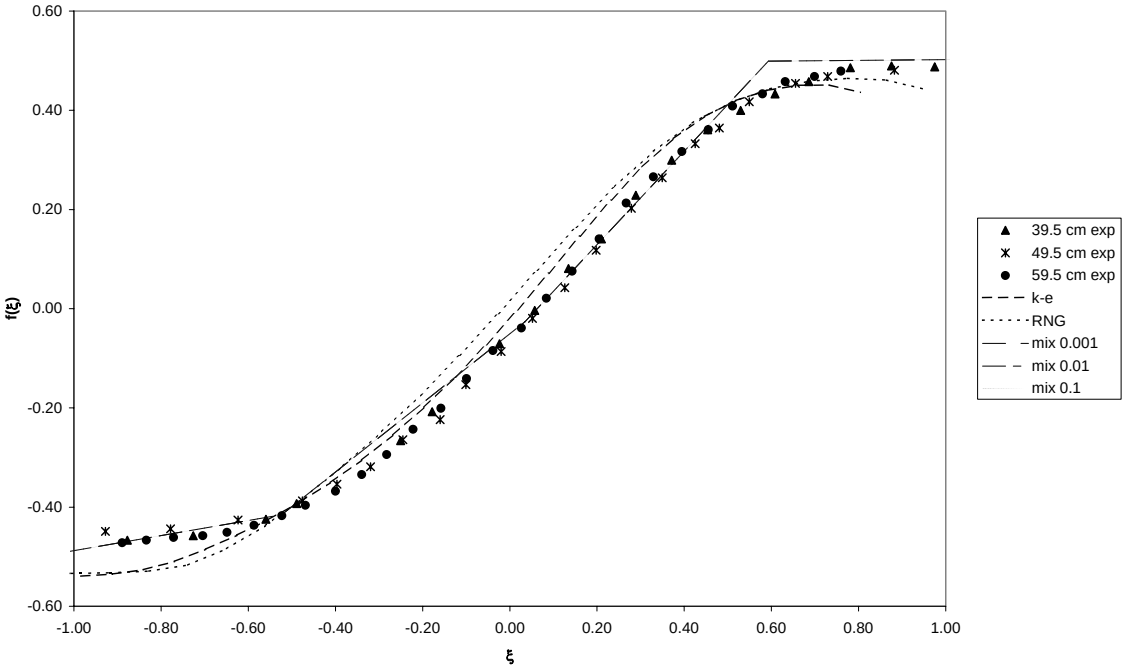

Figure 5.21: Comparison of mixing layer velocity profiles for different models (y=4)

Mixing layer growth rates for cross-stream locations at $z_{0.1}$, $z_{0.5}$, and $z_{0.95}$ are show in Figure 5.22 through Figure 5.25. In Figure 5.22 the growth rate of the cross-stream location at $z_{0.1}$ shows that the RNG model most closely predicts the data points given by experiment. However, the k-ε model most closely matches the slope of the regression line, which is the actual growth rate of the mixing region. In fact, a very close approximation of the experimental data can be shown with the k-ε model if the distances are offset by 0.115 ft, as is shown in Figure 5.23. The mixing length models predict a very slow growth rate, which is not consistent with experiment. At $z_{0.5}$ (Figure 5.24) the mixing length model data points are the closest in magnitude to the experimental data. However, the growth rate of the mixing region is much smaller, as it was at $z_{0.1}$. Interestingly enough, both the k-ε and RNG models predict identical values and growth rates for this cross-stream distance. As with the $z_{0.1}$ k-ε profile, the k-ε and RNG profiles can be offset to provide an accurate representation of the experiment. This again shows that the growth rate for these models is consistent with experiment. The same general observations for the k-ε and RNG model at $z_{0.1}$ also hold for $z_{0.95}$. Here, again, the RNG model predicts closer values to the experimental data, but the growth rates of the k-ε model are nearly identical to that of experiment. For this case, the three mixing length models all predict no growth of the mixing region, which is obviously incorrect. Overall, the RNG model predicts the magnitudes of the mixing region most accurately while the k-ε model predicts the growth rate correctly.

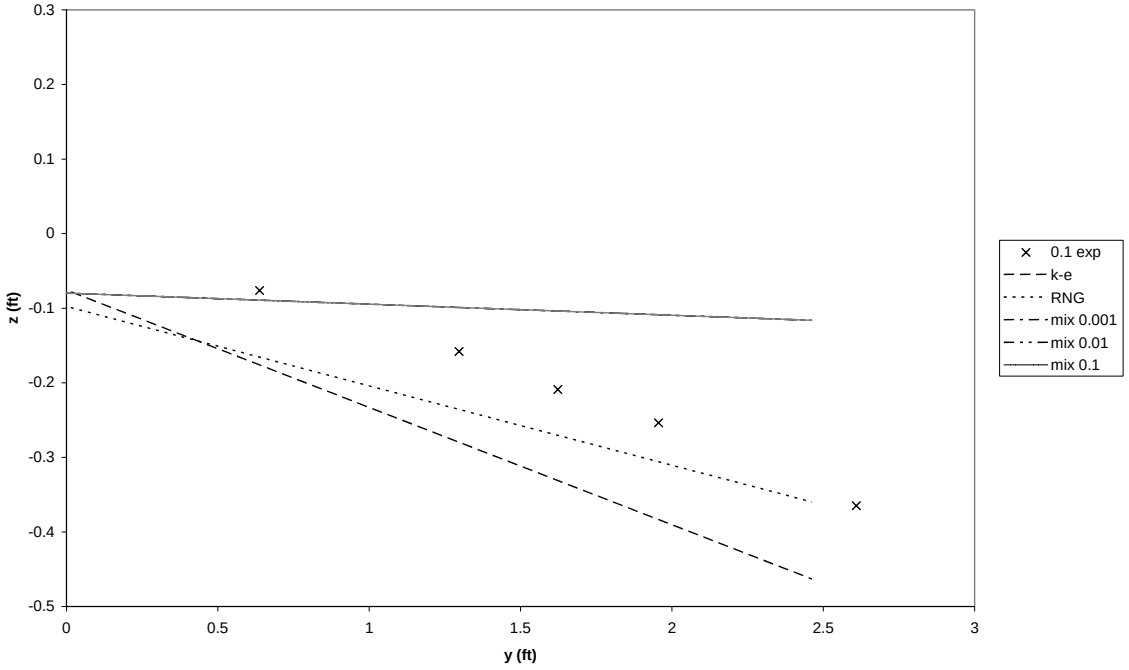

Figure 5.22: Comparison of mixing region growth rates ($z_{0.1}$)

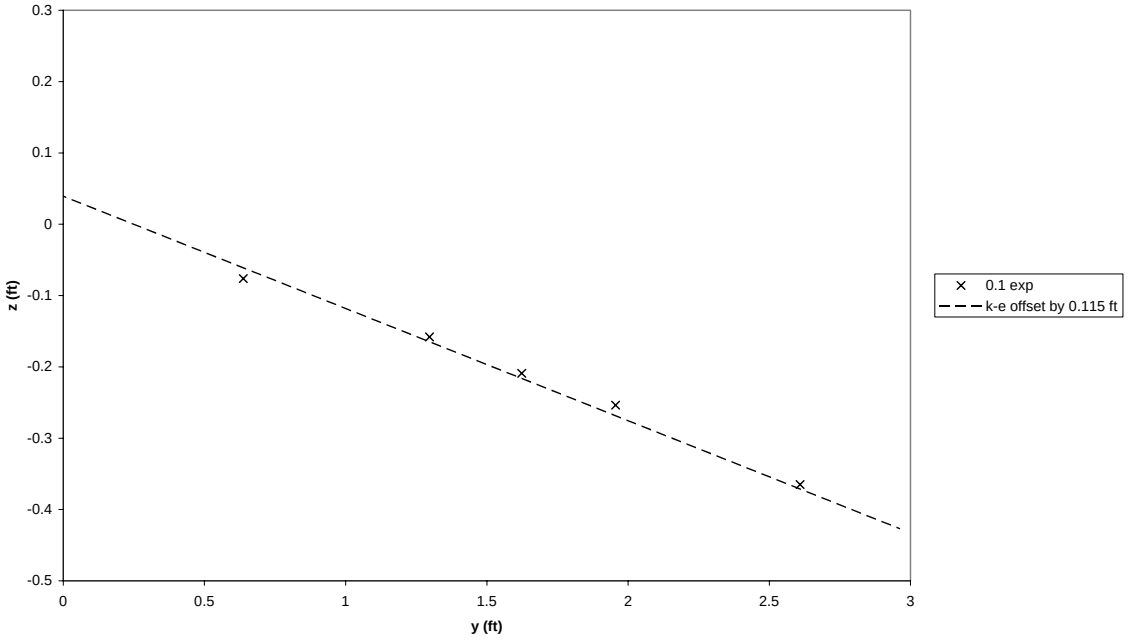

Figure 5.23: Mixing region growth rate for k-ε model offset by 0.115 ft.

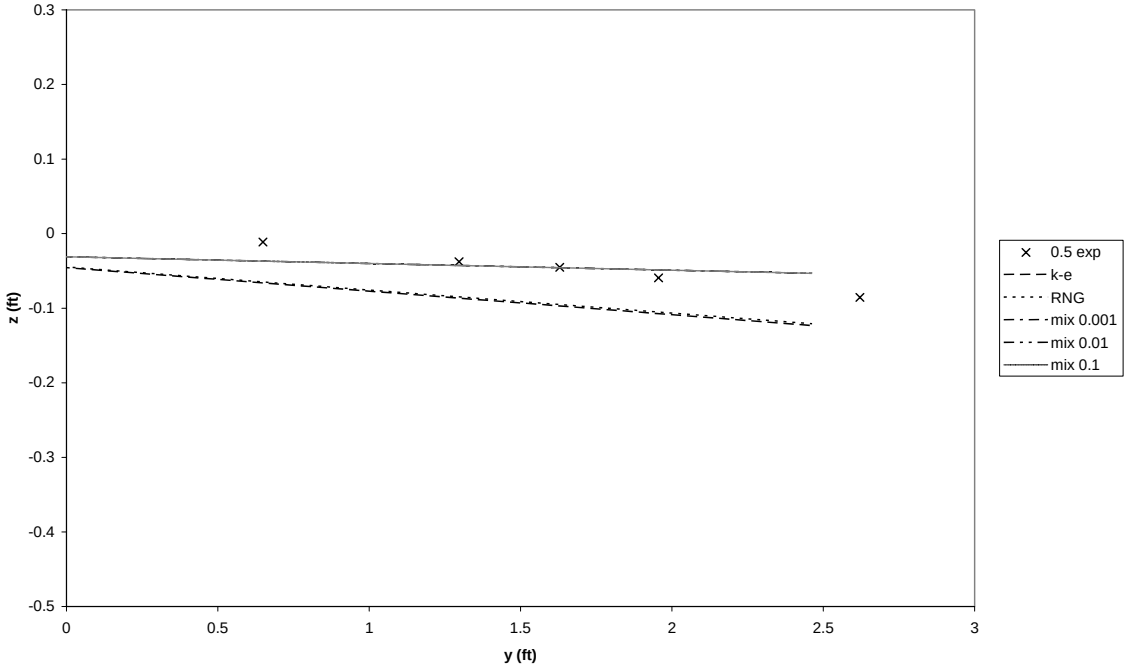

Figure 5.24: Comparison of mixing region growth rates ($z_{0.5}$)

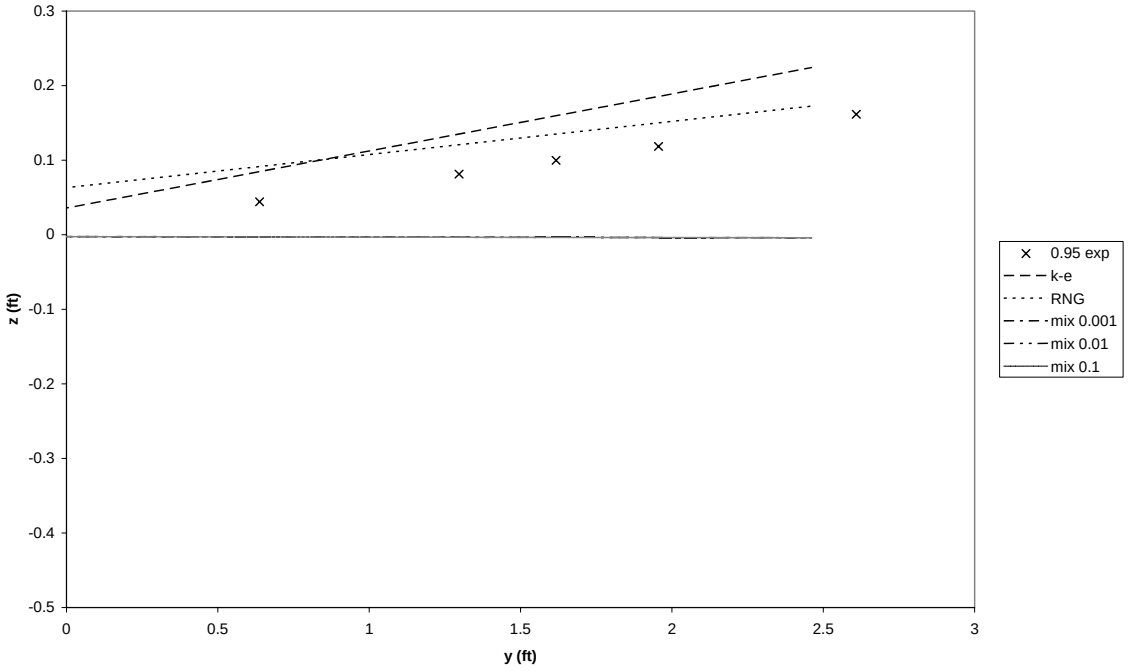

Figure 5.25: Comparison of mixing region growth rates ($z_{0.95}$)

The normalized kinetic energy profiles for each of the turbulence models are shown in Figure 5.26 below. As was discussed in Section 5.3.1, the kinetic energy predicted by the mixing length models is incorrect by a significant margin. These profiles are shown as the markers located near the bottom of the graph, creating a horizontal line across the figure. The k-ε model most accurately predicts the magnitudes of the turbulent kinetic energy, although the profile appears skewed toward negative ζ values. Additionally, the values predict are significantly smaller than given by experiment. Toward negative ζ values, the k-ε and RNG values approach each other. However, as one moves toward positive ζ values, the RNG kinetic energy is significantly smaller than predicted by the k-ε model and experiment. Overall, the k-ε model gives the most accurate representation of the experimental kinetic energy data available for the mixing layer.

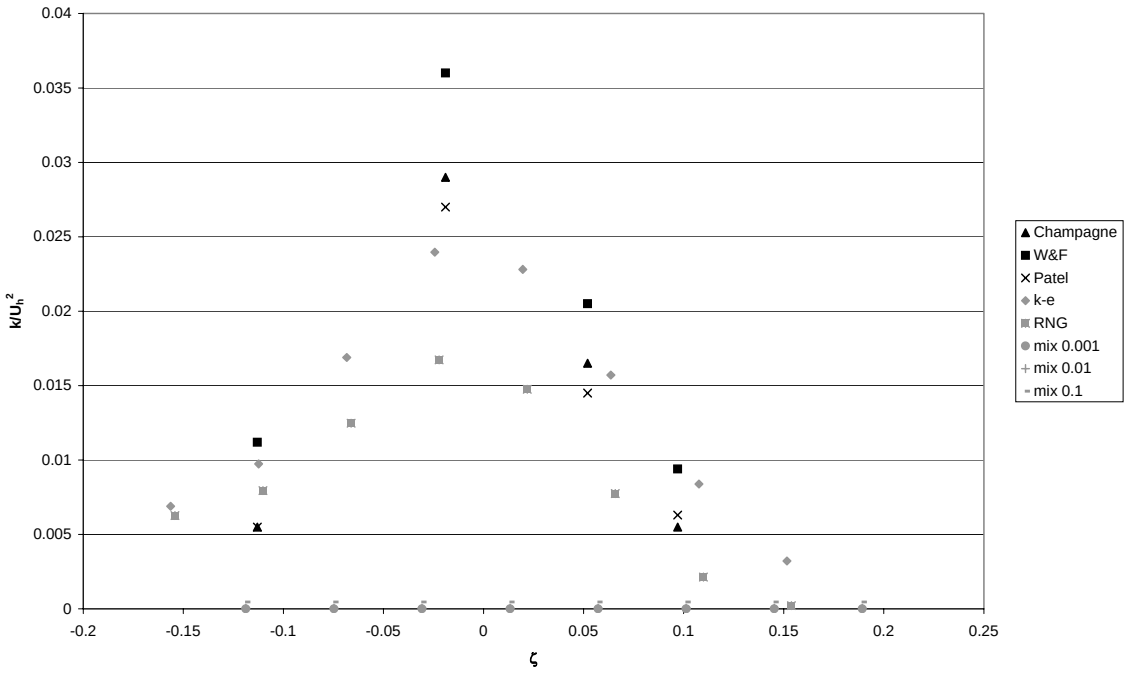

Figure 5.26: Comparison of kinetic energy profiles of mixing region

6. Conclusions

Models for several experiments from literature were created with GOTHIC. Comparisons of GOTHIC's computed flow properties for an axi-symmetric jet, mixing layer flow, and channel flow were compared to experimental results. Flow properties analyzed included turbulent kinetic energy, spreading rates, velocity profiles, mixing region growth rates, and centerline velocities. Comparisons of the predictions of the different turbulence models to each other are also made. The ability of GOTHIC to predict such flow properties with coarse grids is essential to validating the code.

Of the three models analyzed, the standard k-ε model provides the best prediction of the flow properties in each of the experiments modeled. For the axi-symmetric jet case, the k-ε model most closely approximates the turbulent kinetic energy and jet centerline velocities. For the channel flow, this model gives the closest values for the velocity parameters such as normalized velocity profile and velocity defect profile. The standard k-ε model also most closely predicts the mixing layer velocity and kinetic energy profiles. Since these profiles make up the majority of the properties analyzed, the standard k-ε model is the most accurate of the turbulence models analyzed.

The RNG k-ε model provides the second closest overall prediction of the flow properties. For the axi-symmetric jet, the normalized mean velocity and lateral velocity profiles are most accurately predict by the RNG model. In the channel flow, the RNG model only provides the closest approximation for turbulent kinetic energy. Of the three models, the mixing layer's growth rate is most similar to that predicted by the RNG model. Thus, the RNG model gives the most accurate prediction of various flow properties for several of the experiments modeled.

As these results show, no generalizations can be made on whether the standard k-ε model or the RNG model more accurately represents the flows. Depending on the flow configuration either of the models may give the most accurate prediction of the kinetic energy and velocity profiles. One would expect that a generalization of specific properties could be made based on whether the flow is wall bounded (channel flow) or a free shear flow (axi-symmetric jet and mixing layer). However, as has been shown, the turbulence models' accuracy cannot be grouped based on these parameters. Thus, the determination of the most accurate model for predicting flow properties in GOTHIC must be explored on a case-by-case basis that is dependent on the system geometry.

The performance of the mixing length model was disappointing for all of the experiments modeled. While it was not anticipated that an algebraic turbulence model would provide more accurate results than the two-equation models, the dismal results of the mixing layer model were particularly disappointing. For many of the flow properties predicted the mixing length model significantly over or under predicted the parameters. This is likely due to the mixing length being a constant value that is provided by the user. If the mixing length were provided in the form of a wall function (i.e., if it was proportional to the distance to the walls of the volume), it would likely provide much better results. However, such a function would not be useful for the two free shear flow experiments modeled here. Overall, the mixing length model provided few reasonable approximations of the experimental flows modeled.

A comparison of the computational times for determining the flow properties showed that the RNG model takes slightly longer to run than the standard k-ε model. This is not unexpected since the RNG model has an additional term that must be computed by the solver. The computational time for the mixing length model is by far the smallest for each of

the cases analyzed (one to two orders of magnitude smaller than the two-equation models). Computational times for the mixing length models are greatly reduced since the kinetic energy and dissipation are linear equations that can be solved directly. For the RNG and standard k-ε models, the kinetic energy and dissipation are differential equations that must be solved for each cell at each time step. This adds a considerable load to the computational requirements of the solver. Thus, the mixing length model provides the fastest run-time of all the models while the standard k-ε model is the fastest of the two-equation models.

The findings of this work and the conclusions above can be summarized with the following statements:

1. The standard k-ε model most accurately predicts the most flow properties for the experimental flows/geometries modeled here.
2. No generalization can be made as to whether the RNG or standard k-ε model more accurately predicts wall bounded or free shear flows.
3. The mixing length model provided in GOTHIC does a poor job of predicting flow properties for all of the experiments modeled.
4. The computational time requirements are most demanding for the RNG model, followed by the standard k-ε and mixing length models.

GOTHIC's ability to predict turbulent flow properties should be researched in the future. A possible area of study would be the analysis of the 2nd and 3rd order k-ε models identified in the Introduction for the experiments provided here. Other flow configurations such as wake flows or flow over a backward-facing step could also be explored. Sensitivity of the calculated flow properties to the grid resolution should also be examined. Integration and

testing of additional turbulence models into GOTHIC, such as the k-ω model, would also be helpful. This work provides a basis for future research in these and other areas.

7. References

1. "About EPRI." Electric Power Research Institute. 20 Aug. 2005. <http://my.epri.com>.
2. Analytis, G. Th. "Implementation and assessment of the renormalization group (RNG), quadratic and cubic non-linear eddy viscosity k–ε models in GOTHIC." Nuclear Engineering and Design. 210 (2001): 177–191.
3. Analytis, G. Th., and M. Andreani. "On the boundary conditions of the k–ε model in 3D coarse-mesh models for containment analysis." Nuclear Engineering and Design. 205 (2001): 53–67.
4. Analytis, G. Th. "Implementation of the Renormalization Group (RNG) k-ε Turbulence Model in GOTHIC 6.1b: Solution Methods and Assessment." Annals of Nuclear Energy. 30 (2003).
5. Andreani, M., F. Putz, T.V. Dury, C. Gjerloev, and B.L. Smith. "On the application of field codes to the analysis of gas mixing in large volumes: case studies using CFX and GOTHIC." Annals of Nuclear Energy. 30 (2003): 685–714.
6. Block, Nathan R. "HNP Essential Services Chilled Water Loss of Accumulator Tank Pressure Analysis." Numerical Applications, Inc. Report NAI-1188-001, Revision 1, June 2005.
7. Cebeci, Tuncer., and A.M.O. Smith. Analysis of Turbulent Boundary Layers. New York: Academic Press, 1974.

8. Champagne, F.H., Y.H. Pao, and I.J. Wygnanski. "On the two-dimensional mixing region." Journal of Fluid Mechanics. 74.2 (1976): 209-250.
9. Eckelmann, H. "The structure of the viscous sublayer and the adjacent wall region in a turbulent channel flow." Journal of Fluid Mechanics. 65.3 (1974): 439–459.
10. GOTHIC Containment Analysis Program Technical Manual, Version 7.2, July 2004, EPRI, Palo Alto, CA.
11. GOTHIC Containment Analysis Program User Manual, Version 7.2, July 2004, EPRI, Palo Alto, CA.
12. Jones, W.P., and B.E. Launder. "The Prediction of Laminarization with a Two-Equation Model of Turbulence." International Journal of Heat and Mass Transfer. 15 (1972): 301-314.
13. Kim, John, Parviz Moin, and Robert Moser. "Turbulence statistics in fully developed channel flow at low Reynolds number." Journal of Fluid Mechanics. 177 (1987): 133-166.
14. Kreplin, H. P., and H. Eckelmann. "Behavior of the three fluctuating velocity components in the wall region of a turbulent channel flow." Physical Fluids. 22.7 (1979): 1233–1239.
15. "NAI Products: GOTHIC/FATHOMS." Numerical Applications Inc. – Solutions in Engineering and Software. 20 Aug. 2005. <http://www.numerical.com/fathoms.html>.
16. Patel, Rajini P. "An Experimental Study of a Plane Mixing Layer." A.I.A.A. Journal. 11.1 (1973): 67-72.

17. Pope, Steven B. Turbulent Flows. New York: Cambridge University Press, 2002.

18. Rodi, W. Turbulence Models for Environmental Problems. Prediction Methods for Turbulent Flows. Ed. W. Kollman. Washington: Hemisphere Publishing Corp., 1980.

19. Sinodis, Joe. "SLC Pump Voiding Potential During SLC Tank Sparger Operation." Numerical Applications, Inc. Report NAI-1156-001, Revision 0, May 2004.

20. Wilcox, David C. Turbulence Modeling for CFD. 2nd Ed. La Canada, California: DCW Industries, 2002.

21. Wygnanski, I., and H.E. Fiedler. "Some measurements in the self preserving jet." Boeing Research Laboratories, Report D1-82-0712, April 1968.

22. Wygnanski, I., and H.E. Fiedler. "The two-dimensional mixing region." Journal of Fluid Mechanics. 31 (1970): 327-361.

23. Yakhot, V., and S.A. Orszag. "Renormalization Group Analysis of Turbulence." Journal of Scientific Computing. 1.1 (1986).

Appendix A. Axi-Symmetric Jet GOTHIC Input Deck

Control Volumes								
Vol #	Description	Vol (ft3)	Elev (ft)	Ht (ft)	Hyd. D. (ft)	L/V IA (ft2)	S Wave Damper	Burn Opt
1	atmosphere	1000000.	0.	100.	10.	DEFAULT	1.	NONE
2s	room	1020.	0.	7.5	7.16	DEFAULT	1.	NONE

Laminar Leakage									
Vol #	Lk Rate Factor (%/hr)	Ref Press (psia)	Ref Temp (F)	Ref Humid (%)	Sink /Src BC	Model Option	Rep Wall	Subvol Option	Leak Area (ft2)
1	0.					CNST T		UNIFORM	DEFAULT
2s	0.					CNST T		UNIFORM	DEFAULT

Turbulent Leakage										
Vol #	Lk Rate Factor (%/hr)	Ref Press (psia)	Ref Temp (F)	Ref Humid (%)	Sink /Src BC	Model Option	Rep Wall	Subvol Option	Leak Area (ft2)	fL/D
1	0.					CNST T		UNIFORM	DEFAULT	
2s	0.					CNST T		UNIFORM	DEFAULT	

X-Direction Noding Volume 2s		
Cell Plane	Distance (ft)	Width (ft)
1	0.	0.380952
2	0.380952	0.380952
3	0.761905	0.380952
4	1.14286	0.380952
5	1.52381	0.380952
6	1.90476	0.182195
7	2.08695	0.0869567
8	2.17391	0.0869566
9	2.26087	0.0869566
10	2.34783	0.0869565
11	2.43479	0.0869564

X-Direction Noding (cont.)
Volume 2s

Cell Plane	Distance (ft)	Width (ft)
12	2.52175	0.0869563
13	2.60871	0.0869562
14	2.69567	0.0869561
15	2.78263	0.086956
16	2.86959	0.0869559
17	2.95655	0.0869558
18	3.04351	0.0869557
19	3.13047	0.0869555
20	3.21743	0.0869554
21	3.30439	0.0869553
22	3.39135	0.0869551
23	3.47831	0.086955
24	3.56526	0.0869551
25	3.65222	0.0869549
26	3.73917	0.0869551
27	3.82613	0.0869549
28	3.91308	0.0869551
29	4.00004	0.0869549
30	4.08699	0.0869552
31	4.17395	0.0869549
32	4.2609	0.0869552
33	4.34786	0.0869549
34	4.43481	0.0869552
35	4.52177	0.0869549
36	4.60872	0.0869552
37	4.69568	0.0869549
38	4.78263	0.0869552
39	4.86959	0.0869549
40	4.95654	0.0869553
41	5.0435	0.0869549
42	5.13045	0.0869549
43	5.2174	0.0869549
44	5.30435	0.0869548
45	5.3913	0.0869548
46	5.47825	0.0869548
47	5.5652	0.0869548
48	5.65215	0.0869547
49	5.7391	0.0869547
50	5.82605	0.0869545
51	5.913	0.18219
52	6.09524	0.380952
53	6.47619	0.380952
54	6.85714	0.380952

X-Direction Noding (cont.)
Volume 2s

Cell Plane	Distance (ft)	Width (ft)
55	7.2381	0.380952
56	7.61905	0.380952

Y-Direction Noding
Volume 2s

Cell Plane	Distance (ft)	Depth (ft)
1	0.	3.4
2	3.4	3.4
3	6.8	3.4
4	10.2	3.4
5	13.6	3.4

Z-Direction Noding
Volume 2s

Cell Plane	Distance (ft)	Height (ft)
1	0.	0.357143
2	0.357143	0.357143
3	0.714286	0.357143
4	1.07143	0.357143
5	1.42857	0.357144
6	1.78571	0.357144
7	2.14285	0.357144
8	2.49999	0.357144
9	2.85713	0.357145
10	3.21427	0.357145
11	3.57141	0.357145
12	3.92856	0.357145
13	4.28571	0.357144
14	4.64285	0.357145
15	4.99999	0.357146
16	5.35714	0.357145
17	5.71429	0.357144
18	6.07143	0.357145

Z-Direction Noding (cont.)
Volume 2s

Cell Plane	Distance (ft)	Height (ft)
19	6.42858	0.357143
20	6.78572	0.357143
21	7.14286	0.357144

Cell Blockages - Table 1
Volume 2s

Blockage No.	Description	Type			

Cell Blockages - Table 2
Volume 2s

Blockage No.	Coordinates & Dimensions (ft) X1	Y1	Z1	X2	Y2	Z2	X3	Y3	Z3	L	Curb Height

X-Direction Cell Face Variations
Volume 2s

Cell No.	Blockage No.	Area Porosity	Hyd. Dia. (ft)	Loss Coeff.	Drop De-ent. Factor
def	0	1.	1000000.	0.	0.

Y-Direction Cell Face Variations
Volume 2s

Cell No.	Blockage No.	Area Porosity	Hyd. Dia. (ft)	Loss Coeff.	Drop De-ent. Factor
def	0	1.	1000000.	0.	0.

Z-Direction Cell Face Variations Volume 2s						
Cell No.	Blockage No.	Area Porosity	Hyd. Dia. (ft)	Loss Coeff.	Drop De-ent. Factor	Curb Ht (ft)
def	0	1.	1000000.	0.	0.	

Volume Variations Volume 2s			
Cell No.	Blockage No.	Volume Porosity	Hyd. Dia. (ft)
def	0	1.	1000000.

Boundary Slip Conditions Volume 2s					
North	South	East	West	Top	Bottom
NO SLIP	NO SLIP	NO SLIP	NO SLIP	NO SLIP	NO SLIP

Turbulence Parameters							
Vol #	Molec. Diff.	Turb. Model	Liquid Mix.L. (ft)	Vapor Mix.L (ft)	Liquid Pr/Sc No.	Vapor Pr/Sc No.	Phase Option
1	NO	NO			1.	1.	VAPOR
2s	YES	ke-STD	0.001	0.001	1.	1.	VAPOR

Turbulence Sources						
Vol #	Type	Phase	Kinetic Energy (ft2/s2) [*lbm/s]	FF	Dissipation (ft2/s3) [*lbm/s]	FF

Fluid Boundary Conditions - Table 1

BC#	Description	Press. (psia)	FF	Temp. (F)	FF	Flow (lbm/s)	FF	S P	J O	ON Trip	OFF Trip	Elev. (ft)
1F	Boundary Condit	14.6944		59		0.10307		N	N			3.7067
2P	Out flow	14.6944		59				N	N			0.

Fluid Boundary Conditions - Table 2

BC#	Liq. V. Frac.	FF	Stm. V. Frac.	FF	Drop D. (in)	FF	Cpld BC#	Flow Frac.	FF	Heat (Btu/s)	FF	Outlet Quality	FF
1F	0.		0		NONE							DEFAULT	
2P	0.		0		NONE							DEFAULT	

Fluid Boundary Conditions - Table 3
Volume Fractions

BC#	Air Gas 1	FF	Gas 2	FF	Gas 3	FF	Gas 4	FF
1F	1.							
2P	1.							

Fluid Boundary Conditions - Table 4
Volume Fractions

BC#	Gas 5	FF	Gas 6	FF	Gas 7	FF	Liq Comp	FF
1F								
2P								

Flow Paths - Table 1

F.P. #	Description	Vol A	Elev (ft)	Ht (ft)	Vol B	Elev (ft)	Ht (ft)
1	jet	2s2827	3.7067	0.0433	1F	3.7067	0.0433
2	out for atmosph	1	0.	10.	2P	0.	10.

Flow Paths - Table 2								
Flow Path #	Flow Area (ft2)	Hyd. Diam. (ft)	Inertia Length (ft)	Friction Length (ft)	Relative Rough-ness	Dep Bend (deg)	Mom Trn Opt	Strat Flow Opt
1	0.005899	0.04333	17.	0.			-	NONE
2	60.	8.	10.	0.			-	NONE

Flow Paths - Table 3						
Flow Path #	Fwd. Loss Coeff.	Rev. Loss Coeff.	Comp. Opt.	Critical Flow Model	Exit Loss Coeff.	Drop Breakup Model
1	0.	0.	OFF	OFF	0.	OFF
2	0.	0.	OFF	OFF	0.	OFF

3D Connectors						
Connector No.	Description	Volume A	Volume B	Fwd. Loss Coeff.	Rev. Loss Coeff.	LP Vol Momentum
1		2s225-5880	1			CONSERVE

Volume Initial Conditions						
Vol #	Total Pressure (psia)	Vapor Temp. (F)	Liquid Temp. (F)	Relative Humidity (%)	Liquid Volume Fract.	Liq. Comp. Fract.
def	14.69444	59.	59.	0.	0.	0.

Initial Volume Fractions								
Vol #	Air Gas 1	Gas 2	Gas 3	Gas 4	Gas 5	Gas 6	Gas 7	Liq Comp
def	1.	0.	0.	0.	0.	0.	0.	0.

Noncondensing Gases						
Gas No.	Description	Symbol	Type	Mol. Weight	Lennard-Jones Parameters Diameter (Ang)	e/K (K)
1	Air	Air	POLY	28.97	3.617	97.

Noncondensing Gases - Cp/Visc. Equations						
Gas No.	Cp Tmin (R)	Equation Tmax (R)	(Required) Cp (Btu/lbm-R	Visc. Tmin (R)	Equation Tmax (R)	(Optional) Viscosity (lbm/ft-hr)
1	360.	2880.	0.2385-6.20065e			

Control Variables								
CV #	Description	Func. Form	Initial Value	Coeff. G	Coeff. a0	Min	Max	Upd. Int. Mult.
1C		write	0.	1.	0.	-1e+03	1e+032	0.

Function Components
Control Variable 1C

write
Y=write(FileX1,a2X2,a3X3,...,anXn)

#	Gothic_s Name	Variable location	Coef. a
1	Vol_Var.txt	st	0.
2	Cdxf	cV	1.
3	Cdxr	cV	1.
4	Cdyf	cV	1.
5	Cdyr	cV	1.
6	Cdzf	cV	1.
7	Cdzr	cV	1.
8	Dispv	cV	1.
9	P	cV	1.
10	Qvap	cV	1.
11	Rv	cV	1.

Function Components (cont.)
Control Variable 1C

write
Y=write(FileX1,a2X2,a3X3,...,anXn)

#	Gothic_s Name	Variable location	Coef. a
12	Shearxv	cV	1.
13	Shearyv	cV	1.
14	Shearzv	cV	1.
15	Temv	cV	1.
16	Tkev	cV	1.
17	Tvisv	cV	1.
18	Totvisv	cV	1.
19	Uxv	cV	1.
20	Uyv	cV	1.
21	Uzv	cV	1.
22	Viscv	cV	1.
23	Visv	cV	1.
24	Xiv	cV	1.

Run Control Parameters (Seconds)

Time Dom	DT Min	DT Max	DT Ratio	End Time	Print Int	Graph Int	Max CPU	Dump Int	Ph Chng T Scale	L Flow Shutoff
1	1e-005	2.	1.	100.	100.	0.5	1e+006	0.	DEFAULT	DEFAULT

Solution Options

Time Dom	Solution Method	Imp Conv Limit	Imp Iter Limit	Pres Sol Method	Pres Conv Limit	Pres Iter Limit	Differ Scheme	Burn Sharp
1	AUTO-IMP	0.001	100	SPARSE	0.	1	FOUP	0.

Run Options

Option	Setting
Start Time	0
Restart Time Step #	0

Run Options (cont.)	
Option	Setting
Restart Time Control	NEW
Revaporization Fraction	DEFAULT
Fog Model	OFF
Maximum Mist Density (lbm/ft3)	DEFAULT
Drop Diam. From Mist (in)	0
Minimum HT Coeff. (B/h-ft2-F)	0.0
Reference Pressure (psia)	IGNORE
Forced Ent. Drop Diam. (in)	DEFAULT
Vapor Phase Head Correction	IGNORE
Kinetic Energy	INCLUDE
Vapor Phase	INCLUDE
Liquid Phase	NONE
Drop Phase	NONE
Force Equilibrium	INCLUDE
Drop-Liq. Conversion	INCLUDE
QA Logging	OFF
Debug Output Level	0
Restart Dump on CPU Interval (sec)	3600.
Version 6.1 Formulations	OFF

Graphs							
Graph			Curve Number				
#	Title	Mon	1	2	3	4	5
0	M&E Imbalance		EM	EE			
1			VV1				
2			vy2s111	vy2s112	vy2s112	vy2s112	vy2s112
3			vy2s108	vy2s110	vy2s112	vy2s114	
4			FV1	FV2			
5			2sVV103				
6			FV2				
7			vy2s101				
8			2sVV296				
9			2sVV302				
10			2sVV285				
11			2sVV169				
12			vy2s299	vy2s300	vy2s300	vy2s298	vy2s298

Envelope Sets			
Set No.	Description	Set Type	No. Items

Data Files					
File #	Name	Type	Inter-polate	Output Files	Detail Level
1	what.txt	SPACE	YES	SINGLE	FULL

Appendix B. Channel Flow GOTHIC Input Deck

Control Volumes

Vol #	Description	Vol (m3)	Elev (m)	Ht (m)	Hyd. D. (m)	L/V IA (m2)	S Wave Damper	Burn Opt
1s	channel	0.08	0.	0.02	0.038	DEFAULT	1.	NONE
2	inlet	0.001	0.	0.02	0.01	DEFAULT	1.	NONE
3	outlet	0.001	0.	0.02	0.01	DEFAULT	1.	NONE

Laminar Leakage

Vol #	Lk Rate Factor (%/hr)	Ref Press (kPa)	Ref Temp (C)	Ref Humid (%)	Sink /Src BC	Model Option	Rep Wall	Subvol Option	Leak Area (m2)
1s	0.					CNST T		UNIFORM	DEFAULT
2	0.					CNST T		UNIFORM	DEFAULT
3	0.					CNST T		UNIFORM	DEFAULT

Turbulent Leakage

Vol #	Lk Rate Factor (%/hr)	Ref Press (kPa)	Ref Temp (C)	Ref Humid (%)	Sink /Src BC	Model Option	Rep Wall	Subvol Option	Leak Area (m2)	fL/D
1s	0.					CNST T		UNIFORM	DEFAULT	
2	0.					CNST T		UNIFORM	DEFAULT	
3	0.					CNST T		UNIFORM	DEFAULT	

X-Direction Noding
Volume 1s

Cell Plane	Distance (m)	Width (m)
1	0.	0.4

Y-Direction Noding Volume 1s		
Cell Plane	Distance (m)	Depth (m)
1	0.	1.66667
2	1.66667	1.66667
3	3.33334	1.66667
4	5.	1.66667
5	6.66667	1.66667
6	8.33333	1.66667

Z-Direction Noding Volume 1s		
Cell Plane	Distance (m)	Height (m)
1	0.	0.00363492
2	0.00363492	0.00225916
3	0.00589408	0.0016434
4	0.00753748	0.0012924
5	0.00882988	0.00106526
6	0.00989514	9.062e-004
7	0.0108013	7.885e-004
8	0.0115898	6.979e-004
9	0.0122877	6.259e-004
10	0.0129136	5.675e-004
11	0.0134811	5.19e-004
12	0.014	4.615e-004
13	0.0144615	4.615e-004
14	0.0149231	4.615e-004
15	0.0153846	4.615e-004
16	0.0158462	4.615e-004
17	0.0163077	4.615e-004
18	0.0167692	4.615e-004
19	0.0172308	4.615e-004
20	0.0176923	4.615e-004
21	0.0181538	4.615e-004
22	0.0186154	4.615e-004
23	0.0190769	4.615e-004
24	0.0195385	4.615e-004

Cell Blockages - Table 1
Volume 1s

Blockage No.	Description	Type			

Cell Blockages - Table 2
Volume 1s

Blockage No.	Coordinates & Dimensions (m) X1	Y1	Z1	X2	Y2	Z2	X3	Y3	Z3	L	Curb Height

X-Direction Cell Face Variations
Volume 1s

Cell No.	Blockage No.	Area Porosity	Hyd. Dia. (m)	Loss Coeff.	Drop De-ent. Factor
def	0	1.	1000000.	0.	0.

Y-Direction Cell Face Variations
Volume 1s

Cell No.	Blockage No.	Area Porosity	Hyd. Dia. (m)	Loss Coeff.	Drop De-ent. Factor
def	0	1.	1000000.	0.	0.

Z-Direction Cell Face Variations
Volume 1s

Cell No.	Blockage No.	Area Porosity	Hyd. Dia. (m)	Loss Coeff.	Drop De-ent. Factor	Curb Ht (m)
def	0	1.	1000000.	0.	0.	

Volume Variations Volume 1s			
Cell No.	Blockage No.	Volume Porosity	Hyd. Dia. (m)
def	0	1.	1000000.

Boundary Slip Conditions Volume 1s					
North	South	East	West	Top	Bottom
NO SLIP	NO SLIP	SLIP	SLIP	NO SLIP	SLIP

Turbulence Parameters							
Vol #	Molec. Diff.	Turb. Model	Liquid Mix.L. (m)	Vapor Mix.L (m)	Liquid Pr/Sc No.	Vapor Pr/Sc No.	Phase Option
1s	YES	ke-STD			1.	1.	VAPOR
2	YES	ke-STD			1.	1.	VAPOR
3	YES	ke-STD			1.	1.	VAPOR

Turbulence Sources						
Vol #	Type	Phase	Kinetic Energy (m2/s2)[*kg/s]	FF	Dissipation (m2/s3)[*kg/s]	FF

Fluid Boundary Conditions - Table 1												
BC#	Description	Press. (kPa)	FF	Temp. (C)	FF	Flow (kg/s)	FF	S P	J O	ON Trip	OFF Trip	Elev. (m)
1F	inlet	100.		20		V0.0170	1T	N	N			0.
2P	outlet	100.		20		0		N	N			0.

Fluid Boundary Conditions - Table 2

BC#	Liq. V. Frac.	FF	Stm. V. Frac.	FF	Drop D. (cm)	FF	Cpld BC#	Flow Frac.	FF	Heat (kJ/s)	FF	Outlet Quality	FF
1F	0.		0		NONE							DEFAULT	
2P	0.		0		NONE							DEFAULT	

Fluid Boundary Conditions - Table 3
Volume Fractions

BC#	Air Gas 1	FF	Gas 2	FF	Gas 3	FF	Gas 4	FF
1F	1.							
2P	1.							

Fluid Boundary Conditions - Table 4
Volume Fractions

BC#	Gas 5	FF	Gas 6	FF	Gas 7	FF	Liq Comp	FF
1F								
2P								

Flow Paths - Table 1

F.P. #	Description	Vol A	Elev (m)	Ht (m)	Vol B	Elev (m)	Ht (m)
1	inlet flow	2	0.	0.02	1F	0.	0.02
2	outlet flow	3	0.	0.02	2P	0.	0.02

Flow Paths - Table 2

Flow Path #	Flow Area (m2)	Hyd. Diam. (m)	Inertia Length (m)	Friction Length (m)	Relative Rough-ness	Dep Bend (deg)	Mom Trn Opt	Strat Flow Opt
1	0.008	0.038	1.	0.			-	NONE

Flow Paths - Table 2 (cont.)								
Flow Path #	Flow Area (m2)	Hyd. Diam. (m)	Inertia Length (m)	Friction Length (m)	Relative Rough-ness	Dep Bend (deg)	Mom Trn Opt	Strat Flow Opt
2	0.008	0.038	1.	0.			-	NONE

Flow Paths - Table 3						
Flow Path #	Fwd. Loss Coeff.	Rev. Loss Coeff.	Comp. Opt.	Critical Flow Model	Exit Loss Coeff.	Drop Breakup Model
1			OFF	OFF	0.	OFF
2			OFF	OFF	0.	OFF

3D Connectors						
Connector No.	Description	Volume A	Volume B	Fwd. Loss Coeff.	Rev. Loss Coeff.	LP Vol Momentum
1	inlet	2	1s1-115		1e+025	CONSERVE
2	outlet	1s6-138	3		1e+025	CONSERVE

Volume Initial Conditions						
Vol #	Total Pressure (kPa)	Vapor Temp. (C)	Liquid Temp. (C)	Relative Humidity (%)	Liquid Volume Fract.	Liq. Comp. Fract.
def	100.	20.	20.	0.	0.	0.

Initial Volume Fractions								
Vol #	Air Gas 1	Gas 2	Gas 3	Gas 4	Gas 5	Gas 6	Gas 7	Liq Comp
def	1.	0.	0.	0.	0.	0.	0.	0.

Noncondensing Gases						
Gas No.	Description	Symbol	Type	Mol. Weight	Lennard-Jones Parameters Diameter (Ang)	e/K (K)
1	Air	Air	POLY	28.97	3.617	97.

Noncondensing Gases - Cp/Visc. Equations						
Gas No.	Cp Tmin (K)	Equation Tmax (K)	(Required) Cp (kJ/kg-K)	Visc. Tmin (K)	Equation Tmax (K)	(Optional) Viscosity (centipoise)
1	200.	1600.	0.9986-4.67268e			

Forcing Function Tables				
FF#	Description	Ind. Var.	Dep. Var.	Points
0	Constant	-	-	0
1T		Ind. Var.	Dep. Var.	3

Function 1T Ind. Var.: Dep. Var.:			
Ind. Var.	Dep. Var.	Ind. Var.	Dep. Var.
0. 1000000.	0. 1.	1.	1.

Control Variables								
CV #	Description	Func. Form	Initial Value	Coeff. G	Coeff. a0	Min	Max	Upd. Int. Mult.
1C		write	0.	1.	0.	-1e+03	1e+032	1.

Function Components
Control Variable 1C

write
Y=write(FileX1,a2X2,a3X3,...,anXn)

#	Gothic_s Name	Variable location	Coef. a
1	Vol_Var_channel_k-e_	st	0.
2	Cdxf	cV	1.
3	Cdxr	cV	1.
4	Cdyf	cV	1.
5	Cdyr	cV	1.
6	Cdzf	cV	1.
7	Cdzr	cV	1.
8	Dispv	cV	1.
9	P	cV	1.
10	Qvap	cV	1.
11	Rv	cV	1.
12	Shearxv	cV	1.
13	Shearyv	cV	1.
14	Shearzv	cV	1.
15	Temv	cV	1.
16	Tkev	cV	1.
17	Tvisv	cV	1.
18	Totvisv	cV	1.
19	Uxv	cV	1.
20	Uyv	cV	1.
21	Uzv	cV	1.
22	Viscv	cV	1.
23	Visv	cV	1.
24	Xiv	cV	1.

Run Control Parameters (Seconds)

Time Dom	DT Min	DT Max	DT Ratio	End Time	Print Int	Graph Int	Max CPU	Dump Int	Ph Chng T Scale	L Flow Shutoff
1	1e-006	1.	1.	25.	1.	0.01	1e+006	7200.	DEFAULT	DEFAULT

Solution Options								
Time Dom	Solution Method	Imp Conv Limit	Imp Iter Limit	Pres Sol Method	Pres Conv Limit	Pres Iter Limit	Differ Scheme	Burn Sharp
1	AUTO-IMP	0.001	100	CONJUGATE	1e-004	40	FOUP	0.

Run Options	
Option	Setting
Start Time	0
Restart Time Step #	0
Restart Time Control	NEW
Revaporization Fraction	DEFAULT
Fog Model	OFF
Maximum Mist Density (kg/m3)	DEFAULT
Drop Diam. From Mist (cm)	0
Minimum HT Coeff. (J/s-m2-K)	0.0
Reference Pressure (kPa)	IGNORE
Forced Ent. Drop Diam. (cm)	DEFAULT
Vapor Phase Head Correction	IGNORE
Kinetic Energy	IGNORE
Vapor Phase	INCLUDE
Liquid Phase	NONE
Drop Phase	NONE
Force Equilibrium	IGNORE
Drop-Liq. Conversion	IGNORE
QA Logging	OFF
Debug Output Level	0
Restart Dump on CPU Interval (sec)	3600.
Version 6.1 Formulations	OFF

Graphs							
Graph #	Title	Mon	Curve Number 1	2	3	4	5
0	M&E Imbalance		EM	EE			
1			1sVV4-2				
2			vy1s233	vy1s227	vy1s221	vy1s215	
3			vy1s35	vy1s95	vy1s130	vy1s155	vy1s77
4			vy1s5	vy1s17	vy1s29	vy1s41	vy1s53
5			vy1s5	vy1s41	vy1s83	vy1s125	vy1s167
6			vy1s77				

Graphs (cont.)							
Graph #	Title	Mon	Curve Number 1	2	3	4	5
7			FV2				
8			FV2	FV1			

Envelope Sets			
Set No.	Description	Set Type	No. Items

Appendix C. Mixing Layer Flow GOTHIC Input Deck

Control Volumes

Vol #	Description	Vol (m3)	Elev (m)	Ht (m)	Hyd. D. (m)	L/V IA (m2)	S Wave Damper	Burn Opt
1s		10.	0.	2.	10.	DEFAULT	1.	NONE
2		1000.	0.	2.	1e+006	DEFAULT	1.	NONE
3		10.	0.	2.	1e+006	DEFAULT	1.	NONE

Laminar Leakage

Vol #	Lk Rate Factor (%/hr)	Ref Press (kPa)	Ref Temp (C)	Ref Humid (%)	Sink /Src BC	Model Option	Rep Wall	Subvol Option	Leak Area (m2)
1s	0.					CNST T		UNIFORM	DEFAULT
2	0.					CNST T		UNIFORM	DEFAULT
3	0.					CNST T		UNIFORM	DEFAULT

Turbulent Leakage

Vol #	Lk Rate Factor (%/hr)	Ref Press (kPa)	Ref Temp (C)	Ref Humid (%)	Sink /Src BC	Model Option	Rep Wall	Subvol Option	Leak Area (m2)	fL/D
1s	0.					CNST T		UNIFORM	DEFAULT	
2	0.					CNST T		UNIFORM	DEFAULT	
3	0.					CNST T		UNIFORM	DEFAULT	

X-Direction Noding
Volume 1s

Cell Plane	Distance (m)	Width (m)
1	0.	0.127
2	0.127	0.127
3	0.254	0.127
4	0.381	0.127

Y-Direction Noding Volume 1s		
Cell Plane	Distance (m)	Depth (m)
1	0.	0.25
2	0.25	0.25
3	0.5	0.25
4	0.75	0.75
5	1.5	0.5

Z-Direction Noding Volume 1s		
Cell Plane	Distance (m)	Height (m)
1	0.	0.019802
2	0.019802	0.019802
3	0.039604	0.019802
4	0.059406	0.019802
5	0.079208	0.0198021
6	0.0990101	0.0198021
7	0.118812	0.0198021
8	0.138614	0.0198021
9	0.158416	0.0198022
10	0.178218	0.0198022
11	0.19802	0.0198022
12	0.217822	0.0198022
13	0.237624	0.0198022
14	0.257426	0.0198023
15	0.277228	0.0198023
16	0.29703	0.0198023
17	0.316832	0.0198024
18	0.336634	0.0198024
19	0.356436	0.0198024
20	0.376238	0.0198024
21	0.39604	0.0198025
22	0.415842	0.0198025
23	0.435644	0.0198025
24	0.455447	0.0198026
25	0.47525	0.0198026
26	0.495053	0.0198026
27	0.514856	0.0198027
28	0.534659	0.0198027
29	0.554462	0.0198027

Z-Direction Noding (cont.) Volume 1s		
Cell Plane	Distance (m)	Height (m)
30	0.574265	0.0198028
31	0.594068	0.0198028
32	0.613871	0.0198029
33	0.633674	0.0198029
34	0.653477	0.0198029
35	0.67328	0.019803
36	0.693083	0.019803
37	0.712886	0.0198031
38	0.732689	0.0198031
39	0.752492	0.0198032
40	0.772295	0.0198032
41	0.792098	0.0198033
42	0.811901	0.0198033
43	0.831704	0.0198034
44	0.851507	0.0198034
45	0.87131	0.0198035
46	0.891114	0.0198036
47	0.910918	0.0198036
48	0.930722	0.0198037
49	0.950526	0.0198038
50	0.97033	0.0198038
51	0.990134	0.0198039
52	1.00994	0.0198039
53	1.02974	0.0198039
54	1.04954	0.0198039
55	1.06934	0.0198039
56	1.08914	0.0198039
57	1.10894	0.0198039
58	1.12874	0.0198039
59	1.14854	0.0198039
60	1.16834	0.0198039
61	1.18814	0.0198039
62	1.20794	0.0198039
63	1.22774	0.0198039
64	1.24754	0.0198039
65	1.26734	0.0198039
66	1.28714	0.0198039
67	1.30694	0.0198039
68	1.32674	0.0198039
69	1.34654	0.0198039
70	1.36634	0.0198039
71	1.38614	0.0198039
72	1.40594	0.0198039

Z-Direction Noding (cont.)
Volume 1s

Cell Plane	Distance (m)	Height (m)
73	1.42574	0.0198039
74	1.44554	0.0198039
75	1.46534	0.0198039
76	1.48514	0.0198038
77	1.50494	0.0198038
78	1.52474	0.0198038
79	1.54454	0.0198038
80	1.56434	0.0198038
81	1.58414	0.0198038
82	1.60394	0.0198038
83	1.62374	0.0198038
84	1.64354	0.0198038
85	1.66334	0.0198038
86	1.68314	0.0198038
87	1.70294	0.0198037
88	1.72274	0.0198037
89	1.74254	0.0198037
90	1.76234	0.0198037
91	1.78214	0.0198036
92	1.80194	0.0198036
93	1.82174	0.0198036
94	1.84154	0.0198035
95	1.86134	0.0198036
96	1.88114	0.0198035
97	1.90094	0.0198035
98	1.92074	0.0198035
99	1.94054	0.0198035
100	1.96034	0.0198035
101	1.98014	0.0198035

Cell Blockages - Table 1
Volume 1s

Blockage No.	Description	Type			

Cell Blockages - Table 2 Volume 1s											
Blockage No.	Coordinates & Dimensions (m) X1	Y1	Z1	X2	Y2	Z2	X3	Y3	Z3	L	Curb Height

X-Direction Cell Face Variations Volume 1s					
Cell No.	Blockage No.	Area Porosity	Hyd. Dia. (m)	Loss Coeff.	Drop De-ent. Factor
def	0	1.	1000000.	0.	0.

Y-Direction Cell Face Variations Volume 1s					
Cell No.	Blockage No.	Area Porosity	Hyd. Dia. (m)	Loss Coeff.	Drop De-ent. Factor
def	0	1.	1000000.	0.	0.

Z-Direction Cell Face Variations Volume 1s						
Cell No.	Blockage No.	Area Porosity	Hyd. Dia. (m)	Loss Coeff.	Drop De-ent. Factor	Curb Ht (m)
def	0	1.	1000000.	0.	0.	

Volume Variations Volume 1s			
Cell No.	Blockage No.	Volume Porosity	Hyd. Dia. (m)
def	0	1.	1000000.

Boundary Slip Conditions Volume 1s					
North	South	East	West	Top	Bottom
NO SLIP	NO SLIP	NO SLIP	NO SLIP	NO SLIP	NO SLIP

Turbulence Parameters							
Vol #	Molec. Diff.	Turb. Model	Liquid Mix.L. (m)	Vapor Mix.L (m)	Liquid Pr/Sc No.	Vapor Pr/Sc No.	Phase Option
1s	YES	ke-STD	0.1	0.1	1.	1.	VAPOR
2	YES	NONE			1.	1.	VAPOR
3	YES	NONE			1.	1.	VAPOR

Turbulence Sources						
Vol #	Type	Phase	Kinetic Energy (m2/s2) [*kg/s]	FF	Dissipation (m2/s3) [*kg/s]	FF

Fluid Boundary Conditions - Table 1													
BC#	Description	Press. (kPa)	FF	Temp. (C)	FF	Flow (kg/s)	FF	S P	J O	ON Trip	OFF Trip	Elev. (m)	
1F		100.		25		V0.7233		N	N			0.	
2P	100	100.		25				N	N			0.	

Fluid Boundary Conditions - Table 2													
BC#	Liq. V. Frac.	FF	Stm. V. Frac.	FF	Drop D. (cm)	FF	Cpld BC#	Flow Frac.	FF	Heat (kJ/s)	FF	Outlet Quality	FF
1F	0.		0		NONE							DEFAULT	
2P	0.		0		NONE							DEFAULT	

Fluid Boundary Conditions - Table 3
Volume Fractions

BC#	Air Gas 1	FF	Gas 2	FF	Gas 3	FF	Gas 4	FF
1F	1.							
2P	1.							

Fluid Boundary Conditions - Table 4
Volume Fractions

BC#	Gas 5	FF	Gas 6	FF	Gas 7	FF	Liq Comp	FF
1F								
2P								

Flow Paths - Table 1

F.P. #	Description	Vol A	Elev (m)	Ht (m)	Vol B	Elev (m)	Ht (m)
1		3	0.	1.	1F	0.	1.
2		2	0.	1.	2P	0.	1.

Flow Paths - Table 2

Flow Path #	Flow Area (m2)	Hyd. Diam. (m)	Inertia Length (m)	Friction Length (m)	Relative Rough-ness	Dep Bend (deg)	Mom Trn Opt	Strat Flow Opt
1	1.	1.	1.	0.			-	NONE
2	1.	1.	1.	0.			-	NONE

Flow Paths - Table 3

Flow Path #	Fwd. Loss Coeff.	Rev. Loss Coeff.	Comp. Opt.	Critical Flow Model	Exit Loss Coeff.	Drop Breakup Model
1			OFF	OFF	0.	OFF

Flow Paths - Table 3 (cont.)						
Flow Path #	Fwd. Loss Coeff.	Rev. Loss Coeff.	Comp. Opt.	Critical Flow Model	Exit Loss Coeff.	Drop Breakup Model
2			OFF	OFF	0.	OFF

3D Connectors						
Connector No.	Description	Volume A	Volume B	Fwd. Loss Coeff.	Rev. Loss Coeff.	LP Vol Momentum
1		1s2017-140	2			CONSERVE
2		3	1s1841-2004			CONSERVE

Volume Initial Conditions						
Vol #	Total Pressure (kPa)	Vapor Temp. (C)	Liquid Temp. (C)	Relative Humidity (%)	Liquid Volume Fract.	Liq. Comp. Fract.
def	100.	25.	25.	0.	0.	0.

Initial Volume Fractions								
Vol #	Air Gas 1	Gas 2	Gas 3	Gas 4	Gas 5	Gas 6	Gas 7	Liq Comp
def	1.	0.	0.	0.	0.	0.	0.	0.

Noncondensing Gases						
Gas No.	Description	Symbol	Type	Mol. Weight	Lennard-Jones Parameters Diameter (Ang)	e/K (K)
1	Air	Air	POLY	28.97	3.617	97.

Noncondensing Gases - Cp/Visc. Equations						
Gas No.	Cp Equation (Required)			Visc. Equation (Optional)		
	Tmin (K)	Tmax (K)	Cp (kJ/kg-K)	Tmin (K)	Tmax (K)	Viscosity (centipoise)
1	200.	1600.	0.9986-4.67268e			

Control Variables								
CV #	Description	Func. Form	Initial Value	Coeff. G	Coeff. a0	Min	Max	Upd. Int. Mult.
1C		write	0.	1.	0.	-1e+03	1e+032	0.

Function Components
Control Variable 1C

write
Y=write(FileX1,a2X2,a3X3,...,anXn)

#	Gothic_s Name	Variable location	Coef. a
1	Vol_Var_k-e.txt	st	0.
2	Cdxf	cV	1.
3	Cdxr	cV	1.
4	Cdyf	cV	1.
5	Cdyr	cV	1.
6	Cdzf	cV	1.
7	Cdzr	cV	1.
8	Dispv	cV	1.
9	P	cV	1.
10	Qvap	cV	1.
11	Rv	cV	1.
12	Shearxv	cV	1.
13	Shearyv	cV	1.
14	Shearzv	cV	1.
15	Temv	cV	1.
16	Tkev	cV	1.
17	Tvisv	cV	1.
18	Totvisv	cV	1.
19	Uxv	cV	1.
20	Uyv	cV	1.
21	Uzv	cV	1.

Function Components (cont.) Control Variable 1C write Y=write(FileX1,a2X2,a3X3,...,anXn)			
#	Gothic_s Name	Variable location	Coef. a
22	Viscv	cV	1.
23	Visv	cV	1.
24	Xiv	cV	1.

Run Control Parameters (Seconds)										
Time Dom	DT Min	DT Max	DT Ratio	End Time	Print Int	Graph Int	Max CPU	Dump Int	Ph Chng T Scale	L Flow Shutoff
1	1e-008	1.	1.	50.	10.	0.1	1e+006	0.	DEFAULT	DEFAULT

Solution Options								
Time Dom	Solution Method	Imp Conv Limit	Imp Iter Limit	Pres Sol Method	Pres Conv Limit	Pres Iter Limit	Differ Scheme	Burn Sharp
1	SEMI-IMP	0.	1	DIRECT	0.	1	FOUP	0.

Run Options	
Option	Setting
Start Time	0
Restart Time Step #	0
Restart Time Control	NEW
Revaporization Fraction	DEFAULT
Fog Model	OFF
Maximum Mist Density (kg/m3)	DEFAULT
Drop Diam. From Mist (cm)	DEFAULT
Minimum HT Coeff. (J/s-m2-K)	0.0
Reference Pressure (kPa)	IGNORE
Forced Ent. Drop Diam. (cm)	DEFAULT
Vapor Phase Head Correction	INCLUDE
Kinetic Energy	IGNORE

Run Options (cont.)	
Option	Setting
Vapor Phase	INCLUDE
Liquid Phase	INCLUDE
Drop Phase	INCLUDE
Force Equilibrium	IGNORE
Drop-Liq. Conversion	INCLUDE
QA Logging	OFF
Debug Output Level	0
Restart Dump on CPU Interval (sec)	3600.
Version 6.1 Formulations	OFF

Graphs							
Graph #	Title	Mon	Curve Number 1	2	3	4	5
0	M&E Imbalance		EM	EE			
1			vy1s199	vy1s185	vy1s179	vy1s167	

Envelope Sets			
Set No.	Description	Set Type	No. Items